Award Number: W81XWH-12-2-0055

TITLE: Sub-lethal Ocular Trauma (SLOT): Establishing a Standardized Blast Threshold to Facilitate Diagnostic, Early Treatment, and Recovery Studies for Blast Injuries to the Eye and Optic Nerve

PRINCIPAL INVESTIGATOR: Walt Gray, Ph.D.

CONTRACTING ORGANIZATION: University of Texas at San Antonio
San Antonio, TX 78249

REPORT DATE: November 2015

TYPE OF REPORT: Final Report

PREPARED FOR: U.S. Army Medical Research and Materiel Command
Fort Detrick, Maryland 21702-5012

REPORT DOCUMENTATION PAGE

Form Approved
OMB No. 0704-0188

1. REPORT DATE	2. REPORT TYPE	3. DATES COVERED
November 2015	Final	15 August 2012 - 14 August 2015

4. TITLE AND SUBTITLE
Sub-lethal Ocular Trauma (SLOT): Establishing a Standardized Blast Threshold to Facilitate Diagnostic, Early Treatment, and Recovery Studies for Blast Injuries to the Eye and Optic Nerve

5a. CONTRACT NUMBER

5b. GRANT NUMBER
W81XWH-12-2-0055

5c. PROGRAM ELEMENT NUMBER

6. AUTHOR(S)
Walt Gray, Matthew Reilly, Brian J. Lund, Jae H. Choi, William E. Sponsel, Randolph D. Glickman

E-Mail: matthew.reilly@utsa.edu

5d. PROJECT NUMBER

5e. TASK NUMBER

5f. WORK UNIT NUMBER

7. PERFORMING ORGANIZATION NAME(S) AND ADDRESS(ES)
University of Texas at San Antonio
One UTSA Circle
San Antonio, TX 78249

8. PERFORMING ORGANIZATION REPORT NUMBER

9. SPONSORING / MONITORING AGENCY NAME(S) AND ADDRESS(ES)
U.S. Army Medical Research and Materiel Command
Fort Detrick, Maryland 21702-5012

10. SPONSOR/MONITOR'S ACRONYM(S)

11. SPONSOR/MONITOR'S REPORT NUMBER(S)

12. DISTRIBUTION / AVAILABILITY STATEMENT
Approved for Public Release; Distribution Unlimited

13. SUPPLEMENTARY NOTES

14. ABSTRACT
Blast experiments on enucleated porcine eye specimens and *in vivo* rabbits were conducted in a large diameter shock tube and supported with computational analysis using the finite volume blast and shock physics code CTH and finite element code LS-DYNA. The shock tube produced a broad array of closed-globe injuries in the porcine eyes including angle recession, cyclodialysis, peripheral chorioretinal detachments, radial peripapillary retinal detachments, and internal scleral delaminations. The most frequently observed injuries were angle recession and chorioretinal detachments, while the most severely damaged tissues were the sclera and retina. Globe rupture was not observed. Post-blast examination of the exposed rabbits revealed increases in thickness of the cornea, inner retinal, and nerve fiber layers immediately and 48 hours after blast exposure. Post-blast immunoassays of rabbit aqueous and blood plasma showed significant correlations of NGF-β, NSE, G-CSF, Eotaxin, MIP-1a, Il-4, IL-13, IL-12(p)70, MCP-1, LiX, and MIP-2 with blast impulse. Computational eye models revealed differential movement of internal structures relative to the vitreous to be a likely mechanism of injury to the retina, sclera, and ciliary body. An ocular incapacitation risk model was developed based on the *ex vivo* porcine eye experiments and tissue-specific injury scores. The data significantly increased our understanding of ocular injury due to primary blast.

15. SUBJECT TERMS
Ocular Trauma, Primary Blast, Shock Tube Experiments, Trauma Prediction, *ex vivo* Porcine Model, *in vivo* Rabbit Model, Trauma Biomarkers, Numerical Modeling, Risk Curves, Ocular Incapacitation Model

16. SECURITY CLASSIFICATION OF:			17. LIMITATION OF ABSTRACT	18. NUMBER OF PAGES	19a. NAME OF RESPONSIBLE PERSON
a. REPORT	b. ABSTRACT	c. THIS PAGE			USAMRMC
U	U	U	UU	135	19b. TELEPHONE NUMBER *(include area code)*

TABLE OF CONTENTS

ABSTRACT

This report summarizes results of all tasks undertaken as part of U.S. Army Medical Research and Material Command Vision Research Program Grant W81XWH-12-2-0055, “Sub-lethal Ocular Trauma (SLOT): Establishing a Standardized Blast Threshold to Facilitate Diagnostic, early Treatment, and Recovery Studies for Blast Injurieσ to the Eye and Optic Nerve.” Ocular injuries resulting from penetration of blast-driven fragments and debris (secondary blast) are well documented and understood, but injuries resulting from only the air shock or blast wave (primary blast) have received little attention. Thus the data generated in in this study significantly increased our understanding of ocular injury due to primary blast. The approach taken was a fully integrated experimental and computational study. Blast experiments on enucleated porcine eye specimens and *in vivo* rabbits were conducted at the ISR Shock Tube Laboratory (STL) located at Joint Base San Antonio, Fort Sam Houston, TX. Computational analysis was performed using the finite volume blast and shock physics code CTH and finite element code LS-DYNA. Although the magnitude of blast waves generated by the shock tube were below the whole body lethal criteria as predicted by Bowen et al. (1968), the sub-lethal blast waves produced a broad array of closed-globe injuries, many of which would seriously compromise visual function and have both immediate and lifelong adverse effects.

Enucleated porcine eyes were exposed to 6 peak blast overpressure levels of approximately 35, 85, 115, 135, 155, and 230 kPa, and reflected specific impulses of approximately 26, 55, 85, 115, 130, and 210 Pa-s, respectively. In order of increasing severity the observed injuries included angle recession, internal scleral delamination, cyclodialysis, peripheral chorioretinal detachments and radial peripapillary retinal detachments. The most frequently observed injuries were angle recession and chorioretinal detachments, while the most severely damaged tissues were the sclera (delaminations) and retina (detachments). Globe rupture was not observed. The severity of ocular injuries generally increased with increasing blast energy (reflected specific impulse).

During the *in vivo* rabbit blast experiments, rabbits were exposed to single peak blast overpressure levels of approximately 55 kPa, 85 kPa, and 130 kPa, and reflected specific impulses of approximately 60, 100, and 160 Pa-s, respectively. Thicknesses of the cornea and inner retinal layers increased significantly with specific impulse immediately and 48 hours after blast exposure. Clinically significant changes in corneal thickness arose immediately and were sustained through 48 hours, suggesting possible disruption of endothelial function. Results revealed an overall increase in the nerve fiber layer thickness after blast. Immunoassays were performed on aqueous and blood plasma samples drawn from each of the blast-exposed rabbits using two magnetic bead millipore kits; (1) Milliplex Rat Cytokine/Chemokine Panel (RECYMAG65K27PMX), and (2) Milliplex Human Neurological Disorders Panel (HND1MAG-39K). In the Human Neurological assay panel both NGF-β and NSE in the blood plasma were significantly correlated with blast specific impulse. In the Rat Cytokine assay panel G-CSF in the

aqueous humor along with Eotaxin, MIP-1a, Il-4, IL-13, IL-12(p)70, MCP-1, LiX, and MIP-2 in the blood plasma were significantly correlated with blast specific impulse.

Computational eye models provided the opportunity to visualize the interior structures of a surrogate (computer-generated) eye during the extreme dynamics of a blast event and provided insight into mechanisms of primary blast injury. Of particular interest was the response of the LS-DYNA model at the interface of the vitreous and retina. Differential movement of internal structures, particularly relative to the vitreous was shown to be a likely mechanism of injury to the retina, sclera, and ciliary body. The vitreous accounts for more than 50 percent of the mass of the eyeball, is largely incompressible, and strongly attached to the retina and ciliary body over a relatively small area. These characteristics contribute to the stresses imposed by the movement of the vitreous on the smaller and more delicate structures of the eye. The characteristics of the retina, mainly its compressibility, also plays a role in determining the magnitude of movement of the vitreous and in turn the amount of stress at the sclera and ciliary body.

A simplified predictive model for soldier ocular incapacitation risk was developed by combining tissue risk data into three broad ocular integrity categories (1) optical integrity, (2) neurophysiological integrity, and (3) structural Integrity. The model is based largely on the *ex vivo* porcine eye experiments and tissue-specific injury scores with predictions plotted against reflected specific impulse. Once the blast characteristics of a particular weapon or scenario (e.g. improvised explosive device) are known, the model can predict the likelihood of incapacitation in each category as a function of distance from the detonation point.

The results of our controlled porcine experiments and numerical simulations provide a sobering new revelation as to the ocular risks from the isolated effects of primary blast. Unfortunately, the implications for human blast victims are even worse. The pig eye is thicker and stronger than the human eye, with a strength factor estimated as twofold higher according to experimental studies carried out for automotive impact (Kennedy et al., 2006). Thus, the proportion of human eyes sustaining severe incapacitation at any non-lethal distance from the detonation point would likely be substantially greater than predicted by our data, and the distances at which incapacitation could arise would likely be significantly further than those determined experimentally using the pig model.

Although the abattoir-fresh porcine eye model remains a relatively inexpensive and efficient model for study, its general relationship to human ocular injury levels needs to be more carefully examined, especially for blast. Further controlled blast studies with preserved eye bank human donor eyes would be one option for determining the extent of this difference. Extrapolation by innovative use of computer modeling is also an option, but may be limited due to a general lack of knowledge about tissue response in dynamic blast environments.

1. INTRODUCTION

Blast-related injuries are commonly classified as primary (shock and air pressure effects), secondary (penetration from blast-driven fragments and debris), tertiary (blunt impact after blast acceleration), and quaternary (primarily heat and explosive gas toxicity). Penetration, contusion, and laceration by fragments and blast-driven debris (secondary) are thought to account for over 82% of all combat ocular injuries (Mader et al., 2006; Thach et al., 2008). Penetration-type injuries are readily observable so the trauma mechanisms are well documented and understood. However, a significant number of injuries may also result from explosive overpressure alone (primary blast) resulting in internal injuries that may not be easily recognized. Although blast injury and effects to major body organs have been reasonably well characterized (Bowen et al, 1968; Stewart, 2006; Stuhmiller, 2008a), primary blast-related trauma to the eye has not been extensively studied. The high incidence of ocular injuries relative to its small areal exposure suggests that the eye may be especially vulnerable to blast injury. It has been estimated that in the Iraq and Afghanistan conflicts eye injuries account for more than 13% of all combat injuries; the highest rate since World War I and the fourth most common injury among deployed personnel (Weichel et al., 2009). High energy blast weapons such as improvised explosive devices (IEDs) will become an ever increasing threat to U.S. military personnel in future conflicts, thus knowledge of primary blast effects on the eye takes on increased importance. Currently, protective eyewear available through the Military Combat Eye Protection Program (MCEP) provides ballistic or fragment protection, but the ability of current eyewear to protect eyes from the potentially harmful effects of blast overpressure is largely unknown. Thus, a large gap exists in our understanding of physical mechanisms and progression of blast-induced ocular trauma. This gap hampers our ability to extend the design of effective protective devices, and may contribute to ineffective treatment and rehabilitation due to inadequate awareness of potentially vision-threatening injury.

This effort was motivated in large part by a non-penetrating blunt impact study previously conducted at Southwest Research Institute (SwRI). That study demonstrated that progression of ocular trauma is well correlated with impact energy (Gray, et al., 2008a; Gray et al., 2008b; Sponsel et al., 2011). The research showed that significant internal damage could occur without obvious external evidence. The study used porcine specimens as surrogates for the human eye and highly deformable paintballs to ensure that the impact energy was imparted to the eye without penetration. Until globe rupture occurred (~10 Joules) internal damage was not typically evident from external examination. However, detailed post-impact pathology revealed that, at significantly lower energies (2-7 Joules), internal trauma could be severe, including cyclodialysis, iridodialysis, angle recession, lens displacement, as well as retinal and choroid detachment. Using paintball mass (m_p) and velocity (V), an approximate correlation between impact energy ($E = \frac{1}{2}m_pV^2$) and trauma severity can be shown (Figure 1). Unfortunately injury could only be treated in a qualitative way (Gray et al., 2008a; Sponsel et al., 2011), as there were insufficient test repetitions (at each injury level) to allow for estimation of ocular injury and incapacitation probabilities (at a given energy of impact).

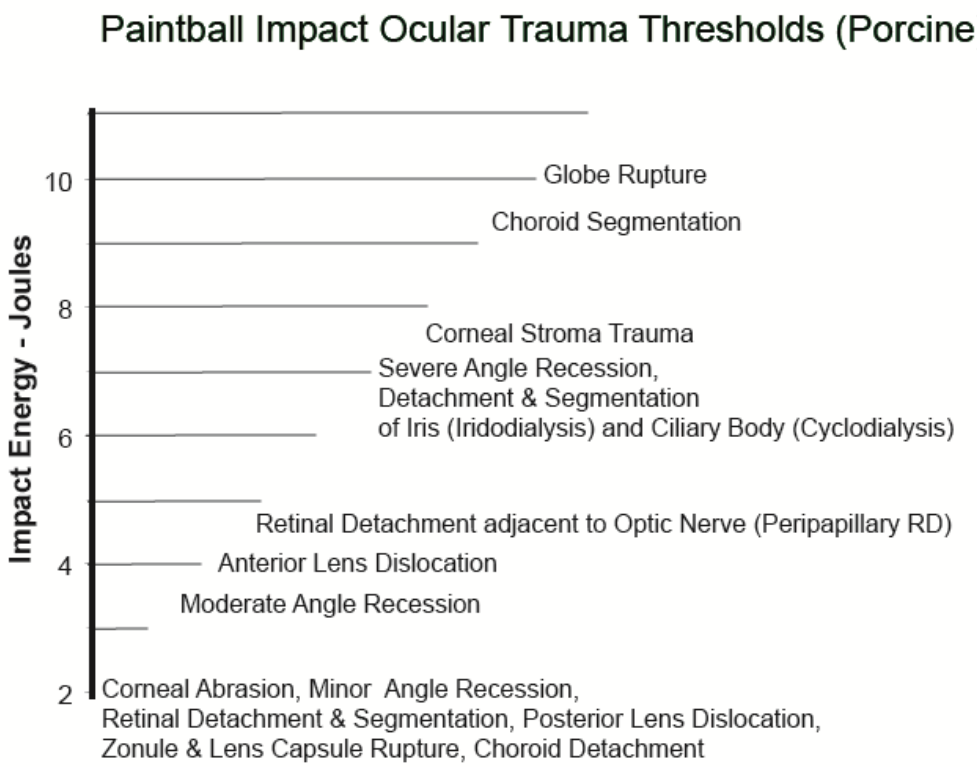

Figure 1. Qualitative trauma thresholds showing lowest energy level for which pathologic entities were observed. Trauma entities were obtained from results of a paintball blunt impact study on porcine eyes (Gray et al., 2008a; Sponsel et al., 2011). The plot illustrates the correlation between impact energy and trauma severity.

Although globe rupture has been used as the injury criterion in a number of previous blunt impact studies (Kennedy et al., 2004; Duma et al., 2004; Kennedy et al., 2006), the energy required to rupture the sclera is large (~ 9 to 10 J) compared to energy thresholds for less catastrophic but potentially serious injuries to the eye's soft inner tissues (Thach et al., 1999; Sponsel et al., 2011). However, soft tissue injuries typically require immediate surgery and numerous follow-up surgeries to prevent immediate or eventual loss of vision. Thach et al. (2008) estimated that approximately 45% of recent combat eye injuries are closed-globe-type injuries. Although studies by Duma and Kennedy (2011) and Gray et al. (2008a) characterized closed globe injuries to eyes subjected to projectile blunt impact, analysis of primary blast has been sparse and inconclusive. Thus, the primary objective of this research effort was to address this knowledge gap by experimentally identifying sub-globe-rupture injury mechanisms and their progression with increasing blast energy and impulse. Blast experiments were conducted using the U.S. Army Institute of Surgical Research (ISR) large diameter shock tube. This device has the capability to reliably produce blast overpressure with the characteristic Friedlander waveform typical of explosive detonation (Figure 2).

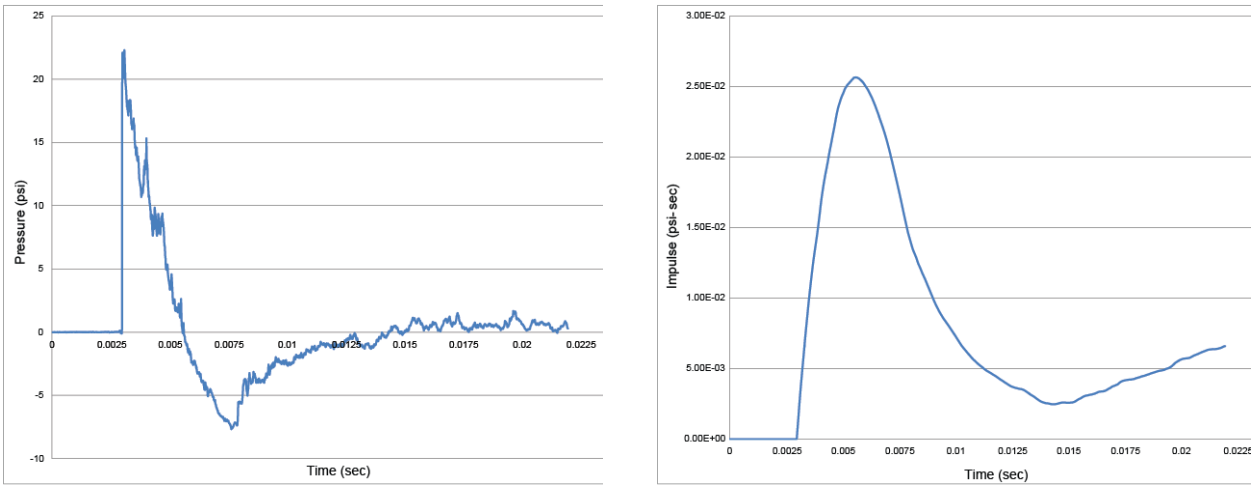

Figure 2. Typical Friedlander waveform (left) and specific impulse (right) for ISR shock tube apparatus. Specific impulse is calculated by time integration of the waveform. (The term specific impulse is used here because it is the pressure-time waveform that is integrated, and not the force-time trace that results in impulse.)

Integration of the measured pressure-time traces provides the required specific impulse information. The term specific impulse is used here because it is the pressure-time waveform that was integrated, and not the force-time trace associated with impulse. The magnitude of blast waves generated by the shock tube were well below the whole body lethal criteria as predicted by Bowen et al. (1968), so closed-globe injuries observed in this study were also sub-lethal, thus the term sub-lethal ocular trauma (SLOT) was adopted.

Experiments increased in complexity from *ex vivo* porcine eyes in Year 1 of the study to *in vivo* rabbit eyes in Year 2. Use of the *in vivo* rabbit model allowed for biochemical marker monitoring and characterization. Although physical trauma was the primary focus, the chemical biomarker assessment in Year 2 allowed for correlation of observed physical trauma with more subtle chemical indicators. It is anticipated that results of the biomarker study may provide fruitful pathways and directions for future research aimed at understanding blast-induced traumatic brain injury, its recognition, and early treatment.

Extensive use of in situ imaging technologies was employed for pre- and post-blast assessments. In-house studies of impact trauma have shown that pre- and post-impact B-scan and UBM ultrasound imaging help differentiate blast-induced trauma from fixative artifact. Scanning abattoir eyes from a posterior approach allows cilio-lenticular imaging with B-scan, and peripapilllary/macular assessment with UBM, greatly increasing the diagnostic specificity of the histopathology studies. Any gross globe deformation that occurred during the blast was documented using high-speed digital video.

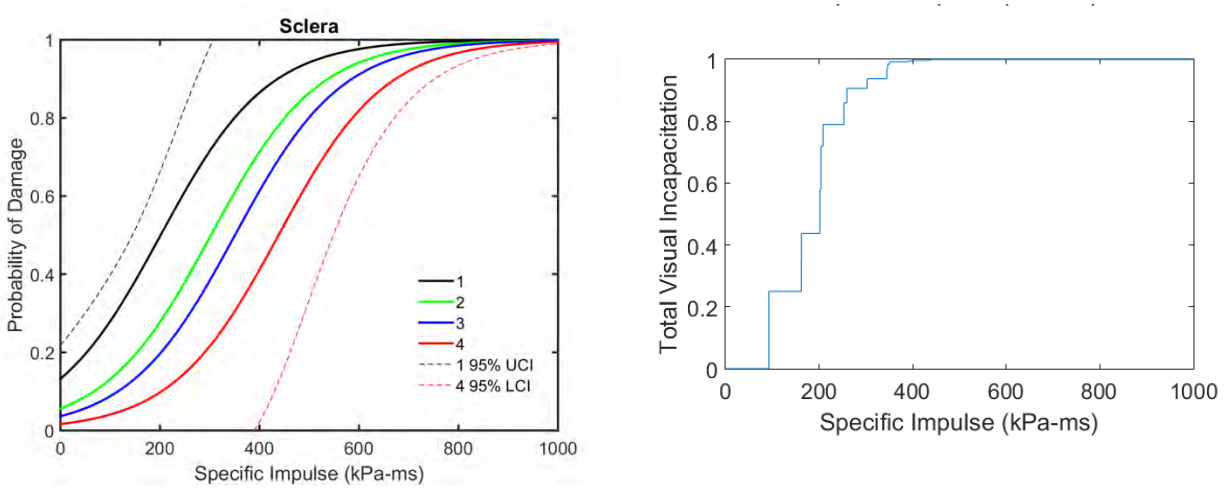

Figure 3. Probability of injury curve (risk function curve) for the sclera (left). Likelihood of total visual incapacitation based on tissue risk curve data and tissue specific injury scores (right). The model predicts that exposure to blasts with specific impulses greater than 400 kPa-ms will result in half of exposed personnel having 100% probability of total visual incapacitation.

Experiments were accompanied by computational analysis using physics-based codes CTH and LS-DYNA. One of the invaluable lessons learned in previous blunt impact studies was that numerical simulations have the potential to identify physical mechanisms responsible for otherwise unobservable and unexplained phenomena (Gray et al., 2008a, 2011). Realistic geometrical and tissue constitutive models of external and internal eye structures were developed for implementation into CTH and LS-DYNA. Co-development of models for both codes allowed us to avoid limitations presented by each code. CTH was used in the initial stages of the shock interaction (i.e., the first few μsec), where it produced the initial boundary condition inputs for LS-DYNA. LS-DYNA was then used to simulate long-term deformation (msec to sec). The simulations carefully mimicked the experiments with the goal of fully reproducing the trauma observed in the experiments. The validated models allowed for analytical extension into impulse regions unattainable with the shock tube experiments. The models were invaluable in providing insights into physics of tissue response. It is hoped that future use of the computational models will allow for more effective design of protective eyewear and virtual identification of physical parameters not measurable in experiments.

The project culminated in Year 3 with development of trauma risk curves and an incapacitation model useful for predicting the likelihood of observing a number of sub-globe-rupture injuries under various blast overpressure-specific impulse environments (Figure 3). The utility of such an approach has been adequately demonstrated by the wide use of so-called Bowen-type curves (whole body response to blast) in a number of warfighter survivability, lethality, and vulnerability (SLV) models (Richmond and White, 1962; Richmond et al., 1966; Bowen et al., 1968; Richmond, et al., 1985; Proud et al., 2009). The individual risk curves reflect the probabilities of observing such injuries as angle recession, iridodialysis/cyclodialysis, and scleral delamination. Ordinal logistic

regression was used to generate the curves from the number of times a specific tissue injury was observed in the porcine blast experiments and subsequent post-blast pathology. The tissue risk probabilities and tissue-specific injury scores (generated during post-blast pathology of porcine specimens) were then combined into an overall visual incapacitation model allowing for estimation of soldier battlefield readiness after exposure to specific blast scenarios (i.e., explosive quantity, specific impulse, and radial distance). Battlefield readiness was based on acute injuries in three categories; (1) optical integrity, (2) neurophysiological integrity, and (3) structural integrity.

The project was undertaken as a collaborative research effort between personnel from the University of Texas at San Antonio, the U.S. Army Institute of Surgical Research (Ocular Trauma Division), the University of Texas Health Science Center-San Antonio, and the Sponsel Professional Association of San Antonio. The project team is especially grateful for the assistance provided by personnel of the Veterinarian Department at the Institute of Surgical Research. Without their help the project could not have been successfully completed. The data and predictive models generated have significantly increased our understanding of blast-induced ocular injury.

2. SUMMARY OF RESEARCH

2.1 Blast Experiments

A total of 85 blast experiments on enucleated porcine eye specimens, and 17 blast experiments on *in vivo* rabbits were conducted at the ISR Shock Tube Laboratory (STL) located at Joint Base San Antonio, San Antonio, TX. Porcine eyes were exposed to 6 peak blast overpressure levels of approximately 35, 85, 115, 135, 155, and 230 kPa. The rabbits were exposed to 3 peak blast overpressure levels of approximately 55 kPa, 85 kPa, and 130 kPa.

All 85 porcine eyes were examined for damage, but 43 were excluded from the subsequent statistical analysis for a variety of reasons including avulsion from the orbit mimic during blast, placement of the orbit-mimic at a different depth within the shock tube's expansion cone (resulting in an unknown blast duration), improper maintenance of pre-blast IOP, and lack of pre-blast screening. The remaining 42 blast-exposed eyes, plus 13 controls, constituted the set of 55 eyes assigned grades of trauma. Commonly observed injuries included angle recession, internal scleral delamination, cyclodialysis, peripheral chorioretinal detachments and radial peripapillary retinal detachments. The most frequently observed injuries in all grades were angle recession and chorioretinal detachments. The most common tissues experiencing severe damage were the sclera (delaminations) and retina (detachments). Some control eyes also exhibited damage, usually involving the angle, choroid, and retina.

Corneal epithelial disruption was observed ubiquitously in exposed and control porcine eyes, and, thus, was not included in our analysis. Macroscopic injury of the iris occurred infrequently and no obvious examples of pupillary sphincter rupture were

observed in eyes lacking pupillary sphincter tone. Anterior segment uveal damage generally was restricted to the angle, where it was common. Anterior lens capsular damage also was not observed, but zonular dehiscence was noted along with some posterior capsular ectasia in multiple instances. Scleral ruptures were not observed.

Post-blast examination of 22 i*n vivo* rabbit eyes (17 exposed to blast, and 5 controls) revealed minimal trauma at the relatively low blast levels used in the experiments (55-130 kPa reflected pressure). Retinal edema observed in fundus images and OCT measurements of the retinal thickness was useful in confirming this qualitative finding. Corneal edema was observed using corneal confocal imaging, but no sphincter ruptures or retinal detachments were observed. The intraocular pressure also lowered in a dose-dependent manner 48 hours after blast exposure

2.2 Shock Tube

Blast exposure testing at the STL was accomplished using a 17-inch diameter compressed air driven shock tube (Figure 4). Blast overpressure was recorded using two pressure transducers to record reflected and side-on pressures. The pressure of most interest is that which results from interaction of the blast wave with a rigid surface such as the human body or eye. In blast-science terminology it is often referred to as the reflected pressure to differentiate it from the side-on pressure that an object experiences solely from the passage of a blast wave (similar to an elevated hydrostatic pressure). The reflected pressure is created by bringing the blast wave to rest at the surface (stagnation), then reflecting from the surface back toward the source (thus the name reflected pressure). For gases such as air, the reflected pressure and associated specific impulse are significantly higher than the side-on pressure and specific impulse. In blast injury studies it is the interaction of blast waves with tissue and bodily surfaces that are important, thus in the following discussion the term overpressure and specific impulse will refer to the reflected pressure and the reflected specific impulse, respectively.

The eye specimen and acrylic holder (orbit mimic) were placed within the expansion cone of the shock tube and isolated from the driver section by a series of thin (0.016 inch thick) aluminum disks. Pressurization of the driver section causes the disks to rupture, sending a pressure wave down the tube. Over the length of the tube the pressure front continually steepens, eventually forming a Friedlander-style shock wave before reaching the eye specimen (Figure 2). The peak pressure of the shock wave is controlled by the number of disks. Experiments have been performed using from 1 to 6 aluminum disks resulting in peak reflected pressures from approximately 48 kPa (7 psi) to 152 kPa (22 psi). Peak reflected pressures up to 241 kPa (35 psi) were achieved by moving the eye-orbit mimic further axially into the expansion cone, while peak reflected pressures as low as 21 kPa (3 psi) were achieved using a single 0.010-inch thick mylar disk. Experiments at a pressure levels lower than 21 kPa were conducted using a 0.007-inch thick mylar disk.

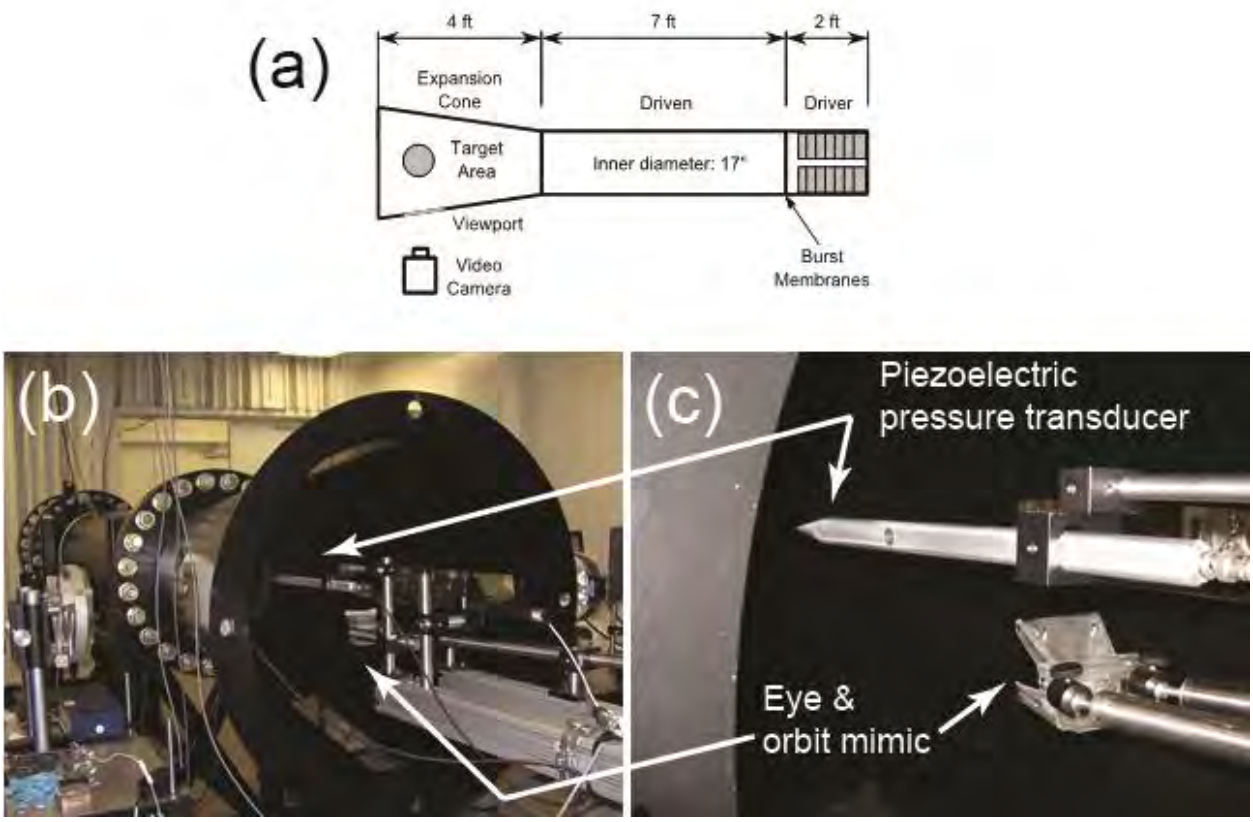

Figure 4. US Army Institute of Surgical Research shock tube showing location and orientation of eye and holder (orbit mimic) along with piezoelectric pressure transducer. A shock wave is created by pressurizing the driver section until the burst membranes ruptures. The target area lies within the expansion cone. Exposures of the pig eyes were recorded using an ultra-high speed video camera looking through an open viewport on the side of the expansion cone.

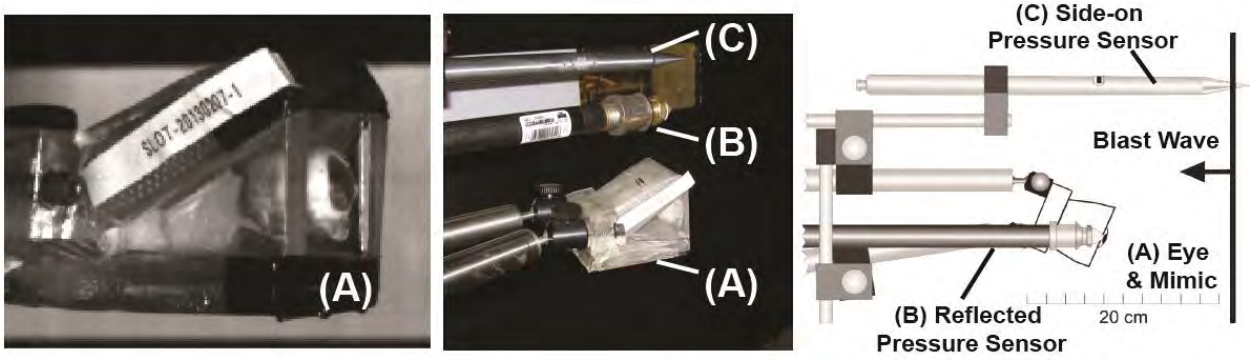

Figure 5. Arrangement of target and pressure sensors used to investigate physical effects of primary blast waves on the eye. A) Water-filled balloon (as substitute for eye) embedded in gelatin, and mounted in acrylic eye orbit mimic. B) Pressure sensor to measure reflected pressure. (Kulite XTL-190 pressure transducer) C) Pressure sensor to measure side-on pressure (PCB Piezoelectronics Model 137A23 ICP Blast Pressure Sensor).

Side-on pressure was recorded using piezoelectric pressure transducers (Model 137A23; PCB Piezotronics, Inc; Depew, New York). Reflected pressure was recorded with a Kulite pressure transducer (Model XTL-190; Kulite Semiconductor Products; Leonia, New Jersey) as shown in Figure 5. Both pressure probes were factory calibrated with appropriate certificates of conformance provided by the manufacturer. Pressure signals were recorded at 200,000 samples per second using a Synergy P Data Acquisition System (Hi-Techniques, Inc.; Madison, Wisconsin). The pulse duration of each experiment was taken as the point where the initially positive phase of the wave form reaches zero pressure, i.e., the negative phase of the waveform is ignored (Figure 2). The specific impulse is calculated by time-wise integration of the entire waveform. Lastly, each blast experiment was documented using high-speed videography at 15,000 frames/second using a Fastcam Ultima APX (Photron USA, Inc; San Diego, California).

2.3 Aluminum Burst Disk

Initial experiments were conducted using burst disk made from 0.016 inch thick 3003-H14 aluminum sheet supplied by McMaster-Carr of Chicago, Illinois. The material was purchased as rolls from which disks of approximately 20" diameter were cut for use in the shock tube. The 3003 alloy is not heat treatable but is supplied in a strain hardened condition achieved by cold working. The H14 designation indicates that the material received a ½ temper, i.e., reduction in hardness of approximately 50%. Reduction of hardness is undertaken to increase the alloys ductility and toughness. Single sheets burst at a pressure of 60 psig forming a series of roughly symmetric petals separating from the center of the disk (Figure 6a). This behavior created blast pressure time profiles that were consistent with the expected Friedlander waveform. Approximately 70 successful experiments were conducted with this batch of material.

However a later batch of material failed by tearing in a very nonsymmetrical pattern at approximately 20 psig, less than half the expected pressure (Figure 6b). This behavior produced a nonsymmetrical pressure-time profile that did not achieve the steep initial pressure rise associated with Friedlander waveforms. As this type of waveform was deemed unacceptable for blast testing, shock tube experiments were suspended pending resolution of the issue. In response to inquiries from ISR personnel, McMaster-Carr indicated that the aluminum supplier changed the processing procedure for the aluminum sheet in order to be in compliance with a recent change in material standards. However, they were unable to provide any insight as to why this affected the aluminum's burst behavior.

Further inquiries to metallurgist at Southwest Research Institute (SwRI) revealed that changes in cold working procedures can greatly affect material failure characteristics, especially if rolling directions and associated grain boundary orientations are altered. They indicated that failure behavior in cold worked materials is difficult to predict and control, and consistency difficult to maintain. Their recommendation was to pick a heat treatable alloy and experimentally recalibrate for the desired pressure and burst characteristics.

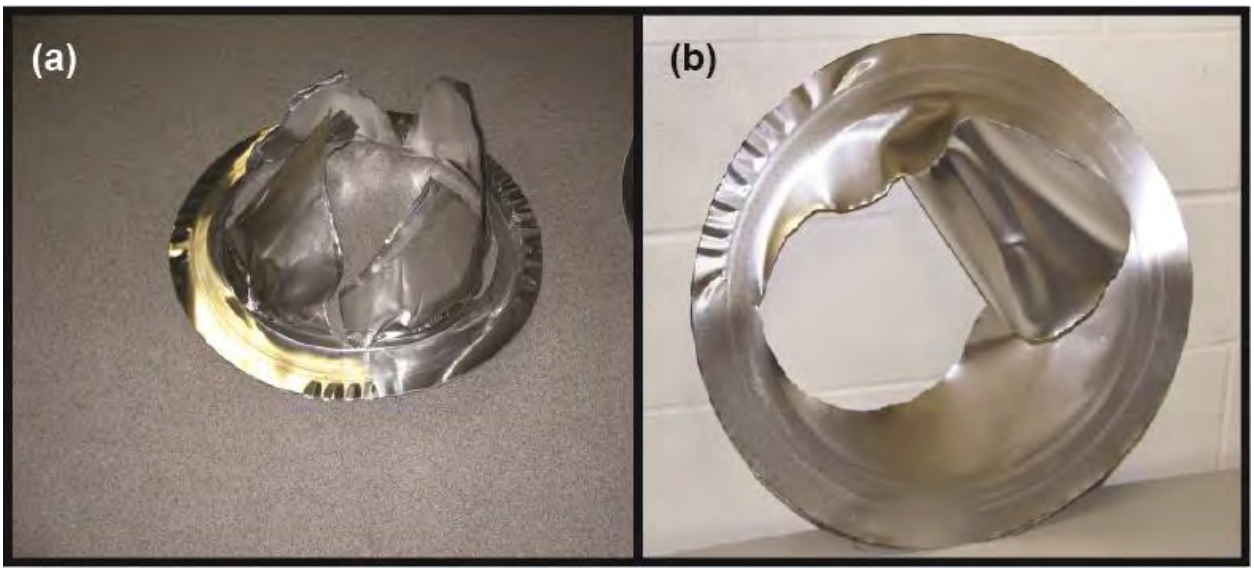

Figure 6. (a) The initial batch of 3003-H14 aluminum sheet burst at a pressure of 60 psig forming a series of roughly symmetric petals separating from the center of the disk. (b) A subsequent batch of aluminum sheet failed by tearing in a very nonsymmetrical pattern and at approximately 20 psig.

In support of the alternate aluminum alloy search, a series of LS-DYNA numerical simulations were undertaken. Based on recommendations from SwRI, our efforts focused on two alloys, 2024-T4 and 6061-T6. Each alloy was simulated in LS-DYNA using a preexisting non-linear material model (Material 24-piecewise linear plasticity), and a stress-strain curve to define the behavior of the material. Stress strain curves for the alloys were obtained from various internet sources (Figure 7a). Each simulation assumed that the burst disk was 20 inches in diameter, 0.016 inches thick and constrained all around its periphery. The disk was then loaded uniformly with by a slowly rising pressure (consistent with pressurization in the shock tube driver section) until failure occurred. Failure of the material was modeled by input of the alloys maximum plastic strain (Figure 8b). The LS-DYNA results suggested that alloy 6061-T6 would fail at driver pressures similar to those observed in previous successful tests.

Based on recommendations from SwRI, Applied Research Associates (ARA), and LS-DYNA simulation results, we procured sheets of 6061-T6 aluminum for further investigation. Preliminary testing revealed that scoring the aluminum disk (scratching a shallow groove in the metal) prior to pressure loading was an effective technique to control the initial failure mode and location when the disks burst. During experiments in the shock tube, we were able to consistently force the aluminum disks to split into two large clam-shell-like pieces, thus eliminating the fragmentation hazard. The initial burst pressure was reasonably consistent, allowing us to effectively control the test conditions. Further testing revealed that the new burst disk configuration produced consistent and acceptable Friedlander waveforms. As an added precaution, a fragment catcher screen was fabricated and installed inside the shock tube just downstream of the driver section.

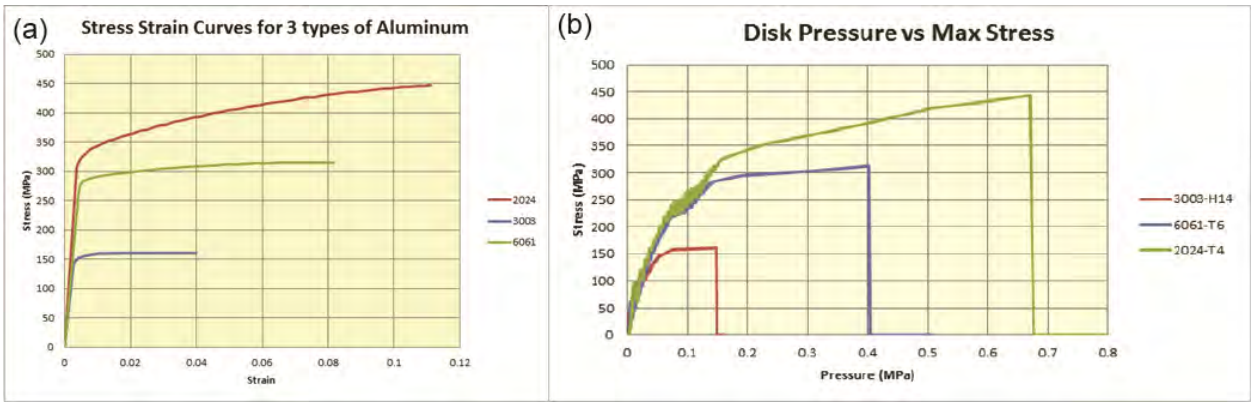

Figure 7. (a) Typical stress vs. strain curves for 3003, 2024, and 6061 aluminum alloys. (b) LS-DYNA predictions as to the failure stress and burst pressure for 3003-H14, 6061-T6, and 2024-T4 aluminum disks.

2.4 Porcine Eye Specimen Preparation

Enucleated porcine eyes, including eyelids and extraocular muscles, were purchased from Animal Technologies, Inc. (Tyler, Texas) and shipped overnight on wet ice. All animal tissues were handled in accordance with the ARVO Statement for the Use of Animals in Ophthalmic and Visual Research and protocols approved at each institution. The superior sclera was first marked using a surgical marker based on eyelid position to allow repeatable identification of locations on each eye. Skin, muscles, eyelids, and fatty tissues were removed to expose the surface of the globe, then placed in Hanks Balanced Salt Solution (HBSS; Fisher Scientific; Hampton, New Hampshire) and transported to the pathology laboratory.

Despite transfer on ice, the hydraulic conductivity of the scleral membrane and the necrotic state of the tissue, rendered the initial intraocular pressure (IOP) of the porcine eyes low. Evidence for this was the observed flaccid cornea, soft eyewall, and failed readings from our Tono-Pen VET (Dan Scott & Associates; Westerville, Ohio). It was often necessary to re-inflate the porcine eyes to a normal level (10-20 mmHg) with HBSS before scanning and blast testing. We found that injections at the pars plana increased the fluid content of the posterior chamber, allowing subsequent anterior chamber injections to maintain a normal IOP. At the pathology laboratory, each eye was re-inflated via pars plana injection of HBSS using a 30 gauge needle until the IOP was between 10-20 mmHg as determined by the Tono-Pen. B-scan (Compact Touch; Quantel Medical; Bozeman, Montana) and ultrasound biomicroscopy (UBM; OIS-100; i-Science Interventional; Menlo Park, CA) were used to assess the condition of each pressurized eye prior to blast exposure. B-scans were taken from 3 to 9 o'clock, 6 to 12 o'clock, and 9 to 3 o'clock axially and posterior near the optic nerve to visualize the anterior chamber. UBM was used to image each eye from pars plana, equator, and peripapillary regions from clock hours 12, 3, 6, and 9. Approximately 10% of received

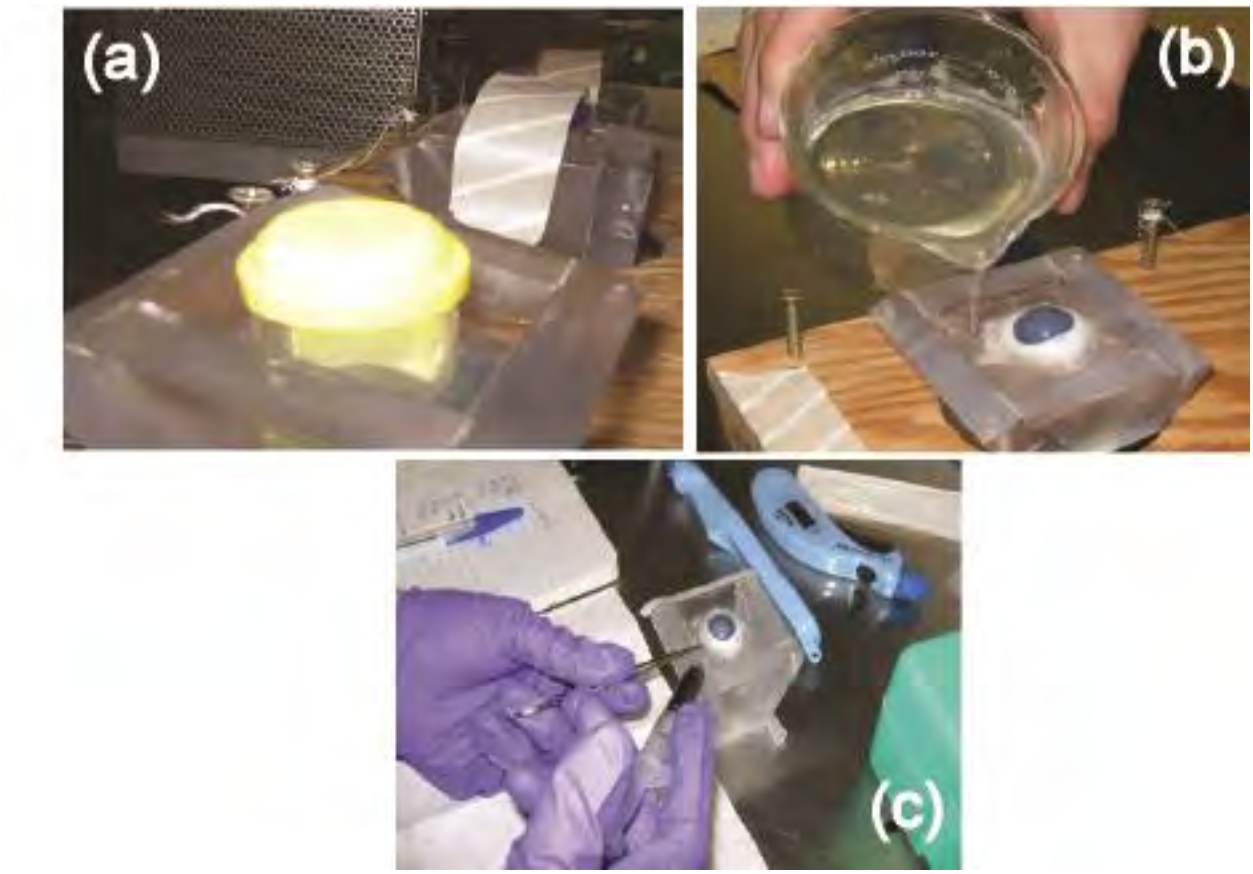

Figure 8. (a) Gelatin is preformed into acrylic holders that simulate the interior dimensions of the orbit. (b) Eyes are oriented and set within the preformed gelatin and sealed in place. (c) Just prior to blast testing, HBSS is injected in to the anterior chamber at the pars plana. The needle is inserted nearly parallel to the corneal surface in an attempt to provide for some degree of self-sealing once the intraocular pressure is raised.

eyes were excluded because the B-scan and UBM ultrasonic pre-screening demonstrated the presence of pre-existing damage to the eye.

After screening, eyes were stored refrigerated (4°C) overnight in HBSS then transported to the shock tube laboratory. Several acrylic orbital mimics were fabricated with internal dimensions and geometry similar to the orbital structure (Sponsel et al., 2011; Kennedy at al., 2007; Weaver et al., 2010). A plastic cup with spherical bottom (diameter roughly equivalent to the porcine globe) was placed in the center of the orbit mimic and the remaining internal volume filled with a 3.6 % liquid gelatin mixture (Knox Gelatin; Kraft Foods; New York, New York) which was cooled overnight prior to delivery of the eyes (Figure 8a). This 3.6% gelatin has been shown to provide nearly equivalent mechanical strength as the periorbita fat and surrounding tissues (Yoo et al., 2011).

Each eye was re-inflated via pars plana injection with HBSS, the plastic cup removed from the gelatin, and the re-inflated eye set in its place. Additional liquid gelatin was then poured around the eye filling the holder to the top (Figure 8b). The eye-orbit mimic

assembly was then refrigerated for approximately 30 minutes to fully set the gelatin. During refrigeration, each eye was covered with parafilm to prevent dehydration of the specimen.

Just prior to blast exposure HBSS was injected into the anterior chamber via a shallow angle through a 30-gauge needleport paracentesis tangential to the limbus in the peripheral cornea (Figure 8c). The eye–orbit mimic assembly was then photographed and placed into a rigid mount inside the shock tube. Once secured, the IOP was measured again and recorded. The eye-orbit mimic was tilted 20 degrees laterally to simulate the convergence of the human eye and placed 25 cm into the expansion cone of the shock tube. The test chamber was cleared, the driver section of the shock tube pressurized, and the blast test conducted.

For each day of testing, this procedure was repeated for several exposed eyes and one control eye. The control eye was treated in an identical fashion to the test eyes, i.e., placed into the expansion cone for several minutes but never subjected to an actual overpressure. After the test, IOP was measured and recorded; the eye-holder assembly was removed from the rigid mount, and another series of photographs taken. The eye specimen was then removed from the gelatin and placed into a HBSS-filled container. The containers were then transported in small plastic containers on ice to the pathology laboratory for blind post-test damage assessment.

Upon arrival at the pathology laboratory, another corneal HBSS injection was used to raise the IOP to between 10-20 mmHg through a 30-gauge needleport paracentesis tangential to the limbus. Trauma damage to each eye was then evaluated and documented using a combination of B-Scan and UBM ultrasound imaging along the meridians and directions examined previously. The specimens were then placed in formalin in preparation for detailed examination via manual dissection (in which the anterior surface was removed with a diamond knife) or histological analysis. Anterior chamber and optic nerve status were further assessed via stained paraffin sections of a subset of specimen eyes representing controls and blast-exposed eyes. Additional eyes were used in preliminary testing to develop the methods described above.

2.5 Porcine Eye Pathology

Using terminology consistent with the Ocular Trauma Classification Score (OTCS, Pieramici et al., 1997), the majority of ocular injuries resulting from blast exposure were found to be lamellar injuries. Probability of injury was found to increase with peak overpressure in Zone 1 (external surface; $p=0.024$) and Zone 3 (internal posterior segment; $p=0.023$) while no significant correlation was found in Zone 2 (interior anterior segment $p=0.6242$). Injuries included angle recession, cyclodialysis, peripheral chorioretinal detachments, radial peripapillary retinal detachments, and internal scleral delamination. No full-thickness openings of the eyewall (scleral rupture) were observed in any of the eyes tested. A summary of exposure information for the 55 eyes is provided in Appendix I. Any type or level of trauma observed in the subject area (i.e., angle, choroid, etc.) is reported in that category regardless of the severity. Peak

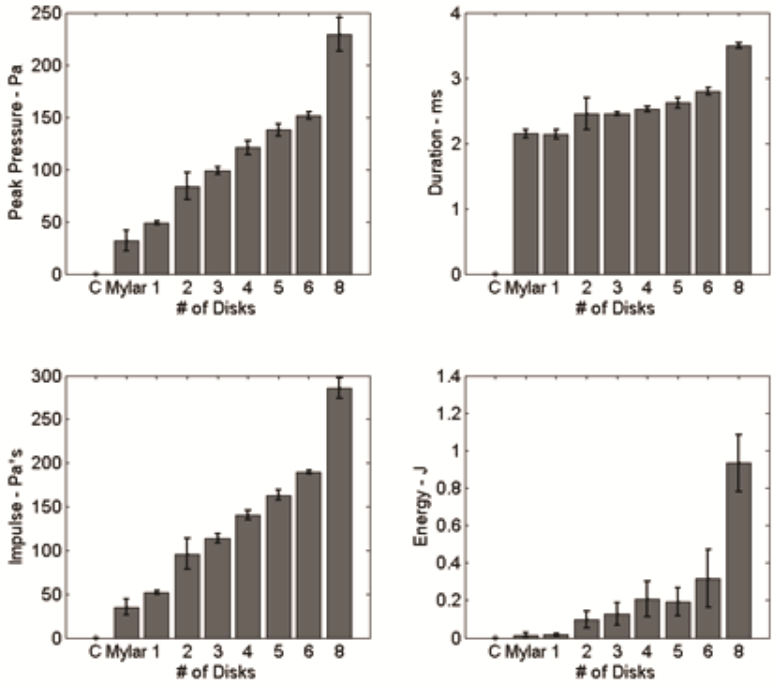

Figure 9. Histographic representation of the association of the number of mylar or aluminum disks secured between the pressure chamber and shock tube and peak pressure (upper left), duration (upper right), impulse (lower left), and energy (lower right)

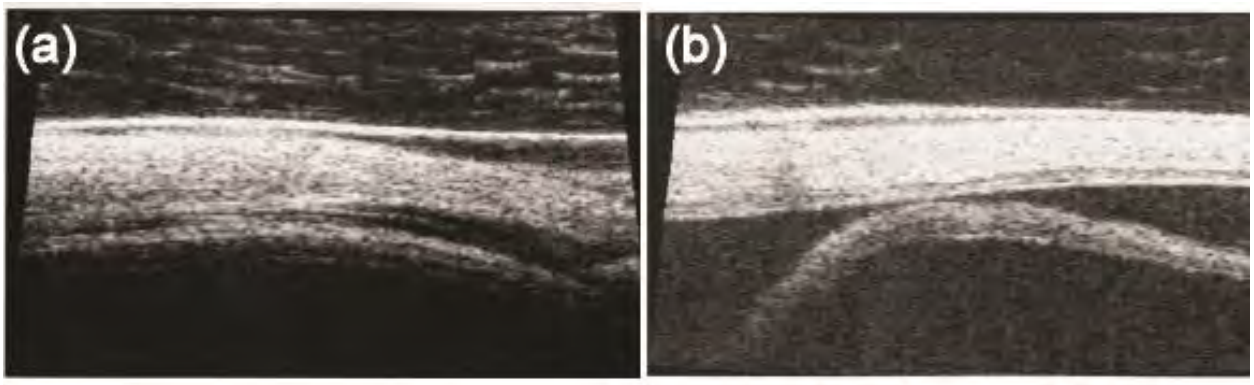

Figure 10. Scleral delamination and multiple chorioretinal detachments were observed before fixation using B-scan and UBM, and were confirmed through dissection and histopathology. Scleral delamination (a) following exposure to a 138 kPa (20 psi) blast, and extensive chorioretinal detachment and, (b) in eye exposed to a 113 kPa (16 psi) blast.

pressure was not independent of the duration of the positive phase: as the peak pressure increased, the duration increased as well (Figure 9), Corneal abrasion was ubiquitously observed in exposed eyes and so was not counted in the linear regression analysis. Macroscopic injury of the iris and anterior chamber occurred infrequently and was generally restricted to the angle. The increase in severity and occurrence of injury did not appear to be a deterministic event, but the results support the idea that certain ocular tissues are more sensitive to increases in blast energy than others. The retina appears to be the very sensitive to increasing blast energy. The sclera demonstrated the strongest associative tendency for increasing injury with increased overpressure (Figure 10). Remarkably, at very high levels of specific impulse (>300 Pa-s) the injury quotient for the sclera and the various other ocular tissues tested returned to control eye values (Figure 11). Angle injuries also showed a bell-curve response, with injuries beginning to appear at the 50 Pa-s level and tapering back to baseline at 200 Pa-s. There was no obvious impulse threshold value for the appearance of lower-grade injury to any ocular structure, but thresholds were in evidence for more extreme damage levels readily apparent for the optic nerve (~125 Pa-s), anterior chamber (~100 Pa-s), and sclera (~90 Pa-s). These injuries were cataloged into three zones in accordance with the Ocular Trauma Classification System (OCTS) for close globe mechanical injuries (Pieramici et al., 1997).

Pathology– Zone 1 (outer surfaces including sclera and cornea): Scleral delamination and multiple chorioretinal detachments were observed before fixation using B-scan and UBM, and were confirmed through dissection and histopathology. Figure 10a shows a chorioretinal delamination following exposure to 138 kPa (20 psi) blast. Figure 10b shows a detachment in an eye that was exposed to 113 kPa (16 psi) blast. These lamellar lacerations occurred in multiple meridians. UBM scans also showed significant chorioretinal disruption with probe oriented postero-anteriorly (Figure 12b) following exposure to 38 kPa (5.5 psi) blast and with the probe oriented equatorially (Figure 13a). One of the strengths of using UBM was the ability to place the probe in the same location before and after blast testing. Figure 13 shows three eyes exposed to three different peak pressures. Figure 13b shows an eye exposed to a peak pressure of 152 kPa, which caused significant delamination of the chorioretina. Figure 14c shows an eye that was exposed to a peak pressure of 134 kPa. Figure 13f shows an eye that was exposed to a peak pressure of 126 kPa, which caused the retina to detach and crumple.

Pathology– Zone 2 (anterior segment, posterior to cornea): Angle obliteration was observed via histopathology after the eye was exposed to peak overpressure of 113 kPa (16 psi; Figure 14). UBM was generally unable to resolve this injury. However, histopathology revealed the angle as a common location for injury, even for porcine eyes exposed to low peak overpressures.

Pathology– Zone 3 (posterior of the eye): Images of the optic nerve head (ONH) were taken during manual dissection and from histopathology (Figure 15). The ONH of the control eye was normal when viewed through the vitreous after removal of the

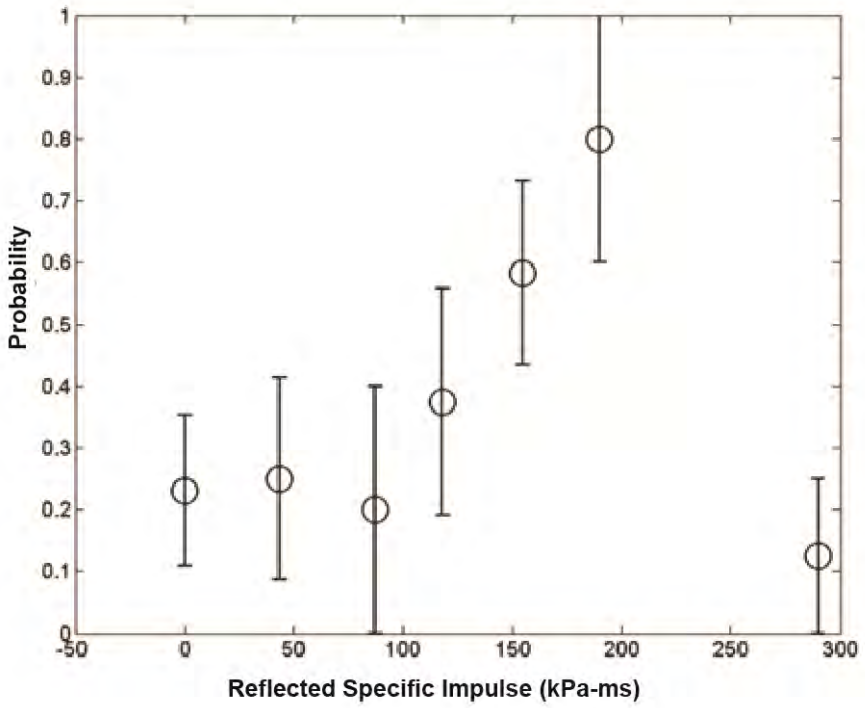

Figure 11. Histogram showing the probability of scleral injury for a given impulse level. Delamination accounted for nearly all observed scleral trauma. Note that the likelihood of injury increased to around 200 kPa (29 psi) above which the probability returned to that of the controls. While the exact mechanism underlying this observation is unknown, similar probability peaks have been observed in other ocular tissues within the present study. A numerical model of the blast may elucidate the underlying cause of this counterintuitive finding.

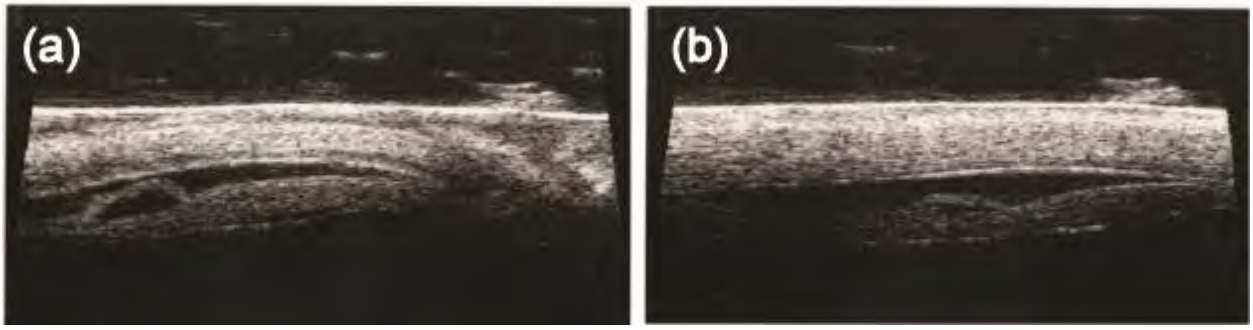

Figure 12. UBM shows significant chorioretinal disruption with probe oriented equatorially (a) and postero-anteriorly (b) following exposure to a 38 kPa (5.5 psi) blast.

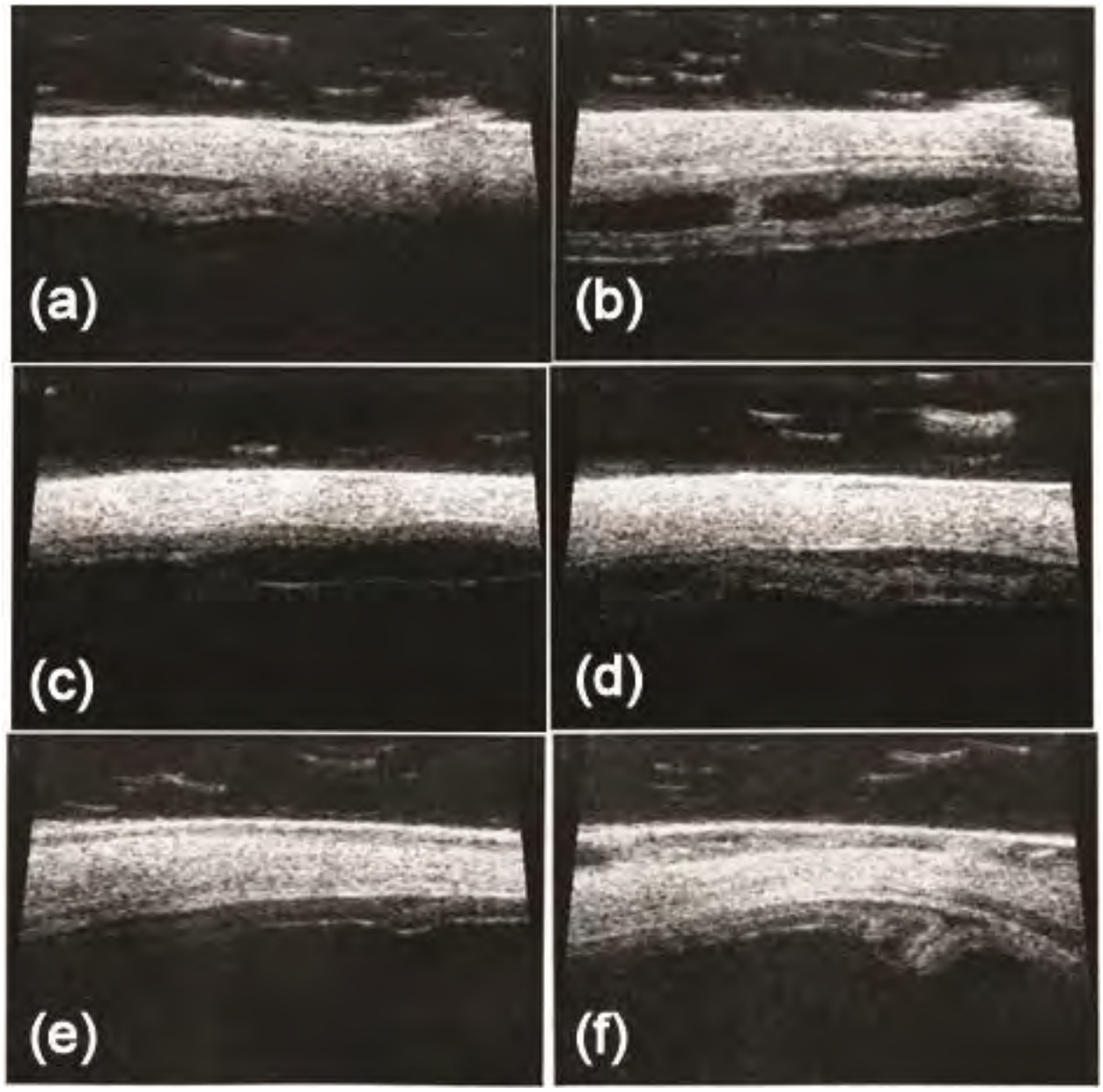

Figure 13. UBM scans of eyes exposed to three different peak reflected pressures showing typical delamination injuries observed after blast exposure. (a, b) severe delamination of the chorioretina after exposure to a peak reflected pressure of 152 kPa, (c, d) similar but less severe injury after exposure to a peak reflected pressure of 134 kPa, and (e, f) detachment and crumpling of retina after exposure to peak reflected pressure of 126 kPa.

anterior chamber. The ONH of an eye exposed to a 207 kPa (30 psi) blast showed retinal elevations coinciding with the location of blood vessels originating from ONH as viewed through the vitreous after removal of the anterior chamber. Examples of such

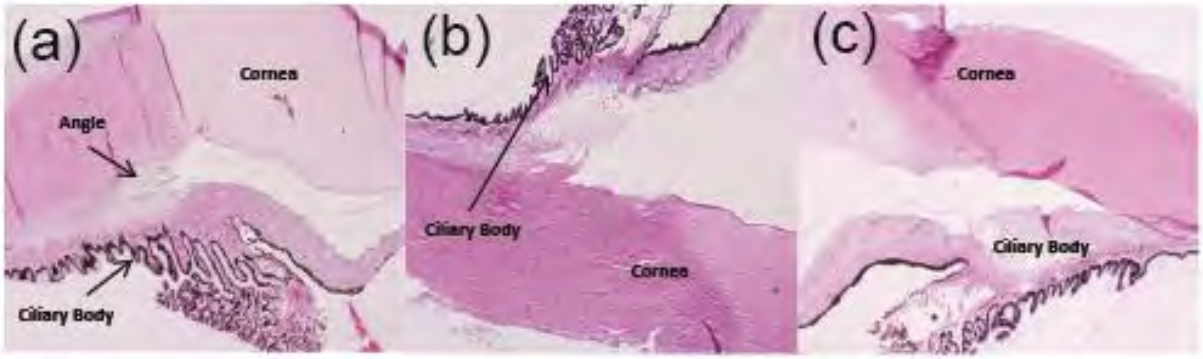

Figure 14. Histopathology of the porcine eye angle in (a) a control eye, and (b, c) eyes exposed to 113 kPa (16 psi) blasts. Both angle recession (b) and cyclodialysis (c) were observed. Significant damage to the angle was commonly observed even after low peak overpressure exposures.

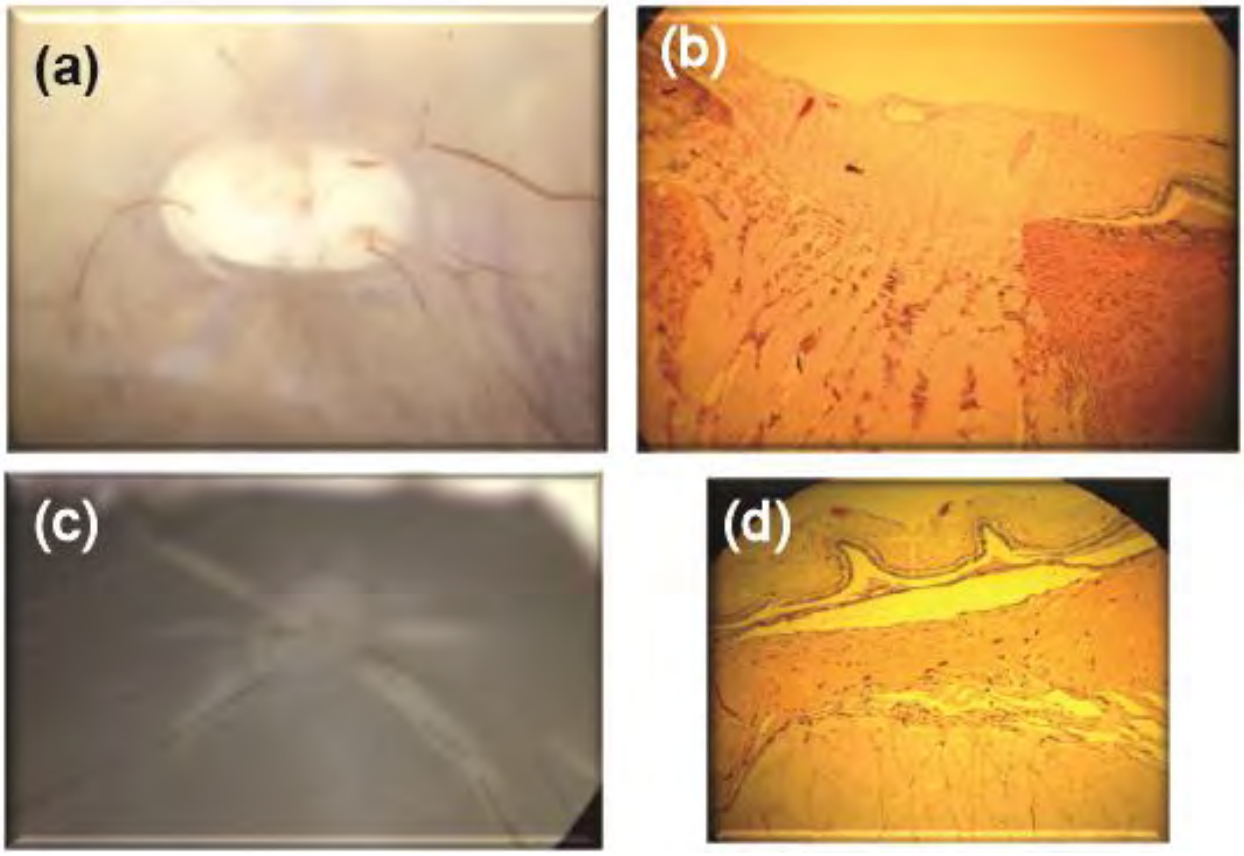

Figure 15. Images of the optic nerve head (ONH) taken during manual dissection (above) and from histopathology (below). (a) Control eye showing clear ONH as viewed through the vitreous after removal of the anterior chamber. (b) Eye exposed to 207 kPa (30 psi) blast shows retinal elevations coinciding with the location of blood vessels originating from ONH as viewed through the vitreous after removal of the anterior chamber. (c) Control eye section shows normal ONH and surrounding tissues. (d) Eye exposed to 126 kPa (18 psi) blast shows retinal folding in the immediate vicinity of blood vessels. Such injuries may be due to rapid oscillations in the tissue following blast exposure and may induce large strains in the region of density gradients such as at the blood vessel-retina interface.

Table 1. Injury Severity Grade

Injury Severity	Observation
Grade 0	No injury observed
Grade 1	One to two significant but mild pathologic defect(s) not present in the pre-impact images for the anatomic tissue/entity being scored
Grade 2	One moderate or One moderate and one mild or Three mild pathologic defects
Grade 3	One severe defect or Two to three moderate defects or Two moderate and any mild defects or Four or more mild pathologic defects
Grade 4	Two or more severe defects or One severe and any number of moderate defects or Four or more moderate defects or Three moderate and any number of additional mild defects

injuries may be due to rapid oscillations in the tissue following blast exposure (see Section 2.11 Numerical Models & Simulations). Such oscillations could induce large strains in regions with density gradients such as at the blood vessel-retina interface.

2.6 Injury Grades

Based on results of post-blast ultrasound, UBM, and histopathology, a surgical ophthalmologist from William E. Sponsel Associates evaluated each porcine eye (regardless of whether it was treated with overpressure or used as a control) for signs of trauma. The ophthalmologist noted the existence, type, and severity of internal or external damage. To ensure accuracy, the ophthalmologist was blind to the eye's exposure status and pre-blast condition. Levels of trauma were designated as none, mild, moderate, or severe for the ultrasound and histopathology data separately, then combined into injury grades on a scale of 0-4 (Table 1, Figure 16). Note that the assigned grade also contains injuries indicative of previous or lower grades, thus the grading scale is cumulative in nature.

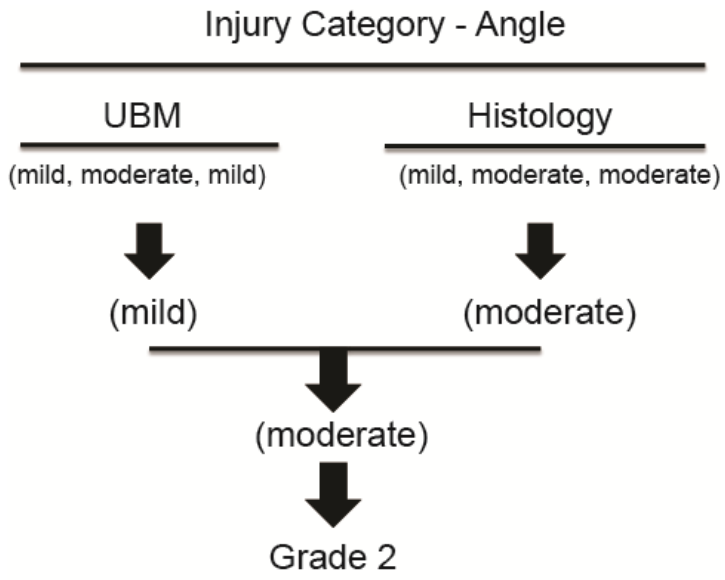

Figure 16. Illustration of combined injury grades from UBM and Histology Observations

Mild defect is defined as one affecting less than 1/16th of the maximal available area for injury of the tissue on the two-dimensional viewing plane. The moderate defect is one affecting from 1/16th to 1/8th of the available area for injury of the tissue on the two-dimensional viewing plane. Lastly, severe defect is one affecting more than 1/8th of the available maximal area for injury of the tissue on the two-dimensional viewing plane. Although the pathology was classified according to OTCS zones, some zones had fewer or greater kinds and severities of injury making it more appropriate to describe injury in terms of the tissue type or ocular structure. Thus the injury categories used for this study were (1) Angle, (2) Choroid (3) Optic Nerve Head, (4) Retina, and (5) Sclera.

2.7 Statistical Analysis of Porcine Eye Blast Data

While the data provided clear evidence of damage due to primary blast (with increased damage as pressure and impulse increased) statistically relevant damage was also observed in some control eyes. This finding leaded us to question whether the specimen preparation methodologies may have had some effect on the observed post-test damage. Thus, in order to more clearly identify specimen preparation effects, as well as place the blast trauma results in a clearer context, a detailed statistical analysis of the results was undertaken.

2.7.1 Statistical Methods

Ordinal Logistic Regression – Because the injury grade takes on values 0-4, the injury categories are *ordinal* data, as each category contains the previous categories. Common practice for injury risk assessment is to apply the log cumulative odds model. This model assumes that all slopes of the different response levels are equal and thus

estimates the individual intercepts for each response level with a common estimated slope. The odds model is:

$$\text{logit}[\,P(Y \le j)] = \ln\left(\frac{P(Y \le j)}{P(Y > J)}\right) = a_j + \beta x \qquad \text{for } j = 1,\ldots,J-1$$

where P is the probability, j is the individual injury grade (0-4), J is the number of injury grades (5), Y is the response, *a* is the respective intercept, and *β* is the respective slope. The slope (β) is also designated as the odds ratio. The odds ratio gives the percent chance of moving from one injury grade to the next with each additional unit of a given predictor.

Multinomial Logistic Regression- When it is inappropriate to apply the ordinal logistic regression, it is necessary to use multinomial logistic regression. Here the log odds are not cumulative. Instead evaluation with respect to a baseline or reference category, for example:

$$\text{logit}[\,P(Y = j)] = \ln\left(\frac{P(Y = j)}{P(Y = J)}\right) = a_j + \beta x \qquad \text{for } j = 1,\ldots,J-1$$

These models were run in JMP Pro 10® with the most relevant predictors selected using the stepwise ordinal logistic regression and the p-threshold option. The stepwise algorithm explicitly tests whether the selected model offers improved correlation relative to a reduced model with no effects (Whole Model test). Once the algorithm ceases to enter or remove predictors, simple ordinal logistic regression was performed on only the relevant predictors. Lack of fit (of the relevant predictors) was then evaluated using both the Wald Effects Test and Likelihood Ratio Test. These tests determine which relevant predictors in the model were statistically significant, i.e., β is different from zero. The test statistic for the Wald Test is simply:

$$Z^* = \frac{b_k}{s\{b_k\}}$$

Where b_k is the estimated slope and $s\{b_k\}$ is the standard deviation. The test statistic for the Likelihood Ratio Test *G* is:

$$G = \sqrt{-2\ln\left[\frac{L(R)}{L(F)}\right]}$$

where L(R) is the likelihood function for the reduced model and L(F) is the likelihood function for the fitted model. Small ratios of L(R)/L(F) (i.e. large values of G2) lead to rejection of the null hypothesis.

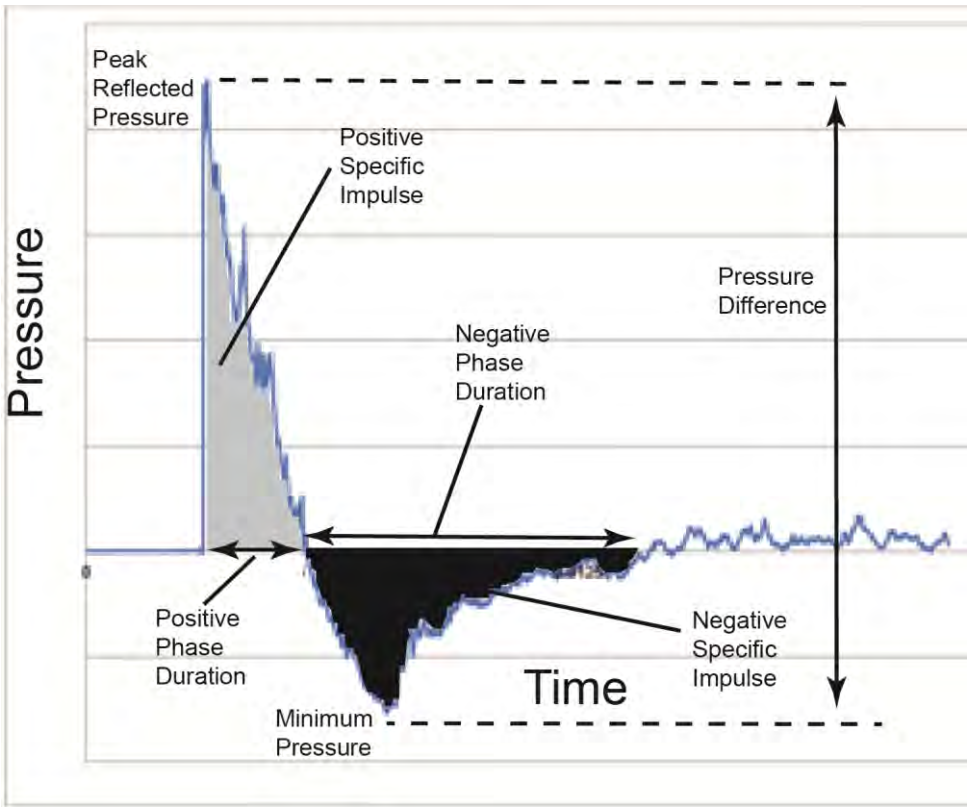

Figure 17. Blast parameters defined by the reflected Friedlander waveform.

2.7.2 Statistical Results

Logistic regression was performed on pathology and injury grade data associated with the injury categories choroid, retina, optic nerve head, angle, and sclera. The predictors selected for correlation analysis came from two distinct groups; (1) blast parameters, and (2) preparation parameters. The blast parameters were defined by the reflected Friedlander waveform and include peak reflected pressure, positive specific impulse, positive phase duration, negative specific impulse, minimum pressure (peak of the negative phase), and pressure difference, i.e., difference between peak reflected pressure and minimum pressure (see Figure 17 for explanation). Preparation parameters included mass of the eye, induced IOP, and pre-IOP. Induced IOP is the pressure recorded after HBSS injection and just prior to setting the eye in the orbit mimic and gelatin. Mass of the eye is the as-received porcine eye mass plus the injected HBSS. Lastly, the pre-IOP is the pressure recorded after loading into the shock and just prior to the blast event.

Stepwise ordinal regression with a p-value threshold stopping rule and parallel/proportional odds assumption was performed using JMP Pro 10® to identify the most relevant predictors (blast or preparation parameters) for each injury category. To appropriately measure the level of significance for the implicated predictors, the Bonferroni Correction was applied. Thus, the nominal significance threshold (α=0.05)

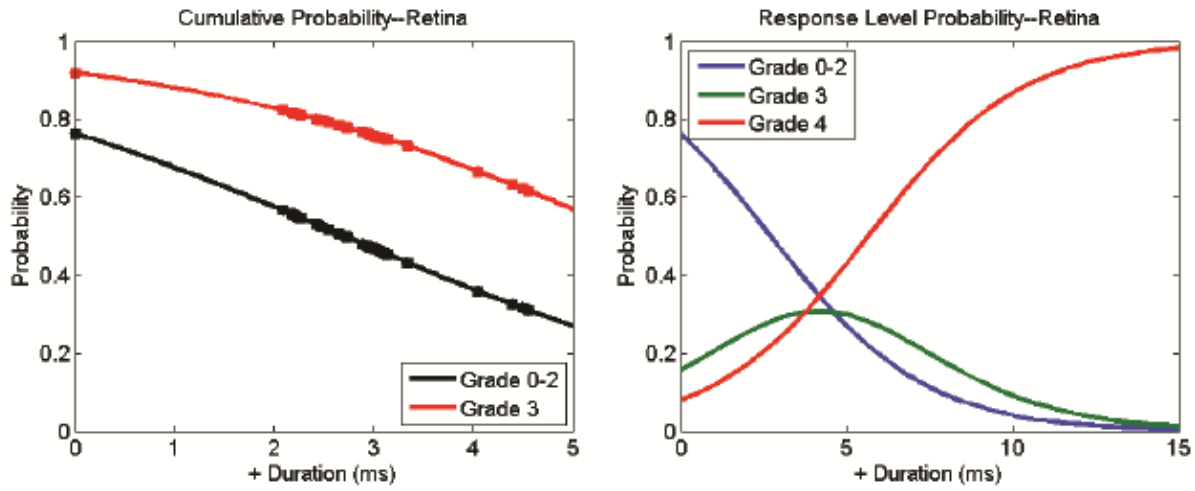

Figure 18. Cumulative probability and response level probability for the retina.

was divided by the total number of predictors to give an adjusted threshold (α = 0.0125). This new alpha was used as the threshold for significance. The predictors selected as relevant where then subjected to simple ordinal logistic regression with Wald and Likelihood Ratio tests used to assess significance of correlations through calculated p-values.

Retina - Only positive phase duration was identified as being significant. The measure of lack of fit returned a large chi-squared value (5.735) and the whole model is significant (p=0.0166). Simple ordinal logistic regression for this single parameter showed p=0.0197 for the Wald Test and p= 0.0166 for the Likelihood Ratio Test, revealing that positive pulse duration is correlated with damage incidence in the retina. The p-values for the intercepts cumulative Grades 2 & 3 is significant, but not for cumulative Grades 0 & 1. As the positive duration of the shock-wave increases, the probability of incurring a Grade 3 reaches a maximal value and then attenuates. The probability of incurring a Grade 4 injury approaches 1, and the probability of incurring a Grade 2 or less approaches zero as the duration increases (Figure 18).

Optic Nerve Head – Again only positive phase duration was identified as being significant. The measure of Lack of Fit has a large chi-squared value (3.183) and the whole model is nearly significant (p=0.0744). Simple ordinal logistic regression was then performed for this parameter with the Wald and Likelihood Ratio Tests returning p values of 0.0834, and 0.0744, respectively. The result suggests that positive phase duration is only weakly correlated with damage incidence in the optic nerve head. The p-values indicated that the intercept for the collapsed Grades 1 & 2 is significant, but Grade 0 is not. As the duration of the positive phase of the shock increases, the probability of incurring a “Grade 3 & 4” injury approaches “1” and the probability of incurring no injury approaches zero (Figure 19).

Choroid- Four blast parameters were identified as relevant, positive phase duration, positive impulse, negative phase duration, and pressure difference. The measured lack

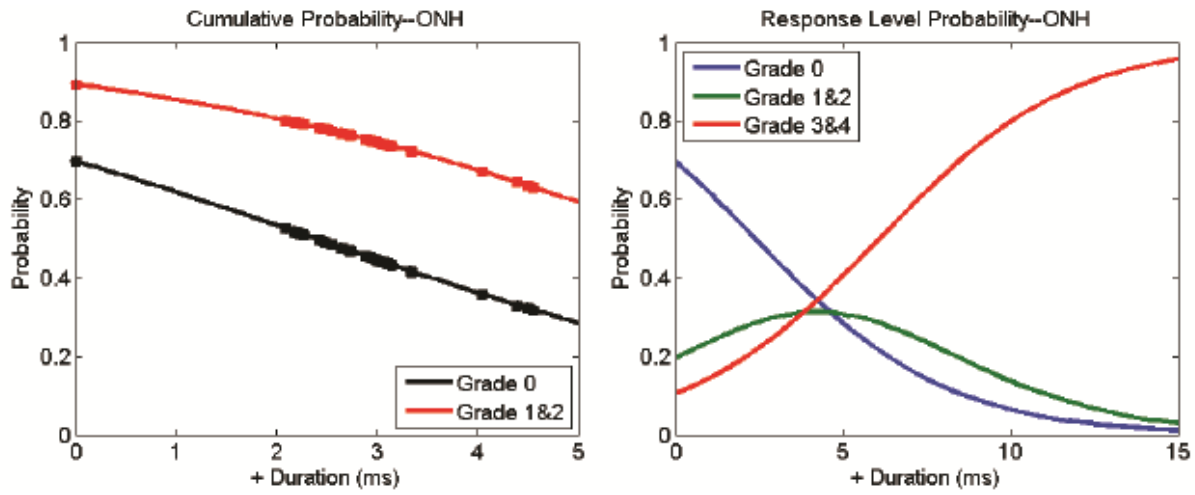

Figure 19. Cumulative probability and response level probability for the optic nerve head.

of fit has a large chi-squared value (9.614) and the whole model is significant (p=0.0475). Simple ordinal logistic regression was then performed for these four parameters. The Wald Test results indicate that only the pressure difference is correlated with damage incidence (p=.0449), but the Likelihood Ratio Test indicates pressure difference, positive impulse, and negative duration as being significant (p=0.0285; p=0.0371; p=0.0371, respectively). The p-values for the cumulative grades 2 & 3 are significant, but not grades 0 and 1.

Angle – JMP Pro 10® identified mass of the eye, induced IOP, pre-IOP, and negative pulse duration as relevant, but additional analysis using SAS® revealed that the parallel odds assumption required for ordinal logistic regression was violated. Thus, multinomial logistic regression was applied, followed by simple ordinal logistic regression. The Likelihood Ratio Test returned the following p-values; negative pulse duration p=0.1667, pre-IOP p=0.2542, eye mass p=0.0782, and induced IOP p=0.0299. Thus, for the angle only induced IOP is significant.

Sclera - JMP Pro 10® identified mass of the eye, induced IOP, positive phase duration, and negative phase pressure as relevant, but again SAS® revealed that the parallel odds assumption was violated. Thus, multinomial logistic regression was applied, followed by simple ordinal logistic regression. The Likelihood Ratio Test revealed that only the mass of the eye is significant (p=0.0275).

Results of the statistical analysis support the conclusions of Sherwood et al. (2014) that primary blast overpressure can cause damage to *ex vivo* porcine eyes exposed 48 hours post mortem. The small p-values for the chi-square test indicate that the observed frequencies for blast-treated eyes are significantly different from control eyes not subjected to the blast environment (Table 2). The results further suggest that different ocular tissues and structures are sensitive to different aspects of the primary blast wave. For example, the choroid appears to be sensitive only to the pressure difference,

Table 2. Grade Frequencies for both Blast-exposed and Control Porcine Eyes

Injury Category	Blast-exposed Eyes Grade Frequencies %					Control Eyes Grade Frequencies %				
	4	3	2	1	0	4	3	2	1	0
Choroid	14.3	31	28.6	11.9	14.3	7.7	15.4	23.1	15.4	38.5
Retina	23.8	28.6	16.7	14.3	16.7	7.7	15.4	23.1	7.7	46.2
Angle	40.5		45.2		16.2	23.1		38.5		38.5
Optic Nerve Head	23.8		30.9		48.6	15.4		15.4		69.2
Sclera	23.8		21.4		51.4	23.1		7.7		69.2

Note: It was necessary to collapse grades 3&4, and grades 1&2 for angle, optic nerve head, and retina because several frequencies were less than one.

positive impulse, and negative duration of the blast wave, whereas the retina and optic nerve head only show sensitivity to the positive phase duration. In contrast, the angle and sclera appear to be sensitive only to preparation parameters, i.e., the induced IOP and mass of the eye, respectively. In all cases, however, the individual tissue p-values were larger than the adjusted significance level of 0.0125. Thus one may conclude that the correlations at present are imprecise, and will require additional testing to obtain a large enough data set to clearly define the exact tissue response-blast wave relationships.

Nonetheless, all of the injury categories were associated with a blast parameter to some degree. The most significant was the positive phase of the blast in association with the retina. The predicted probabilities (Figure 18) show that the probability of observing Grade 4 damage reaches 100% at approximately 15 ms of blast duration. Although not as significant, the positive impulse, positive duration, negative duration, and pressure difference of the primary blast were associated with the severity of injury for the choroid. The presence of minimum negative phase pressure and pressure difference is intriguing, because minimal pressure and overall pressure difference are generally discounted in the literature as a source of significant injury. Previously, only Duke-Elder (1954) speculated that the negative phase may be associated with ocular injuries.

2.7.3 Effect of Porcine Specimen Preparation

As data accumulated over the duration of the project, it has become increasingly evident that some factors other than blast were inducing injury artifacts, as evidenced by a number of false positive injuries in control eyes. For example, internal scleral delamination and mild angle recession was observed in approximately 20% of control eyes. It was hypothesized that such false positives may be due to several factors,

namely (1) handling of the eyes during harvesting at the abattoir or during shipment, (2) preparation factors such as repeated saline injections as the eye is cyclically re-inflated prior to imaging, placement in gelatin (induced IOP), and blast testing (pre-IOP), (3) osmotic-induced damage due to exposing the eye to gelatin and refrigeration, and (4) natural decay of the eye due to biological processes post mortem. Our concern was that significant changes in the eye may occur due to any one of these factors.

As outlined above, the statistical results suggest that the angle and sclera are sensitive to preparation, namely induced IOP for the angle and mass of the eye for the sclera. However, these two parameters are not truly independent, as injection of HBSS to maintain proper IOP elevates the eye's mass. Because of periodic readjustment of the IOP, it is likely that incidental over-inflation contributed to some of the angle recession and scleral delamination damage observed (in the absence of blast exposure).

Adjustment of the IOP (induced IOP and pre-IOP) was often necessary because of its relatively quick decrease to a minimum value. Although the exact cause was unknown, we hypothesized that it was not a blast accelerated phenomena, but due to post-mortem elevated hydraulic conductivity, allowing rapid seepage of internal fluid through the scleral wall into the gelatin. To estimate the hydraulic conductivity (K) of the porcine eyes, the time (t) between pre- and post-blast IOP measurements was averaged for each test day and a MATLAB® script written to find the coefficients of a linear hydraulic conductivity model. The decay of pressure (IOP) with time was taken as:

$$P(t) = P_0 e^{-(t/u)}$$

then a least squares approach used to estimate values for the initial IOP (P_0) *and time constant (u).* The values of the measured IOP of both the control and blast-exposed eyes were compared using a two-sample, homoscedastic t-test assuming that the measurements were normally distributed and that the variances were equal.

The times and the IOP were recorded for 11 eyes exposed to blast and 2 eyes not exposed to blast. The t-test indicated that the null-hypothesis could not be rejected, thus there was no difference between the decline in IOP over time between the blasted and non-blasted eyes for P_0 ($p=0.4248$) or u ($p=0.5909$). The fitted line of the average of all 13 runs (solid black line) and the average of the actual data values (solid black circles) is shown in Figure 20. The curve illustrates that in approximately 4 minutes the porcine eye lost 63% of its IOP, independent of blast exposure. This elevated hydraulic conductivity is probably indicative of the state of decay. Unfortunately for proper mechanical response, IOP levels must be maintained at a physiologically relevant state at time of blast exposure. We also found during preliminary testing that failing to re-inflate the eye prior to blasting resulted in much more extensive damage than that observed in eyes with physiological IOP values.

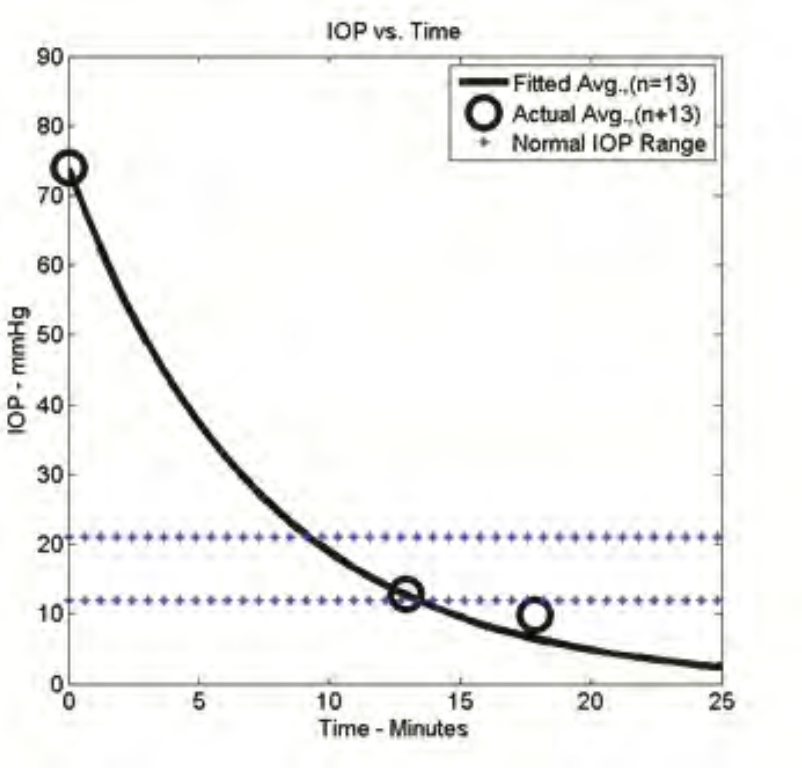

Figure 20. Plot showing IOP decline with time.

In a second control study, six enucleated porcine eyes were delivered, prepared, and pre-screened as normal, but not exposed to blast. Two eyes each were treated as follows:

1. Refrigerated in HBSS to detect natural degradation of the tissue with time and whether the handling of the eye while removing the muscles/eyelids might induce artifacts,
2. Mounted in gelatin as normal to determine whether any temperature/osmotic interactions between the gelatin and coats of the eye might be inducing artifacts, and
3. Injected several times with BSS to determine whether we were causing damage to the eye during the injection process.

After treatment, each eye was again subjected to B-scan ultrasound and UBM scans, and any change from its pre-treatment condition noted. Only exposure to gelatin (method 2) resulted in observed changes to the eye; primarily delamination-type injuries consistent with what might be observed due to thermal strain or osmotic shock. This suggests that exposure to gelatin might also contribute to scleral delamination injuries.

Unfortunately, due to limited funds, a study of the effect of age and post-mortem decay was not possible. The exact age of each eye was not available, but Animal Technologies typically harvests eyes from pigs whose ages vary from 6 months to two

years. Eyes are enucleated and shipped overnight on wet ice. All blast testing and ultrasound screenings were completed with 48 hours of enucleation. Although our testing times were well within those quoted by previous researchers, it is hard to imagine that post-mortem decay was not a factor, as evidenced by the suggested elevated hydraulic conductivity. Even post-mortem decay in control eyes was problematic. Effects of decay could potentially be mitigated by fixatives, but we found that placing control eyes in formalin prior to the post-ultrasound examination introduced artifacts in nearly every control eye.

An additional series of experiments was undertaken to determine whether the ex vivo porcine eye model is mechanically representative of the in vivo human eye. Specifically, blunt impact loading of porcine eyes potted in 3.6% and 10% gelatin was used to evaluate the dynamic response of the eye model. Additional mechanical testing of the gelatin was used to determine whether 3.6% or 10% gelatin more closely approximated the dynamic mechanical properties of human periorbital tissues. This study indicated that the elastic modulus of the 3.6% gelatin very closely matched that of human orbital fat as determined by Yoo et al. (2011), whereas the modulus of the 10% gelatin used by other groups was higher by a factor of five. High-speed videos of blunt impact testing also indicated that the porcine eyes mounted in 3.6% gelatin experienced large posterior translation into the gelatin as is commonly reported in facial injuries, whereas the eyes embedded in 10% gelatin experienced virtually no posterior translation. This indicates the 10% gelatin may alter the damage mechanisms in the ex vivo porcine eye model by mechanically supporting the eye in an artifactual manner.

2.8 Trauma Data Analysis and Modeling

2.8.1 Tissue Specific Trauma Risk Functions

Trauma risk functions estimate the probability of injury occurrence given some value of predictor variable, in this case the reflected specific impulse of the positive blast phase and Cumulative Injury Scale Score (CIS, Sherwood et al., 2014). To determine the probability of achieving a certain CIS damage level a logistic regression was performed for each tissue using the porcine experimental and pathology data shown in Appendix I. A binary data set for each tissue and CIS Score was generated whereby a positive pathology observation at the CIS Score of interest is taken to indicate a probability of 1 and CIS Score less than the score of interest, is taken to indicate a probability of 0 (Collett, 2003). A logistic transformation and regression was then performed on the porcine trauma data and the resulting coefficients input to the general form of the logistic risk function (Proud et al., 2009):

$$p = \frac{1}{1 + e^{-(ax+b)}}$$

where p is the probability of occurrence of the particular injury or CIS category, x is the blast reflected specific impulse, and a and b are the regression parameters. Following

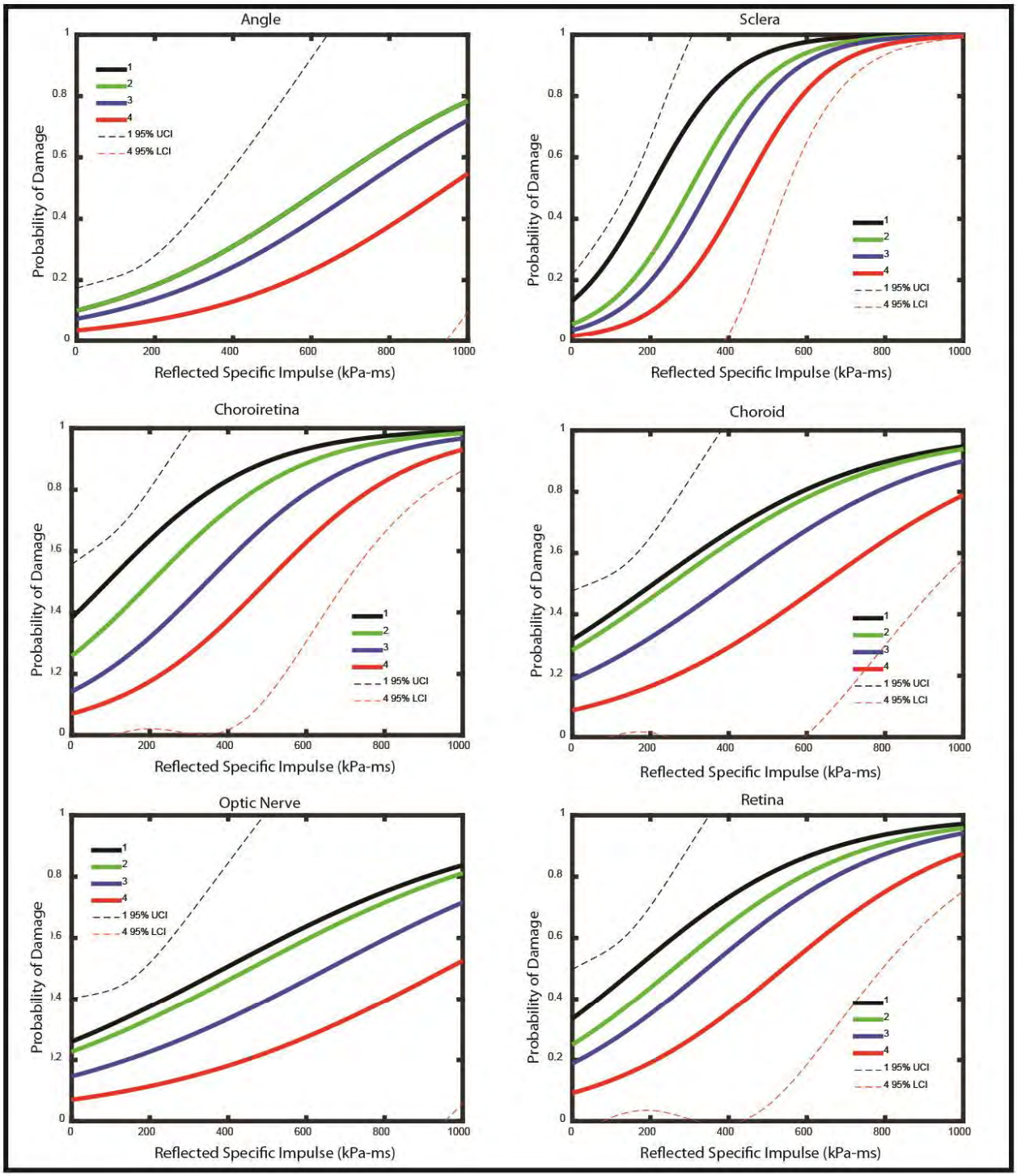

Figure 21. Tissue-specific risk vs. reflected specific impulse. The curves estimate (for each type of ocular tissue) the probability of suffering a CIS score-level damage condition (1 to 4) when the eye is subjected to a blast wave of known reflected specific impulse value. To prevent clutter, only the upper 95% confidence limit for CIS Level 1 (black dashed line), and the lower 95% confidence limit for CIS Level 4 (red dashed line) are shown.

this method, probabilities of occurrence were calculated for each of the injury categories with individual responses plotted versus reflected specific impulse (Figure 21).

It should be noted that corneal abrasion, angle recession, and retinal detachment were observed in the vast majority of porcine post-test specimens and a significant number of control specimens, suggesting that these may be artifacts of the handling or pathology procedures. The logistic regression accounts for such artifacts as an offset in the probability (i.e. the probability of incurring a retinal detachment is non-zero even in the absence of blast exposure). Development of trauma risk functions was further hampered by the generally infrequent tissue damage observed in the shock tube experiments. The maximum reflected peak pressure achievable in the shock tube's current configuration is approximately 221 kPa (32 psi) and ~2 ms pulse width. At this shock condition, ocular tissue damage was less frequent than anticipated. This may also be due to the use of porcine rather than human eyes, as porcine eyes are known to have a higher mechanical toughness than their human counterparts. Thus, uncertainty in the risk curves is due to several factors:

1. Potential presence of artifacts leading to false positives,
2. Non-zero incidence of tissue damage at null blast exposure (owing to #1), and
3. Non-unity incidence of tissue damage at the highest levels of blast exposure.

The ideal case for logistic regression is a dataset with a level of the independent variable at which all responses are negative and a higher level at which all responses are positive. Due to artifacts and the limited blast parameter space available during these experiments, neither of these conditions was met and we are left with quantifiable uncertainty in the predictions (indicated in the curves using 95% confidence intervals). To prevent unnecessary clutter in Figure 21, only the upper 95% confidence limit for CIS Level 1 (black dashed line), and the lower 95% confidence limit for CIS Level 4 (red dashed line) are shown.

2.8.2 Ocular Incapacitation Model

Our objective was to develop a numerical model of overall visual incapacitation based on tissue-specific injury scores. Additional military and clinical input will be needed to map this incapacitation score to a metric for mission readiness, but the model can predict acute or chronic concerns. Here, three categories of acute injuries affecting battlefield readiness were considered:

A. Optical integrity
B. Neurophysiological integrity
C. Structural integrity

Optical Integrity-This category summarizes the optical effects influencing the eye's ability to transmit focused light onto the retina. Factors contributing to optical integrity are transparency of the ocular media, integrity of the accommodative apparatus, and integrity of pupil function. Media transparency would be affected by glare, abrasions/

lacerations/ punctures of the cornea, cataract, and/or vitreous hemorrhage /detachment. Damage to the ciliary muscle, ciliary body, zonules, lens capsule, lens, or vitreous could influence the eye's ability to accommodate. Damage to the ciliary body or iris would affect pupil function. In addition, accommodation and pupil function could be limited by damage to the eye's nervous system blocking either the photoreceptive response or motor signals to the relevant muscles. Thus, damage to the optic nerve could influence the eye's optical integrity. For the purposes of this model, only the motor signals were considered to influence the optical integrity since photoreception is captured under the neurophysiological functionality category.

Neurophysiological Integrity- This category summarizes the neural and other effects influencing the eye's ability to transduce light and/or transmit the resulting information to the brain. Measures of functionality could include retinal blood flow and metabolism, chorioretinal detachment or other damage, optic nerve integrity, and changes to the intraocular pressure.

Structural Integrity-This category summarizes the ability of the eye to maintain its shape, maintain proximity of tissues, and resist further insults. The shape of the eye plays into its optical integrity and proximity of tissues is essential for proper electrophysiological functionality. Furthermore, since we are interested only in acute effects, the eye's ability to mechanically resist further insults is largely irrelevant. This category will therefore be neglected in assessing the potential for acute visual incapacitation. However, in general, damage to the cornea or sclera could compromise the eye's mechanical resilience. Such damage might include delamination, laceration, or puncture-type injuries.

Each of the aforementioned categories must be assigned an incapacitation score (*I)* between zero (fully functional) and one (fully incapacitated). Note that a functionality score *F=1-I*, where one is fully functional and zero is fully incapacitated, could also be chosen for convenience. For each of the three categories, the extreme scores may be interpreted as follows:

A. Optical Integrity
    a. I_A=0 → Clear cornea, lens, and vitreous, fully functional pupil and accommodative apparatus
    b. I_A=1 → No light transmitted to the retina

B. Neurophysiological Functionality
    a. I_B=0 → All light reaching the retina is transduced and transmitted to the brain with high fidelity
    b. I_B=1 → No information from the eye reaches the brain

C. Structural Integrity
    a. I_C=0 → Globe is fully intact
    b. I_C=1 → Globe is ruptured

Thus, an eye which has a perfectly intact retina and optic nerve may still be completely incapacitated if its optical media are opaque or the globe is ruptured. The simplest mathematical model capturing these features has the form:

$$I = 1 - (1 - I_A)(1 - I_B)(1 - I_C)$$

where I_A is the optical integrity incapacitation score, I_B is the neurophysiological functionality incapacitation score, and I_C is the structural integrity incapacitation score. This form gives an overall incapacitation I of zero if $I_A=I_B=I_C=0$ and one if any of I_A, I_B, *or* I_C are one. In the context of the present study, these scores must be estimated based on technical and clinical input which attempts to synthesize information from both the *ex vivo* porcine eye study and *in vivo* rabbit eye study. In both cases, relevant information has been compiled on a tissue-specific basis. Incapacitation within each category ultimately depends on the extent of relevant damage to tissues contributing to that category. The porcine eye study results were tabulated in terms of the Cumulative Injury Scale (CIS) which was developed to account for long-term health effects. Integer CIS scores from 0-4 were assigned to each tissue based on whether the eye would spontaneously recover, require surgical intervention or be un-repairable. The rabbit study was conducted with acute injuries in mind with continuous variations in biometric responses recorded.

The simplest possible model for generating a category incapacitation score based on tissue-specific incapacitation t_i is:

$$I_j = 1 - \prod_i (1 - t_i)$$

This mapping may be used to distinguish between acute and chronic effects. For example, cold cataract may completely blind a person in a cold environment but will resolve itself upon return to warmer temperatures. Cold cataract would be assigned a CIS score of one since it would self-resolve. This is but one example of how the CIS scoring algorithm may not directly translate to estimating the incapacitation of a given tissue. However, for simplicity, the first estimate of tissue incapacitation scores will be calculated as:

$$t_i = \frac{CIS_i}{4},$$

since 4 is the maximum score on the CIS scale.

Risk curves generated via ordinal logistic regression allow an estimate of risk of a given trauma level for a given tissue subjected to a given set of blast parameters. While the data considered herein pertain strictly to ocular tissues, the methods proposed are sufficiently general that they are readily extended to any organ or system. The primary goal may be stated as: given a vector $\boldsymbol{X}$ which parametrically describes the insult,

estimate the risk ***r*** of a given tissue achieving one or more grades of traumatic injury *t*. Note that, for a given ***X***, the risk may be a scalar *r* if only a binary trauma response is considered but it may also be a vector ***r*** if multiple injury grades are allowed. In other words, the risk analysis must return ***r(X)*** for each tissue under consideration based on trauma grade data ***t(X)***.

If *t* is a binary response variable, then this may be achieved using logistic regression regardless of the number of parameters included in ***X***. However, if *t* is instead an ordinal response variable (i.e. it can take on integer values whose magnitude indicates the severity of trauma), then multinomial ordinal logistic regression must be employed. In the latter case, ***r*** must be estimated for each ***X*** and for each possible value of *t*. An increase in *t* indicates an increased severity of trauma. Thus, a multinomial ordinal logistic regression must be undertaken to estimate ***r(X)***. Based on the analysis of Bowen et al. (1968), for short durations, primary blast-induced injuries generally correlate with the specific overpressure impulse *i* more closely than the maximum overpressure P_{max} or duration of the positive phase t_+ of the blast. Therefore, a single predictor variable *i* is expected to predict the risk at each CIS grade such that the output of the model is ***r(i)***.

In the previous section, we attempted to predict the probability of a given tissue requiring surgical intervention to reverse a primary blast-induced injury. Here, we undertake another preliminary analysis attempting to predict the likelihood of achieving a given CIS score in each tissue for a given blast using ordinal multinomial regression. This statistical method allows the construction of a predictive injury model using the blast wave measurements and CIS scores for each tissue as inputs. Multiple blast wave characteristics may then be used to predict whether a given tissue will be damaged to the extent corresponding to a given CIS score rather than simply a binary response. The proportional odds model without interaction between blast parameters is given by:

$$\text{logit}\left[P(Y=j)\right] = \ln\left[\frac{P(Y\le j)}{P(Y>j)}\right] = a_j + \sum_j b_i x_i$$

where P(Y>j) is the probability of achieving a CIS injury score Y greater than j; a_j is the offset probability for CIS score j; b_i is the slope corresponding to a unit change in the logit due to an increase in the blast parameter x_i. Both a_j and b_i are regression coefficients which determine the model's predictions. For example, the Bowen Curves are an example of multinomial regression with a binary response. In the case of the Bowen Curves, x_1 was the duration of the positive blast phase and x_2 was the peak overpressure. Thus far, we have performed ordinal multinomial regression using only a single predictive blast parameter (the specific impulse of the positive phase).

Bowen et al. (1968) postulated that the risk of mortality due to primary blast must depend on a scaled overpressure *P*. In this case the overpressure is the pressure that results from interaction of the blast wave with a rigid surface such as the human body or

eye, i.e., the reflected pressure. Thus in the following discussion the term overpressure will refer specifically to the reflected pressure.

The scaled overpressure P is related to the scaled duration of the positive blast phase T, given by:

$$P = P^*\left(1 + aT^{-b}\right)$$

where P^*, a, and b are fitting parameters. These fitting parameters should be estimated for each tissue. In particular, P* is the pressure producing a given biological response at very high durations (i.e. the long-duration asymptotic pressure value for a given level of risk). Note that, in the present study, only short durations were examined. In this case, the above equation may be approximated as:

$$PT^b = P^* a$$

where PT^b is the scaled reflected specific impulse if b=1. Scaled values of P may be computed based on the raw values for reflected overpressure P_r as:

$$P = P_r \frac{14.7\ psi}{P_0}$$

where P_0 is the ambient pressure. Scaled duration T may be estimated for a given target mass m_J relative to human target mass m_H and positive phase duration t_+ as:

$$T = t_+ \left(\frac{m_H}{m_T}\right)^{1/3} \left(\frac{P_0}{14.7\ psi}\right)^{1/2}$$

Note that in Bowen's analysis, the masses were for the entire body. However, in this case, these masses should be of the eye rather than the animal as a whole. No mass scaling was used due to the similarity in the mass of the porcine eye (mean mass 8.15 g prior to inflation) relative to the human eye (reported mass about 7.5 g) – the quantity $(m_H/m_T)^{1/3}$=0.973. No pressure scaling was used due to the close proximity of the experimental laboratory to sea level (about 650 feet above sea level; i.e. P_0 ~14.7 psi). Thus, P=P_r and T=t_+. In practice, the fitting parameters would be estimated using the following algorithm for each tissue in turn:

1. Guess P^*, a, and b
2. Compute risk curves based on scaled overpressure P as described in the preceding section
3. Compute a goodness-of-fit metric for this parameter set
4. Repeat steps 1-3 until P^*, a, and b until the goodness-of-fit metric is optimal

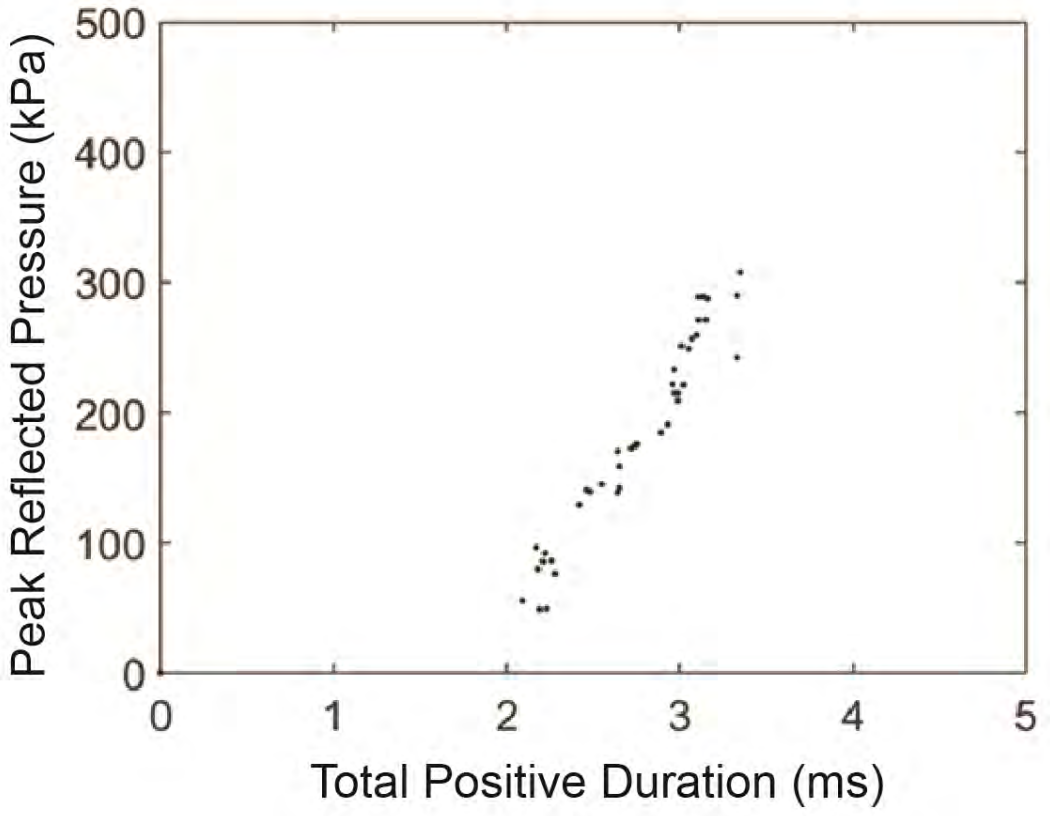

Figure 22. Experimental space of the SLOT experiments.

5. Determine whether the optimal model indicates statistical correlation between *P* and tissue CIS scores

For the present data, the peak overpressure and positive phase duration were highly correlated (Figure 22). This colinearity implies that only one variable is truly independent. Reflected specific impulse was found to have a higher correlation coefficient with the CIS scores than any other characteristic describing the shock experiments. Therefore, risk curves were computed with respect to the reflected specific impulse.

Risk curves generated via ordinal logistic regression allow an estimate of risk of a given trauma level for a given tissue subjected to a given set of blast parameters. The Incapacitation Model allows an estimation of overall visual incapacitation for a set of tissue trauma scores. Some integration of these two mathematical constructs is necessary to enable an estimate of expected incapacitation for a given set of blast parameters.

Table 3. Reflected Specific Impulse (kPa-ms) Corresponding to 50% Risk of CIS Score

	CIS Score			
	1	**2**	**3**	**4**
Angle	629.2	629.2	726.4	945.3
Anterior Chamber	844.1	915.2	1256.6	1506.0
Choroid	208.1	252.7	399.8	640.3
Chorioretina	92.7	203.8	346.2	498.5
Cornea	N/A	N/A	N/A	N/A
Iris	N/A	N/A	N/A	N/A
Lamina Cribosa	N/A	N/A	N/A	N/A
Lens	N/A	N/A	N/A	N/A
Optic Nerve	389.8	456.8	655.9	961.2
Retina	162.0	259.2	344.6	539.9
Sclera	201.4	302.5	350.8	438.4

The simplest method for this integration is to assume the most literal meaning of *expected incapacitation* by computing the effective dose corresponding to 50% risk (ED_{50}) based on the ordinal risk curves for each CIS score level (1, 2, 3, and 4). The assigned tissue score was then one fourth of the highest CIS score for which the reflected specific impulse exceeds the ED_{50}. Then, the soldier incapacitation was calculated as an absolute incapacitation score.

Example: For a blast with specific impulse of 100 kPa-ms, risk curve analysis indicates that the risk vector for the cornea is $\boldsymbol{r}$ = [85% 60% 35% 5%] for CIS = [1 2 3 4]. The vector for the sclera is $\boldsymbol{r}$ = [75% 45% 10% 0%]. From these risk vectors, the most likely CIS score for the cornea is CIS_{cornea}=2 and for the sclera is CIS_{sclera}=1 (i.e. these are the highest CIS scores having a probability of at least 50%). If these are the only two tissues which contribute, and assuming that the incapacitation I of Category C (structural integrity) is well modeled as:

$$I_C = 1 - \prod_i \left(1 - \frac{CIS_i}{4}\right)$$

then the incapacitation I_C would be computed as:

$$I_C = 1 - \left(1 - \frac{2}{4}\right)\left(1 - \frac{1}{4}\right) = 1 - 0.357 = 0.625$$

The probability of suffering a given CIS score-level of damage was correlated with the reflected specific impulse using multinomial ordinal logistic regression. Although some tissues were scored inconsistently and could not be used to reliably estimate risk curves, sufficient data were available to generate meaningful CIS risk estimates for the

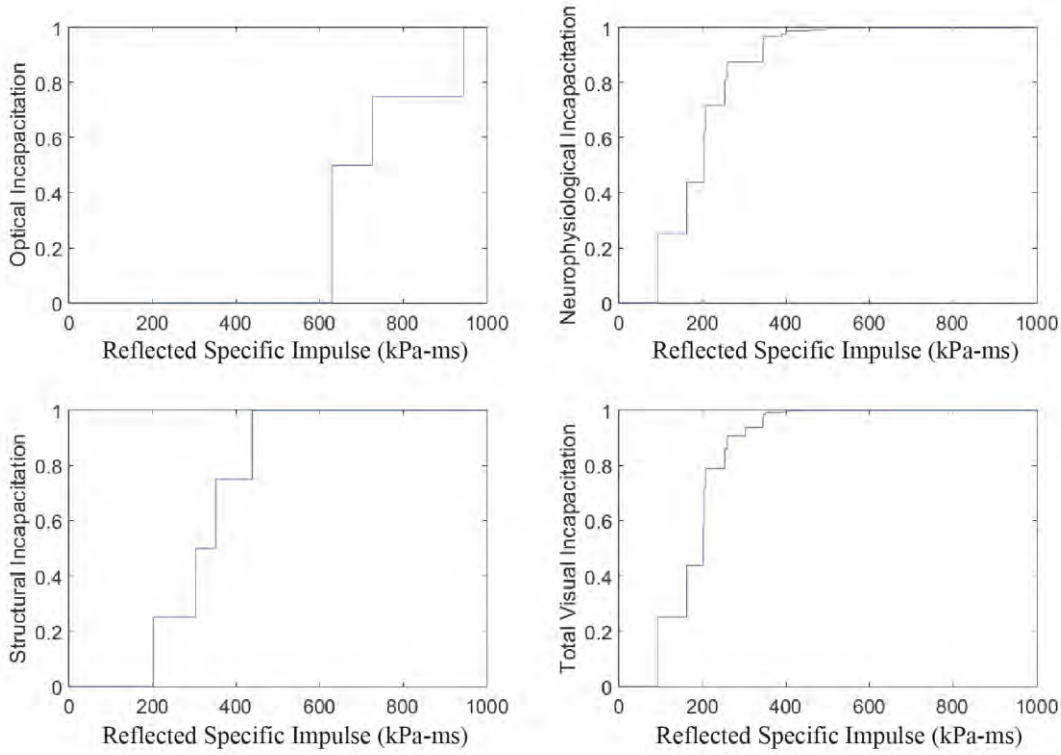

Figure 23. Likelihood of incapacitation vs. reflected specific impulse. In this model likelihood is where 50% of personnel would experience more severe incapacitation and 50% would experience less. For example the structural incapacitation plot predicts that at a specific impulse of 400 kPa-ms, 50% of exposed personnel will experience a structural incapacitation of 75%.

angle, anterior chamber, choroid, chorioretina, optic nerve, retina, and sclera (Figure 21). Using the risk curves the reflected specific impulse corresponding to a 50% probability of achieving a CIS score (ED_{50}) was then computed for each tissue (Table 3). These specific impulse values can be thought of as minimum or critical values for which 50% of personnel would experience more severe incapacitation than the CIS score, and 50% would experience less. This 50% risk criteria is referred to herein as risk likelihood. However, because the specific impulse is scenario dependent (varying with the amount of explosive or weapon type and distance from detonation point) the data presented in Table 3 cannot be used without prior knowledge of the blast characteristics. However, it does provide a baseline from which to compare different blast scenarios if explosive yield can be estimated.

2.8.3 Incapacitation Risk Curves

A simplified predictive model for soldier ocular incapacitation risk was developed by combining tissue risk data into the three broad ocular integrity categories outlined in Section 2.8.3, i.e., (1) optical integrity, (2) neurophysiological integrity, and (3) structural

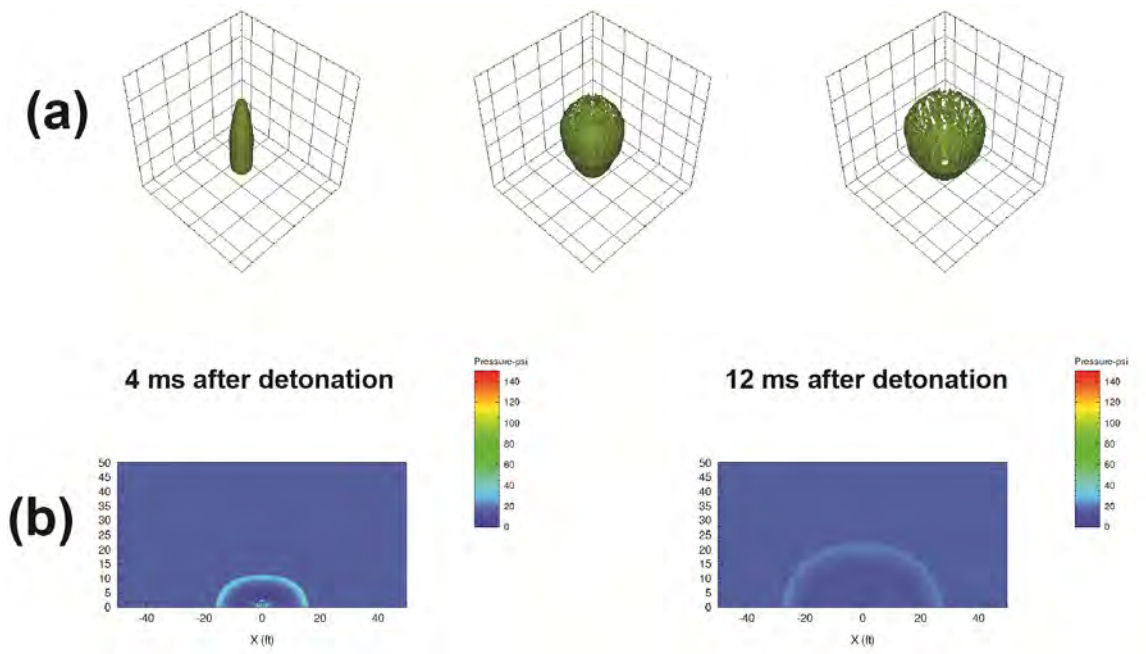

Figure 24. (a) CTH simulation of detonation and fragmentation of a standard US M107 155mm artillery projectile. (b) CTH prediction of side-on pressure and propagation of blast wave 4 ms and 12 ms after detonation.

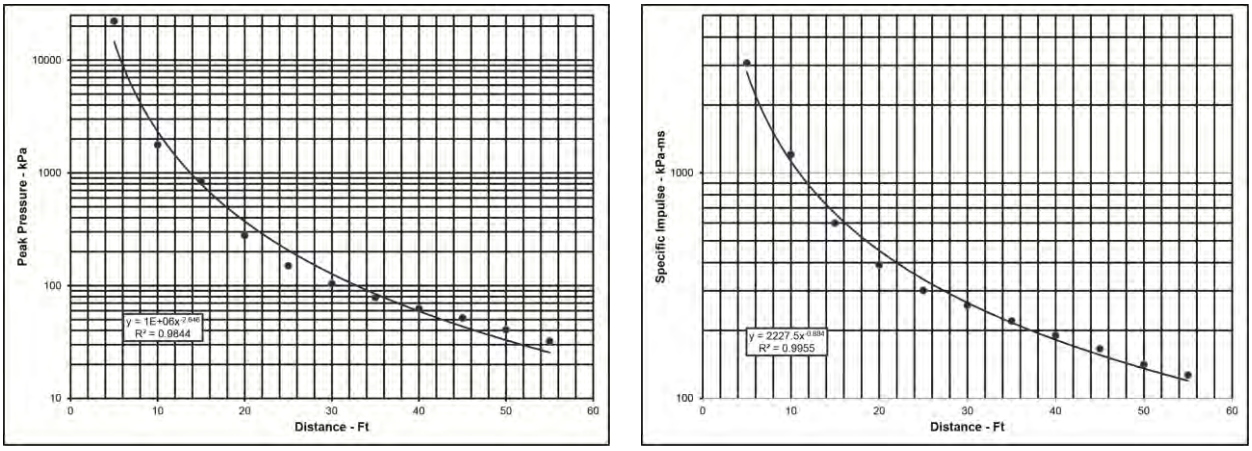

Figure 25. Estimated reflected peak pressure and reflected specific impulse vs. distance.

integrity. The model is based largely on the ex vivo porcine eye experiments and, as above, plotted versus reflected specific impulse (Figure 23).

Unfortunately without knowledge of the blast characteristics, the incapacitation model results may appear vague and difficult to use by most observers. Thus to place

Table 4. Distance from 155mm Projectile Detonation Point (ft) Corresponding to 50% Risk of CIS Score

	CIS Score			
	1	**2**	**3**	**4**
Angle	15.6	15.6	14.0	11.5
Anterior Chamber	12.5	11.7	9.2	8.1
Choroid	36.0	31.1	22.0	15.4
Chorioretina	66.3	36.6	24.5	18.6
Cornea	N/A	N/A	N/A	N/A
Iris	N/A	N/A	N/A	N/A
Lamina Cribosa	N/A	N/A	N/A	N/A
Lens	N/A	N/A	N/A	N/A
Optic Nerve	22.4	19.9	15.1	11.3
Retina	43.5	30.5	24.6	17.5
Sclera	36.9	27.1	24.3	20.5

the results in a more recognizable context a commonly encountered blast scenario is analyzed and the associated incapacitation model predictions outlined. For this illustrative example we have chosen to simulate blast characteristics from the detonation of a standard US M107 155mm artillery projectile. The M107 projectile is very similar to a Soviet 152mm artillery projectile. Large stock piles of these projectiles remained after the US invasion of Iraq and Afghanistan and were used as improvised explosive devices (IEDs) against American soldiers and Marines. Geometrical data for the Soviet 152mm metal shell was not available, so the 155mm projectile was analyzed instead.

Computational code CTH was used to simulate the detonation and blast wave propagation of the 155mm artillery projectile (Figure 24). CTH predicted the side-on pressure vs. time at 5 foot intervals radially outward from the detonation point. Reflected pressure vs. time was then estimated using Sach's scaling (for CTH to calculate reflected pressure directly, rigid surfaces must be placed in the simulation which would unrealistically alter the downstream blast wave characteristics). The estimated reflected peak pressures and specific impulses as a function of distance from the detonation point are shown in Figure 25. Distances were then correlated with ED_{50} specific impulses and the modeling results recast in terms of ocular injury likelihood as a function of distance away from the IED detonation point (Table 4, Figure 26). Using the model, and knowing the weapon involved in the blast (and associated blast wave characteristics), one can now estimate the probability of ocular injury at any radial distance from the detonation point. For example, the model predicts that at a distance of 40 feet from the detonation point of a 155 mm projectile half of exposed personnel will experience 45% total ocular incapacitation (Figure 26).

These controlled prospective masked-evaluation studies on abattoir-fresh porcine eyes have provided clear evidence of a direct graded pathologic response to primary

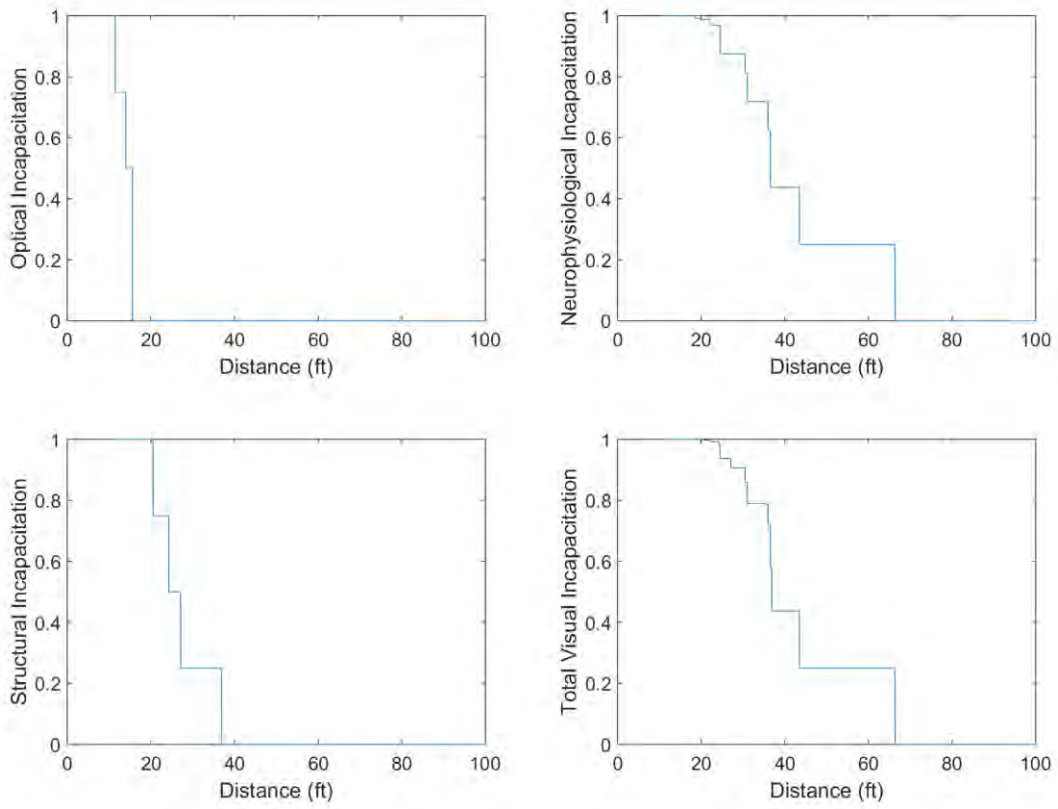

Figure 26. Likelihood of incapacitation vs. distance from 155mm projectile detonation point. In this model likelihood is where 50% of personnel would experience more severe incapacitation and 50% would experience less. For example the total visual incapacitation plot predicts that at a distance of 40 feet from the detonation, half of exposed personnel will experience a total visual incapacitation of 45%.

blast. It is also clear that the ocular injuries sustained would produce visual incapacitation in a high proportion of survivable blast exposures. The results from the 155mm artillery projectile simulation illustrates this nicely. Nearly three-quarters of eyes within 40 feet and around 90% within 30 feet of the explosive device would most likely sustain ocular neurophysiologic incapacitation. Applying the total body Bowen curves (Bowen et al., 1968) to the overpressures used in these studies we would anticipate an approximate 70% survival rate to individuals exposed at this distance interval. Even as far as 65 feet away, with a nearly 100% likelihood of survival from the primary blast insult, nearly a quarter of individuals would suffer ocular neurophysiologic incapacitation. The proportion of these incapacitating injuries that would be transient rather than permanent may be inferred from the related histograms for *visual ncapacitation* and *structural incapacitation*. It may be reasonably assumed that structural damage is generally permanent and would have lifelong visual health implications for the victim. It is thus particularly noteworthy that the preponderance of damage sustained within 40 feet involves such structural incapacitation.

Table 5. In-Vivo Rabbit Blast Test Procedural Sequence

Day	Procedural Sequence
1	**Baseline characterization** Anesthetize Analgesic Imaging: Direct ophthalmoscope, Slit Lamp, Fundus photography, OCT (retinal), HRT Corneal Conformal, Ultrasound (UBM, B-scan) Aqueous Draw Blood Draw Recovery
2	**Blast exposure** Anesthetize Analgesic Ear plug installation Place rabbit in holder IOP Blast exposure IOP Imaging: Direct ophthalmoscope, Slit Lamp, Fundus photography, OCT (retinal), HRT Corneal Conformal, Ultrasound (UBM, B-scan) Anesthetize with isoflurane if required Aqueous Draw Blood Draw Recovery
3	**24 hours post-blast exposure** Anesthetize Aqueous Draw Blood Draw Recovery
4	**48 hours post-blast exposure** Anesthetize Imaging: HRT Corneal Conformal, Other imaging as required Aqueous Draw Blood Draw Euthanize: Harvest eyes, optic nerve, and brain

2.9 *In Vivo* Rabbit Blast Experiments

The *in vivo* rabbit blast experiments were conducted in accordance with Animal Use Protocol A-14-007, approved by ISR IUCAC and the USAMRMC Animal Care and Use Review Office (ACURO). The objectives of this series of experiments were to (1) identify and characterize *in vivo* blast-induced trauma using a series of standard clinically-available imaging techniques, and (2) to collect blood and aqueous samples for use in the biomarker study. Validation of the procedures was accomplished by SLOT team members and the ISR Staff Veterinarian by trial experiments on 3 Dutch-belted rabbits procured from RSI Robinson Services, Inc. (Mocksville, NC) for that purpose. During the trials minor modifications to the protocol were required (again approved by ISR IUCAC and ACURO) to facilitate ease and repeatability of sampling and post-test ophthalmic

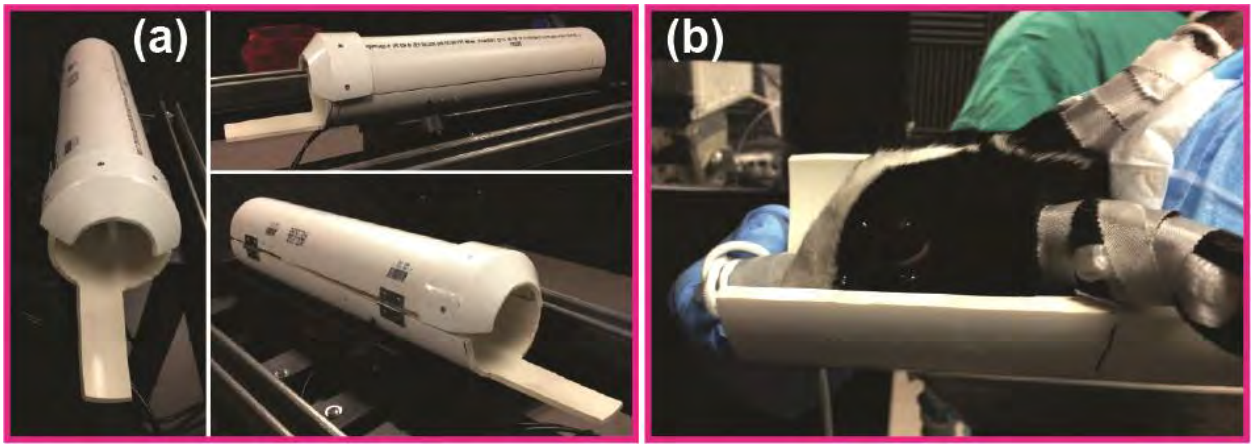

Figure 27. (a) Three views of the custom PVC holder. The holder provides body protection (exposing only the face and eyes) during blast exposure. (b) Ear protection consisting of standard earplugs taped into place with 4x4 gauze.

examination. The validated procedure consisted of the following essential elements (Table 5):

- Anesthesia- the Ketamine/Xylazine injectable anesthetic cocktail and buprenorphine, supplemented with Iso-fluorane gas, was used for sedation and Pain relief for the subjects- Iso-fluorane was used for short procedures, (specifically the 24 hour post-blast blood and aqueous draw) and as a supplement to the Ketamine/Xylazine cocktail (administered via intramuscular injection) used for longer procedures such as the blast exposure.

- Intraocular pressure (IOP) measurement – performed immediately before blast exposure (after rabbit placed in holder inside shock tube) and immediately after blast exposure, and 48 hours after blast exposure. In each case IOP was measured using icare® TONOLAB and TONOVET devices (Icare Finland Oy, Helsinki, Finland).

  Imaging- performed 1 day before blast exposure, immediately after blast exposure, and 48 hours after blast exposure. Imaging consisted of Direct Ophthalmoscopy, Slit Lamp and Fundus photos, OCT, HRT corneal confocal imaging (producing images from which cell counts were obtained in the corneal endothelium), and Ultrasound (UBM and B-scan).

- Blood and aqueous collection – performed 1 day before blast exposure, and at intervals of 4, 24, and 48 hours after blast exposure. Blood was taken from the central ear artery with a 23 gage butterfly needle and a 3cc syringe. Aqueous humor was collected using gentle aspiration with a syringe and plunger.

- Euthanasia and tissue harvest- To increase research program impact, collaboration, and efficiency, it was decided to share harvested tissues between

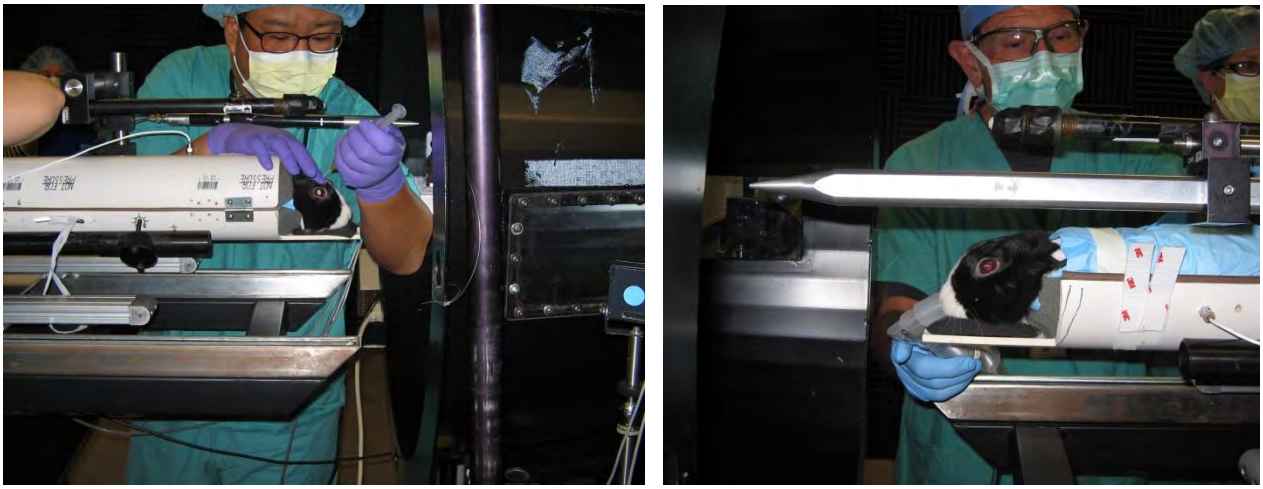

Figure 28. Two views of the Dutch-Belted rabbit secured inside the custom PVC holder. The head of each rabbit faced the open end of the shock tube and extended beyond the holder. The PVC holder firmly held the body of the rabbit in place during the blast.

the SLOT program and researchers at ISR interested in traumatic brain injury (TBI). Thus samples of the eyes, optic nerves, and brains were sent to SLOT team member Dr. Randolph Glickman for identification and characterization of the biomarker proteins, and to Dr. Huey-Ching Wang at ISR for TBI research.

Following procedure validation, *in vivo* blast tests were completed on 17 Dutch-belted rabbits (also procured from RSI Robinson Services, Inc.). Each rabbit was secured at the open end of the ISR shock tube using a custom holder fabricated from two halves of hinged PVC pipe (Figure 27). Ear protection consisting of standard earplugs was taped into place with 4x4 gauze pads (Figure 27). During anesthesia trials it was observed that the eye lids remain open, thus there was no need for tape or sutures to hold the lids open during blast testing. The rabbit was placed inside the holder with its head oriented toward the shock tube and extending beyond the end of the holder (Figure 28). The pipe halves were closed and latched to firmly secure the body of the rabbit inside the holder. Five rabbits served as controls and were subjected to the same procedures, but not exposed to the actual blast overpressure. The blast-exposed rabbits were subjected to low level blast exposures ranging from 54 kPa to 135 kPa (reflected pressure) with durations varying from 2.7 ms to 3.2 ms (Table 6). No animal experienced more than one blast exposure. At intervals of 4 hours, 24 hours, and 48 hours, samples of aqueous fluid and blood were extracted from all rabbits (blast-exposed and controls) for the biomarker study. After the 48 hour blood draw, each rabbit was euthanized followed by extraction of the eyes, optic nerves, and brain.

2.9.1 Rabbit Eye Imaging

An extensive imaging series was conducted on each rabbit before and after blast exposure to identify and characterize any blast-induced ocular trauma. The purpose of

Table 6. Summary of *In Vivo* Rabbit Blast Experiments

Test No.	Peak Reflected Pressure (kPa)	Pulse Duration (ms)	Reflected Specific Impulse (Pa-s)
1	53.8	2.70	59.3
2	54.0	2.69	58.6
3	52.9	2.73	58.2
4	52.6	2.71	58.4
5	52.7	2.69	57.2
6	54.4	2.75	60.6
7	91.1	2.80	102.7
8	87.3	2.83	106.6
9	80.9	2.87	98.6
10	81.8	2.88	99.2
11	84.2	2.76	100.1
12	123.7	2.99	160.0
13	135.7	3.18	160.4
14	125.2	3.05	144.7
15	125.4	3.05	162.0
16	125.2	3.05	144.7
17	125.4	3.05	162.0

*Experiments included 5 control rabbits not subjected to blast exposure

the study was to determine whether clinically significant ocular trauma can be induced by a single survivable primary blast using a live animal model. Both eyes of the

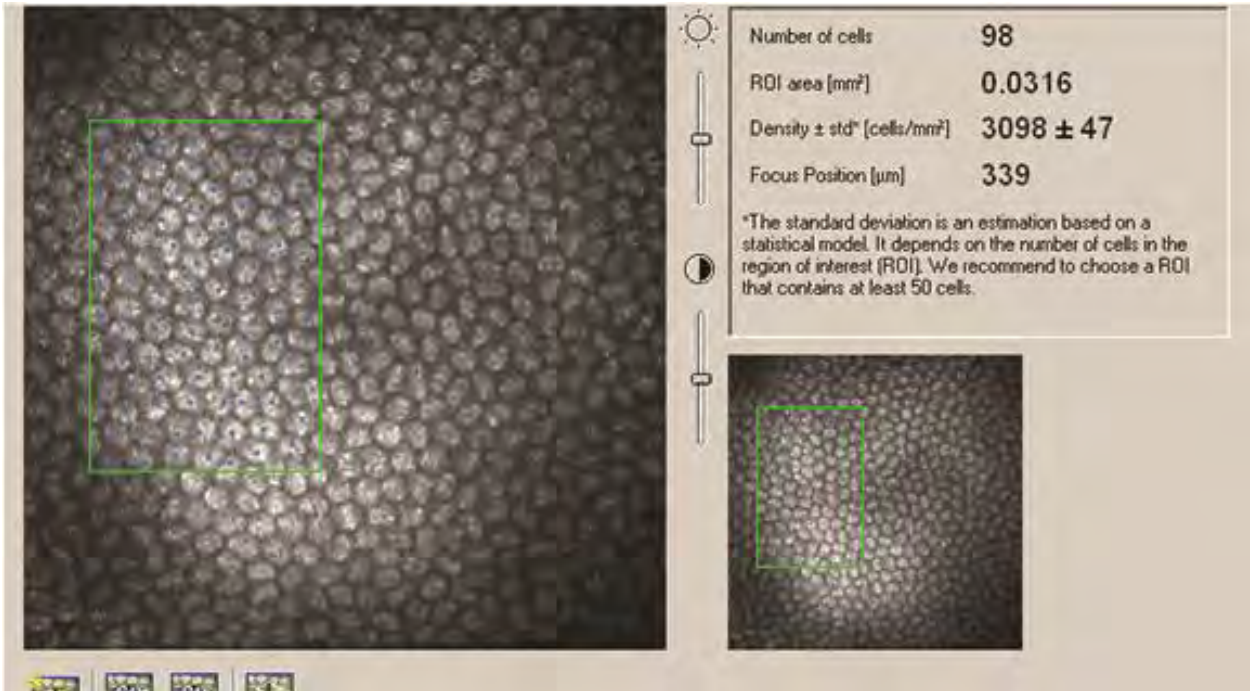

Figure 29. Endothelial cell density acquisition using confocal imaging.

seventeen blast-exposed and five control Dutch Belted rabbits were imaged. The imaging included (1) Direct Ophthalmoscopy, (2) Slit Lamp Photography, (3) Fundus Photography, (4) Ocular Coherence Tomography (OCT), (5) HRT Corneal Confocal Microscopy, and (7) Ultrasound imaging (UBM, B-scan). Slit lamp images were used to observe any surface corneal damage, sphincter ruptures that could be present post-blast, cataract formation, and changes in corneal transparency. Fundus photos were observed for hemorrhaging and/or edema. HRT corneal confocal microscopy images measured the focus, which estimates corneal thickness as well as the density of the endothelial cells. A corneal area of approximately 0.03 mm^2 was obtained and each cell in the specified area was counted and then the total number of the endothelial cells in the area estimated. B-scan image data included corneal confocal (immediate and 48-hours post blast), and OCT images. Retinal nerve fiber layer (NFL) thickness was estimated by combining five pre-blast and five post-blast OCT image measurements. One measurement was taken from each image within 5 mm of the optic cup from the ganglion cell layer to the outer nuclear layer (photorecepters). This measurement was made at a point in each image where the two layers were tangential to the horizontal OCT axis by measuring the length of a vertical (axial) line to ensure maximum spatial resolution. Ultrasound biomicroscopy (UBM) was used to measure the anterior chamber angle pre- and post- blast. Lastly, B-scan ultrasound was used to detect retinal detachment. All measurements were then compared to the pre-blast values.

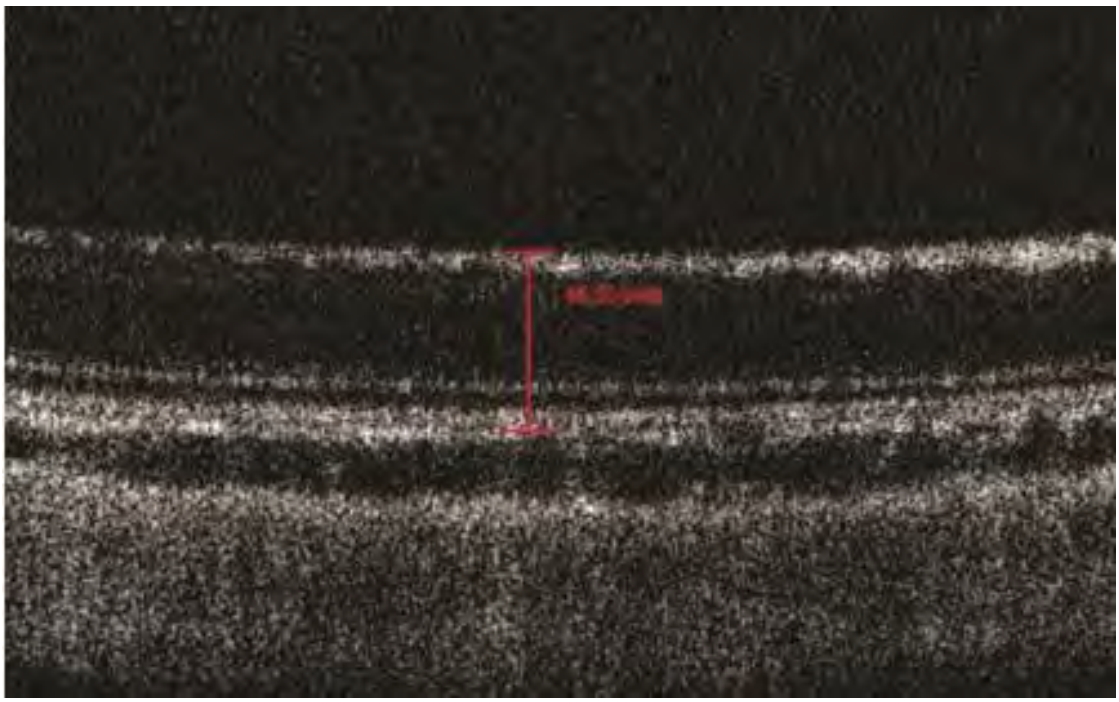

Figure 30. Measurement of neuroretinal thickness taken from the inner ganglion cell layer margin to the junction of the inner nuclear layer and outer plexiform layer.

An apical z-stack of corneal confocal microscopy images was used to estimate corneal thickness and endothelial cell density. Corneal thickness measurements were taken from the top of the epithelial cell layer to the bottom of the endothelial cell layer. Endothelial cell density was estimated using confocal images of an area of approximately 0.03 mm^2 (Figure 29). Each cell was hand counted. Image analysis was performed on both eyes in each animal. In Vivo Vue Clinic v1.4 software (Bioptigen, Inc.) was used to measure inner retinal layer thickness from five pre-blast and post-blast OCT images (Figure 30). This was accomplished by taking one measurement from the inner ganglion cell layer margin (inner limiting membrane) to the junction of the inner nuclear layer and outer plexiform layer from each of five inferior peripapillary images, each within 5 mm of the optic nerve head margin. Note that for the purpose of this study the inner retinal layers exclude the photoreceptors.

2.9.2 Rabbit Blast Test Analysis and Results

Linear regressions were applied to detect whether changes in the eye were significantly correlated with reflected specific impulse. Statistical analysis was performed using normalized data and linear regression. Responses were normalized as:

$$z(t) = \frac{y(t) - y_0}{y_0},$$

where *z(t)* is the normalized response at time *t*, *y(t)* is the experimental measurement at time *t*, and y_0 represents the baseline value at *t=0* (i.e., prior to blast). This normalization accounted for inter-animal variability and changes due to confounding effects such repeated anesthesia. Linear regression was then used to estimate the effect of overpressure specific impulse on each of the normalized responses. Due to the normalization, offsets were set to zero unless the offset was found to be statistically significant during regression. Statistical significance for the offset and/or linear effect was established if the p-value was below 0.05.

The linear regressions results reveal an overall increase in the inner retinal layer thickness after blast relative to control (p-value = 0.00017). Differences for the left eyes reflected the general positive association between overpressure and retinal thickening (Figure 31). The statistical method used was able to incorporate adjustments for differences in baseline thickness values between animals and any effect of time unrelated to blast. The corneal thickness increased progressively over time among blast-exposed eyes, with significant differences between the three blast pressures. Cumulatively for the left eyes, the pre-blast thickness was significantly lower than both the post (p-value=0.0011) and 48-hour post blast (p-value=0.0014; Figure 32). Endothelial cell density did not change significantly from baseline (p=0.50 immediately post-blast; p=0.21 48 hours post-blast). Although not statistically significant, the sudden decrease in density seen immediately post-blast in the 54 and 83 kPa (8 and 12 psi) groups could indicate clinically relevant cell loss or migration (Figure 33). It is known that rabbits are able to regenerate their endothelial cells (Van Horn, et al., 1977), which may explain the observed increases in density of the same groups (54 and 83 kPa) at 48-hours post-blast (Figure 33).

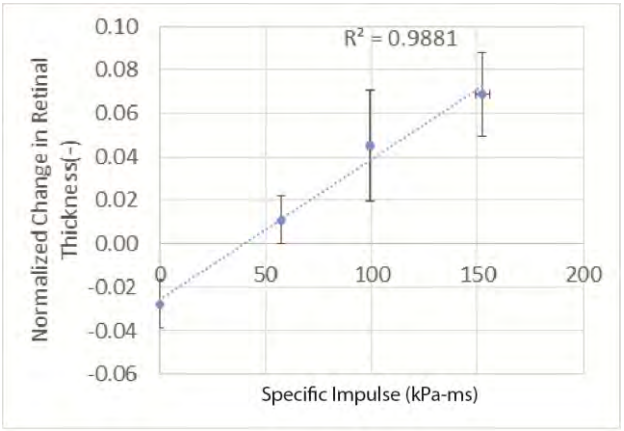

Figure 31. Retinal thickness changes seen immediately after blast in each treatment group.

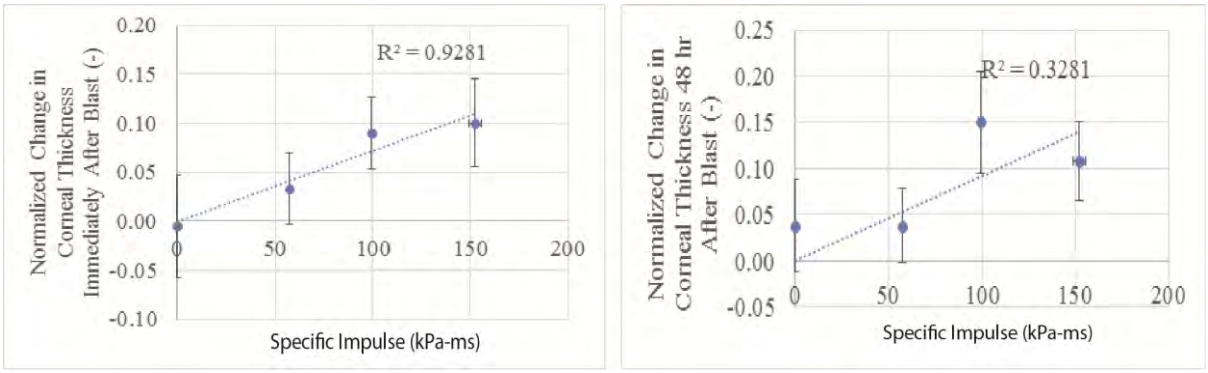

Figure 32. Corneal thickness changes seen in left eyes at base line compared to immediately post-blast (left), and 48 hours post-blast (right).

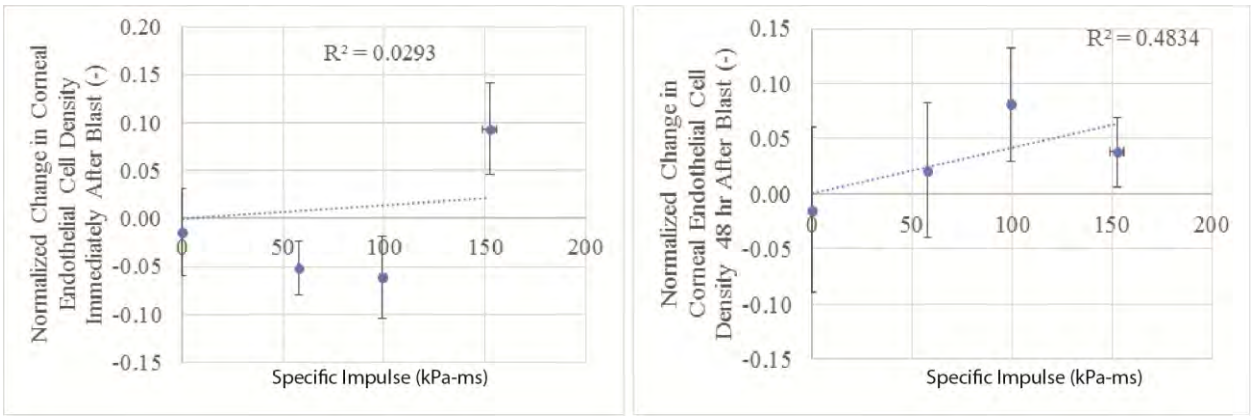

Figure 33. Change in endothelial cell density of the left eye immediately post-blast (left), and 48 hours post-blast (right).

These tomographic data confirm that primary blast insult produced by the shock tube produced immediate changes in the inner retinal layers and cornea of the living eye in rabbits. The immediacy of the effect on the cornea is perhaps not surprising given its superficiality and direct exposure, while the effects on the retina appear to confirm that the effects of blast penetrate the entire globe (e.g. Sherwood et al., 2014). These changes persisted for the duration of the follow-up period (48 hours).

Corneal thickness changes were highly statistically significant. While transient corneal edema is commonplace and typically rapidly resolves, the fact that the observed thickening persisted and indeed increased at 48 hours in left eyes exposed to higher blast energies suggests that endothelial function may have been compromised by a post-blast biological cascade. Sustained corneal thickening has been observed using other in vivo model systems (Hines-Beard et al., 2012; Hyek-Choi et al., 2014).

Peripapillary inner retinal layer thickening was observed immediately post-blast. Although rabbits do not have foveas, the implications of these findings for the macula, optic disc, and posterior pole of other foveated species are likely to be important. Computational modeling of blast effects on the eye suggests that coup-contrecoup positive and negative oscillations of the chorioretina arise almost immediately and are sustained throughout and beyond the primary blast impact (Watson et al., 2014). These changes resemble those noted previously in blunt trauma studies (Gray et al., 2011). The present findings suggest that survivable isolated primary blast is capable of producing acute corneal injuries consistent with a Cumulative Injury Score of level 1, and retinal damage at a potentially much higher level (Sherwood et al., 2014).

In conclusion, normalized thicknesses of the cornea and inner retinal layers increased significantly with specific impulse immediately and 48 hours after blast exposure, providing new *in vivo* evidence of tissue damage due to primary blast (cornea pre- versus immediate post-blast: p=0.0011 and 48-hours post-blast: p=0.0014; retina p=0.00017). Survivable primary blast overpressure caused significant ocular damage in actively perfused living eyes. Clinically significant changes in corneal thickness arose immediately and were sustained through 48 hours, suggesting possible disruption of endothelial function. Likely clinical outcomes are decreased visual acuity (due to increased corneal light scattering), and retinal swelling with potential for subsequent detachment.

2.10 Biomarker Study

Aqueous and blood plasma samples were drawn from each of the 17 blast-exposed and 5 control rabbits in order to evaluate the release of trauma-related biomarkers into the injured eye and the host circulatory system. Sampling included 100 µl of aqueous humor drawn from the rabbit's right eye (od) using a 30 gage needle, and 2 ml of blood drawn from the right ear (ad) using a 20 gage needle. Samples were taken at intervals of pre-blast (baseline) as well as 3, 24, and 48 hours post blast. At each interval, the samples were immediately labeled and placed on ice, followed by freezer storage at ≤ -20°C until needed for analysis. More than 2 freeze and thaw cycles occurred. After thawing, samples were pipetted from centrifuge tubes and chronologically arranged in a 96-well, uncoated microliter assay plate. Approximately 45µl if aqueous humor and 75 µl of blood plasma were used per plate. Immunoassays of protein markers were carried out using Luminex technology, bead-based multiplexed assays. Two magnetic bead millipore kits were utilized; (1) Milliplex Rat Cytokine/Chemokine Panel (RECYMAG65K27PMX), and (2) Milliplex Human Neurological Disorders Panel (HND1MAG-39K). Each kit contained all needed components and reagents (Table 7). Following the kit manufacturer's protocols assays were carried out with the BioRad xMAP instrument located in the CATT Core Facility at the UTHSCSA. An important advantage of the multiplexed xMAP assay is that multiple analytes can be measured in a single sample, which is especially critical when only limited volumes of experimental samples are available. Samples were assayed neat (aqueous humor) or diluted (blood plasma). Following manufacturer's recommendations, blood plasma

Table 7. xMAP Panels Used for the Measurement of Trauma-Related Biomarkers

1. Rat Cytokine/Chemokine Magnetic Bead Panel, Milliplex<u>Analytes</u>:

VEGF, EGF, Eotaxin, Fractalkine, G-CSF, GM-CSF, GRO/KC, IFN-γ, IL-1α, IL-1β, IL-2, IL-4, IL-5, IL-6, IL-10, IL-12 (p70), IL-13, IL-17A, IL-18, IP-10, Leptin, LIX, MCP-1, MIP-1α, MIP-2, RANTES, TNF-α
(This broad panel probes for cytokine and immune system modulators involved in systemic responses to inflammation, cancer, trauma, and cancer. The antibodies are nominally reactive to rat antigens, but showed adequate sensitivity toward the rabbit target analytes).

2. Human Neurological Disorders Magnetic Bead Panel, Milliplex <u>Analytes</u>:

Total tau
Tau phosphorylated (Thr231) neurofibrillary tangle protein
α-Synuclein
NGF-β (nerve growth factor)
NSE (neuron specific enolase)
PARK5/UCHL1 (Parkinson Disease Protein 5)
PARK7/DJ-1 (Parkinson Disease Protein 7)
(Although this kit is designed for the detection of human proteins, it demonstrated adequate sensitivity toward the rabbit proteins).

Notes:
<u>Human Neurological Disorders Panel</u>: NGF-b: Nerve Growth Factor type b; NSE: Neuron Specific Enolase; both NGF and NSE have been found to be upregulated after traumatic brain injury.
<u>Rat Cyto/Chemokine Panel</u>: G-CSF: Granulocyte-Colony Stimulating Factor; Eotaxin: an eosinophil-attracting chemokine; GM-CSF: Granulocyte Macrophage-Colony Stimulating Factor; IL-1A: a pro-inflammatory interleukin; Leptin: primarily known as hormone regulating the amount of stored fat, however, it has other, less-well characterized functions; for example, it may act to reduce phosphorylated tau in the brain (a marker of injury and disease); IL-12p70: a T-cell stimulating cytokine, p70 is a biologically active heterodimer; CRO/KC: also known as CXCL1 and is a factor involved in a variety of stress response such as angiogenesis,inflammation, wound healing (including that of keratinocytes) and tumorigenesis. It is also a possible neuroprotective agent.

samples were prepared with ethylenediaminetetraacetic acid (EDTA) to prevent coagulation, and diluted 1:2 with buffer provided in the millipore kit. Several biomarkers were detected in the aqueous humor and plasma samples that appeared to correlate with changes in blast conditions as well as retinal/corneal thickness and intraocular pressure (Table 8). A summary of all xMap detection data results including biomarkers that were below the detection limit is provided in Appendix II.

Table 8. Biomarkers Detected in Aqueous Humor and Blood Plasma

Biomarkers Detected in Aqueous Humor	
Human Neurological Assay	**Rat Cytokine Assay**
NGF-b	G-CSF
NSE	Eotaxin
	GM-CSF
	IL-1a
	Leptin
	IL-12p 70
	GRO/KC/CINC-
	MIP-2

Biomarkers Detected in Blood Plasma	
Human Neurological Assay	**Rat Cytokine Assay**
UCHL1 (PARK 5)	GM-CSF
NGF-b	GRO/KC/CINC-
DJ-1 (PARK 7)	LIX
NSE	MIP-2
Phospho-Tau (Thr 321)	

Table 9. Tobit Analysis of Biomarkers Showing Correlations with Blast Overpressure (BOP)

Human Neurological Assay-Aqueous Humor	Human Neurological Assay-Blood Plasma	Rat Cytokine Assay-Aqueous Humor	Rat Cytokine Assay-Blood Plasma
No positive results	NGF 3 hrs P=0.033	G-CSF 48 hrs P=0.03	IL-4 3 hrs P=0.03
	NSF 3 hrs 2.1e-5		IL-13 3 hrs .04
			IL-12p70 3 hrs .04
			MCP-1 3 hrs 1.5e-5
			LIX 3 hrs 4.9e-6
			MIP-2 3 hrs .02

2.10.1 Statistical Analysis and Results

The initial statistical analysis of the biomarker data consisted of subjecting each biomarker data set to a two-way analysis of variance analysis (ANOVA), using sampling time (3 hr, 24 hr, and 48 hr post-blast) and reflected blast overpressure (BOP) as the two factors. The absolute levels of the biomarker measured in the biological matrix were used as the input data set. Using this approach, most of the biomarkers listed in the tables above contained significant variances in the data matrix, either at different times or different BOP levels. The possibility existed, however, that these conclusions were potentially biased by two factors: (1) that the different baseline levels of a given biomarker varied considerably among the animals and those differences increased the overall variability, and (2) some of the values, reported by the xMAP instrument for a given biomarker, fell below the limit of quantitation for the particular assay. A common approach is to score measurements below the detection or quantitation limit as “zero”; however, this substitution may introduce erroneous determinations of analyte concentrations, particularly at low levels. To minimize the effect of baseline variation between animals, the biomarker data was normalized so that the changes from baseline

were expressed as fold-changes. To reduce the effect of zero or below quantitation level data, the “Tobit” statistical analysis was utilized.

The Tobit model describes a relationship between a positive dependent variable Y_i, and X_i, the independent variable. Essentially, the model assumes a linear relationship between the dependent and independent variables (i.e., performs a linear regression on the data set), but also allows for the presence of latent (un-measureable) variables, either on the low end or the high end of the data set. Variables above the detection limit are taken as measured, while values below the threshold are censored, i.e. assumed to be zero. Thus:

$$Y_i = Y_i^* \text{ if } Y_i^* > 0$$
$$Y_i = 0 \quad \text{if } Y_i^* \leq 0$$

A coefficient, designated as beta (that is, a weighting factor), is introduced from an estimation made by regressing the observed variables as a function of the X (independent) variable. This parameter reflects the change in Y_i for those values above the censoring threshold, and the change in probability of the dependent value being above the censoring limit and thus measureable. The slope, intercept, and coefficient of regression are determined. For this analysis, the Tobit analysis was “left censored”, to take into account those values falling below the limit of quantitation of the assay.

For aqueous humor samples no biomarkers in the Human Neurological assay panel significantly correlated with BOP, but NGF-β and NSE in the blood plasma were significantly correlated with BOP (Table 9). In the Rat Cytokine assay panel, the Tobit analysis indicated that G-CSF in the aqueous humor was significantly correlated with BOP, while Eotaxin, MIP-1a, Il-4, IL-13, IL-12(p)70, MCP-1, LiX, and MIP-2 in the plasma were significantly correlated with BOP (Table 9). Some of these factors, such as MIP-2, were negatively correlated with the blast, while the others were positively correlated (Figure 34). Interpreting these changes in biomarker expression level, in view of the system roles and signaling pathways involving these factors, may provide a greater insight into the central nervous system responses to blast injury.

The biomarker expressions were also correlated with the rabbit eye imaging results (Table10). The Tobit model analysis showed that NGF (p=0.033), NSE (p=2.1e-5), G-CSF (p=0.03), IL-4 (p=0.03), IL-13 (p=0.04), IL-12p70 (p=0.04), MCP-1 (p=1.5e-5), LIX (p=4.93-6), and MIP-2 (p=0.02) in the aqueous humor and plasma samples appeared to correlate with BOP amplitude. The Tobit results also demonstrate that NGF, NSE, IL-4, IL-13, IL-12p70, and LIX correlate with increased retinal thickness and after 48 hours a decreased IOP (Table 10). Statistical significance for the regression model was established if the p-value was below 0.05.

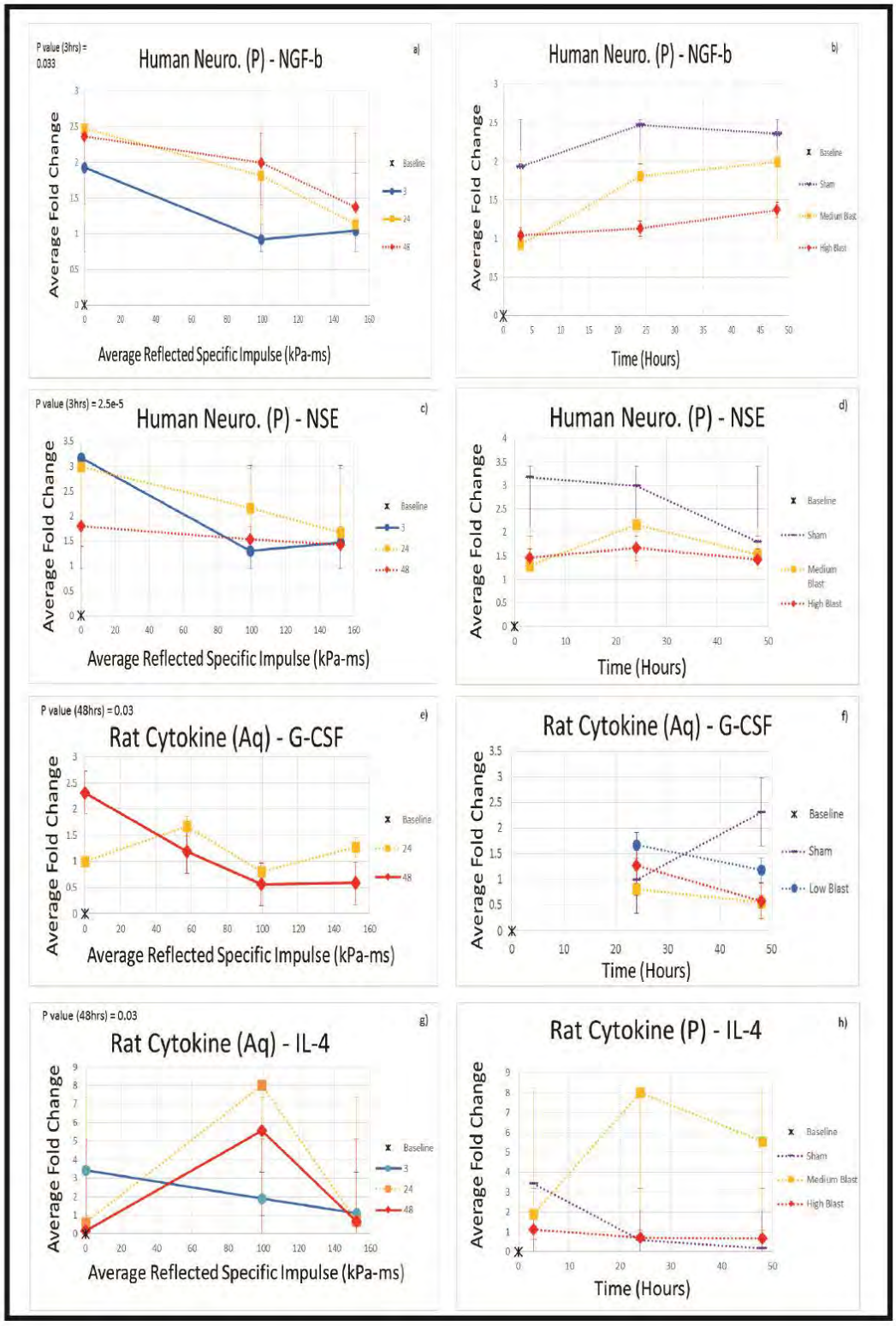

Figure 34. Results of Tobit model analysis showing biomarker expressions as the fold change from baseline value (pre-blast) as a function of reflected specific impulse. Lines show the data trend for each sampling point. Asterisks denote time points at which biomarker expression achieved a significant change from baseline.

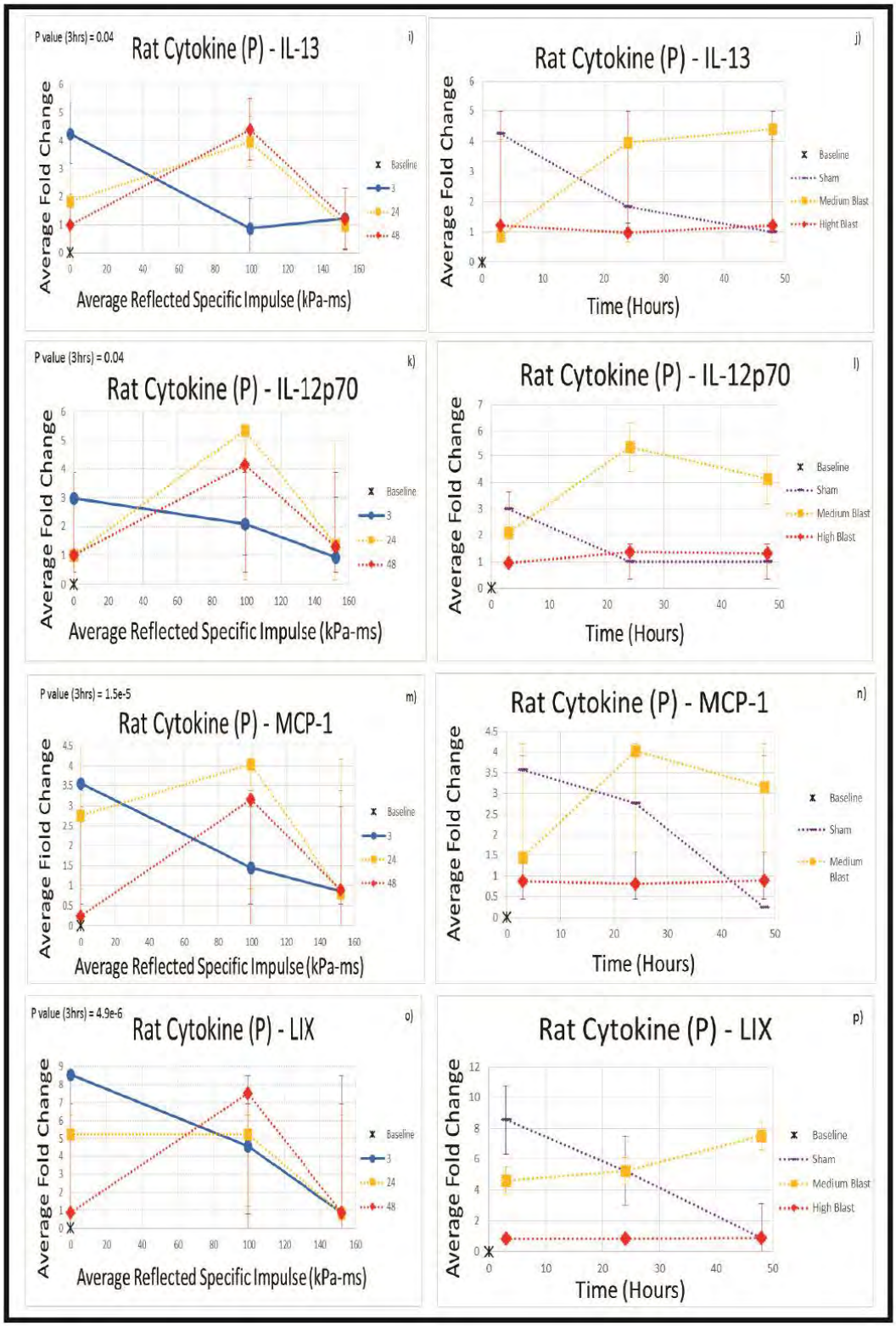

Figure 34 (continued). Results of Tobit model analysis showing biomarker expressions as the fold change from baseline value (pre-blast) as a function of reflected specific impulse. Lines show the data trend for each sampling point. Asterisks denote time points at which biomarker expression achieved a significant change from baseline.

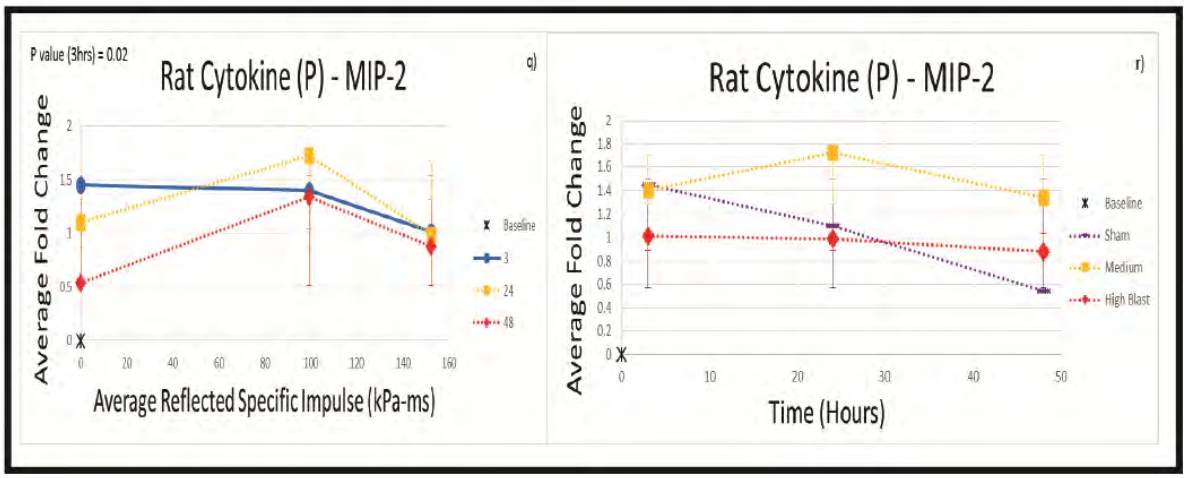

Figure 34 (continued). Results of Tobit model analysis showing biomarker expressions as the fold change from baseline value (pre-blast) as a function of reflected specific impulse. Lines show the data trend for each sampling point. Asterisks denote time points at which biomarker expression achieved a significant change from baseline.

Table 10. Biomarker Correlations with Rabbit Eye Imaging Results.

Biomarker	Comparisons (X,Y)	P value	Possible Mechanism
NGF	IOP 24 hrs, 3 hrs	0.028	Uveitis-induced nerve growth stimulation
	IOP 48 hrs, 3 hrs	0.008	
	IOP 48 hrs, 24 hrs	0.001	
NSE	Retinal Thickness OS, 3 hrs	0.035	Nerve cell damage
	Retinal Thickness Avg. 3 hrs	0.030	
	IOP 48 hrs, 3 hrs	0.032	Uveitis
IL-13	Corneal Thickness 1 hrs, 3 hrs	0.040	Wound healing response
	IOP baseline, 3 hrs	0.027	Uveitis
IL-4	Retinal Thickness OD 48 hrs	0.033	Wound healing response
IL-12p70	Retinal Thickness OD 48 hrs	0.033	Mechanical trauma response
LIX	Retinal Thickness OD 3 hrs	0.050	Neutrophil activation or DNA synthesis
	Retinal Thickness OD 48 hrs	0.011	

Note: Statistical significance for the regression model was established if the p-value was below 0.05.

2.10.2 Significance of Biomarker Results

Although the origin of biomarkers following blast has not been previously established with rigor, our study suggests that concentrations of certain biomarkers do correlate with known ocular injuries. We hypothesize that tissue damage or cell loss due to blast overpressure increases the presence of biomarkers, which correlate to trauma and healing mechanisms. Although speculative at this point, we also believe unavoidable stress related circumstances, such as post-traumatic, oxidative, and environmental

stresses may have played a role in the increase of some biomarkers. Nonetheless, precautions were put in place to minimize involuntary stress unrelated to blast amplitude. To avoid post-traumatic stress the subject was anesthetized with ketamine/xylazine and handled with care prior to aqueous draws and primary blast exposure. The subjects were also given a recovery period of 48 hours to heal. To control oxidative stress, each rabbit was thoroughly monitored throughout the course of the research project's life cycle. The rabbit's health and well-being were made priority. Inspections were documented to avoid infection and any disturbances of the normal cellular redox state. This method made it possible to evade any toxins which may have destroyed cellular components (Haschek, et al., 2013).

We hypothesize that biomarker concentration levels fall after blast exposure due to ocular tissue damage and cell death, resulting in a reduction in the number of cells present and limiting the presence of any biomolecule detected (Fortea, 2014). This should be especially noticeable at high amplitudes of blast, as is suggested by our data (Figure 34). We observed down regulation in biomarker levels in all nine biomolecules within 48 hours (Figure 34). However, NGF has also been shown to repair tissues (especially in post-traumatic brain injury) by promoting nerve cell growth. This information is valuable, but its clinical application is limited due to the lack of feasible methods for delivering NGF into the brain. The blood-brain barrier presents a substantial challenge to NGF delivery to the brain. Therefore, multiple studies suggest the possibility of NGF reaching the brain through the nasal cavity where NGF may be transported rapidly into the CNS (Lawrence, 2002; Covaceuszach, et al., 2009). Unfortunately, we were unable to see potential up-regulation in biomarker expression levels (if they were going to occur) due to our experimental time constraint of 48 hours.

Cytokines and other protein markers demonstrate significant change in concentration levels associated with blast trauma, particularly NSE (RT at 3 hr, $p=0.030$), NGF (IOP at 48 hr, $p=0.001$), IL-4 (RT in OD; $p=.033$), IL-13 (IOP at 0h; $p=.027$), IL-12p70 (RT in OD; $p=0.033$), and LIX (RT in OD; $p=0.01$). The observation of increased retinal thickness (RT) and decreased IOP measurements after 48 hours may suggest that these six biomarkers are indicators of this type of ocular trauma. Research has shown that NSE and NGF are closely related to head injuries or traumatic brain injury (TBI). Structural damage of neuronal cells causes leakage of NSE into the extracellular compartment and the bloodstream, allowing NSE to be detected in serum after neuronal death, traumatic injury, or a cerebrovascular accident (Zurek & Fedora, 2011; Tian et al., 2012; Qiushi, et al., 2014). This may explain the relatively consistent concentration levels of post blast NSE in our blood plasma samples. If neuronal cells were significantly damaged due to BOP, continuous leakage of NSE into the bloodstream, along with surrounding cellular tissue may occur; the effects could be sustained through 48 hours. Abnormal amounts of NSE and NGF can result in neurological deficits within 6 months, as has been observed in patients during post TBI examinations (Bandyopadhyay , et al, 2005; Zurek & Fedora, 2011; Qiushi, et al., 2014,). In our study NSE was observed in the plasma samples, but not in the aqueous humor samples.

The presence of IL-4 and IL-13 cytokines in the plasma raises the possibility that the animals were subjected to thermal stress, as these biomarkers have been associated with thermal injuries in humans (Gardner, et al., 2014). Theoretically the air driven by the blast waves in our experiments could have experienced a temperature rise as high as 90 degrees C (Needham, 2010), but the amount of heat actually transferred into the rabbit tissues by the air was likely small due to the brief duration of the blast pulse (2-3 ms). More likely, the heat resulted from rapid tissue compression associated with the shock (that precedes blast air loading), and it may have been sufficient to contribute to the cytokine release ($p=0.033$). Although severe burns are often observed on the exposed skin of blast victims, they are typically caused by radiation from the very hot explosive gases and debris, and not exposure to the blast air. The shock tube used in our experiments does not produce hot explosive gases or debris.

The observation of IL-12p70 may suggest induced time-dependent analgesia to mechanical stimulation, which has been seen in rats exposed to neuropathic pain. In high dose, this proinflammatory cytokine prompted a significant analgesic effect by measuring the hind paw tactile allogynia from 1 to 4 h after injection (Chen et al., 2013). Therefore, nociceptors (pain receptors) signal to the brain via spinal cord chemical, mechanical, or thermal tissue damage, which may stimulate IL-12p70 to occur in animals post blast.

LIX, a chemokine, is associated with inflammation and neutrophil activation. It is expressed in hematopoietic stromal cells linked with hematopoietic supportive phenotypes. The effects of LIX on primary bone marrow are the increase of long-term culture initiation cells by 34%, DNA synthesis, and in viable cell count (1.11-fold at 96 h after seeding, Choong, et al., 2004), portraying a specific relationship with primitive hematopoietic cells. This relationship could be associated with internal bleeding (other than the eye) caused by the BOP that was not studied for this project.

This study was limited by sampling for only 48 hours post-blast. This time may have been insufficient to detect the full range of biomarker expression. In addition, drawing of aqueous humor from only the right eye may have prompted environmental and oxidative stress bias. Despite these limitations, the identification of blast-related biomarkers, if borne out in future studies, may aid in the development of diagnostic tools for assessing blast injury.

2.11 Numerical Models & Simulations

Two computational software packages were utilized to simulate the response of eyes to blast, LS-DYNA and CTH. CTH is a three-dimensional Eulerian wave propagation code (hydrocode) developed and distributed by Sandia National Laboratories. It has a second order material advection algorithm and an advanced high-resolution interface tracker making it ideally suited for problems involving large distortions caused by blast or impact. In the Eulerian formulation the computational grid is fixed and materials are allowed to flow through the grid. After each time step, the

materials and interfaces are re-projected back into the Eulerian grid avoiding many severe distortion problems commonly encountered in finite element codes such as LS-DYNA.

LS-DYNA is a commercially available Lagrangian finite element program distributed by Livermore Software Technology Corporation (LSTC) of Livermore, California. It is generally considered the industry standard for simulation of vehicle crash and associated biomechanics. In the Lagrangian formulation, the computational grid remains fixed to the materials as they undergo distortion. Thus, large distortions often result in instabilities and early termination of the calculation. In LS-DYNA, the problem is partially solved by incorporation of Eulerian fluid dynamics components. We used CTH to study the short-term effects of wave and shock propagation through the eye, and LS-DYNA to study the longer term effects of acceleration and applied forces on the ocular tissues.

Two types of CTH computations were undertaken, (1) simulations of the shock tube, and (2) simulations of the shock tube and eye. One disadvantage of CTH is that the blast wave must be generated within CTH from an initial static pressure. Thus to achieve the correct blast wave exposure, the entire shock tube must be modeled. In LS-DYNA however, the blast wave can be input as an initial loading condition (For our simulations the Friedlander wave forms measured in the shock tube experiments were input directly.), so only the eye need be modeled. In addition, CTH requires at least 4 elements across the 1 mm thick sclera. Thus, high fidelity CTH modeling of the shock tube and eye requires models with in excess of 1 million computational elements, and very long run times (currently on the order of 1 week of actual time). In LS-DYNA, a fewer number of solid elements are required to define the tissue thickness, thus size and computational times are greatly reduced.

2.11.1 LS-DYNA Model of the Porcine Eye

A validated computational finite element analysis (FEA) model of the porcine eye was developed to provide insight as to the physical trauma mechanisms observed in blast experiments conducted during this program, as well as blunt impact experiments conducted in previous research efforts. The porcine eye is considered a good surrogate for the human eye and used extensively in experiments, but to our knowledge this is the first computer model of the porcine eye. Geometry for the FEA model was created in 3D using the SolidWorks CAD software (Dassault Systèmes SOLIDWORKS Corp., Waltham, MA). Dimensional data for the model came from a variety of sources (Table 11). Because of its rotational symmetry, the eye was modeled in quarter symmetry. The sclera was modeled with continuously variable thickness ranging from 0.43 mm to 0.89 mm. The overall diameter of the globe in the coronal plane was 22.2 mm. The length of the eye in the transverse/sagittal planes was 22.9 mm. Dimensions of the cornea and lens and their positional relationship were taken from a study that determined optically correct geometry (Reilly et al, 2009). The zonules were simplified for computational purposes into a continuous band of material connecting the lens equator to the ciliary

Table 11. Dimensions and Sources for Porcine Eye Model

Geometry	Dimensional Value	Source
Scleral outer radius	11.12 mm (calculated to match area value)	Olsen 2002
Scleral inner radii	various	Olsen 2002
Corneal outer radius	9.01 mm	Reilly 2009
Corneal thickness	0.98 mm (at apex)	Reilly 2009
Lens anterior radius	6.63 mm	Reilly 2009
Lens posterior radius	5.08 mm	Reilly 2009
Lens position	2.5 mm posterior to posterior surface of cornea	Reilly 2009
Zonules	Simplified for simulation purposes.	Burd 2002, Bron et al 1997
Ciliary body	Simplified for simulation purposes.	Asejczyk-Widlicka 2008
Iris root thickness	n/a	Bron et al 1997
Iris collarette thickness	n/a	Bron et al 1997
Pupil diameter	n/a	Bron et al 1997
Chorioretina thickness	0.2 - 0.86 mm	Bron et al 1997, Sanchez 2011

body. The ciliary body was also simplified, combining all the ciliary muscles and connective tissues into one contiguous material. The geometry of these constructs was based on imagery from various sources in the literature (Bron et al., 1997; Sanchez et al., 2011). The iris was not modeled as its relatively thin section would have required the use of many extremely small elements. No significant damage to the iris was observed in physical experiments and so it was postulated that the contribution of the iris to the overall dynamics of the model would be relatively small and not worth the computational expense. The retina and choroid were modeled as a single layer with thickness equal to that of both tissue layers combined. This was done to avoid the computational expense of the very small elements required for the thin cross sections of the retina and choroid. The optic nerve head and optic nerve were not modeled for the same reason. The aqueous and vitreous geometry resulted from the anterior and posterior chamber geometry defined by the previously described components.

Once constructed, parts were exported from SolidWorks in the ACIS SAT file format. The SAT part files were individually imported into the CUBIT (Sandia National Laboratories, Albuquerque, NM) meshing software. Within CUBIT, the parts were cut into meshable volumes and imprinted to ensure mesh coherence at the cut junctions. Hexahedral meshes were generated for each part. Maximum element size was kept near or below 1 mm in the interest of accurately propagating shock waves (Panzer et al., 2013). The meshed model is shown in Figure 35.

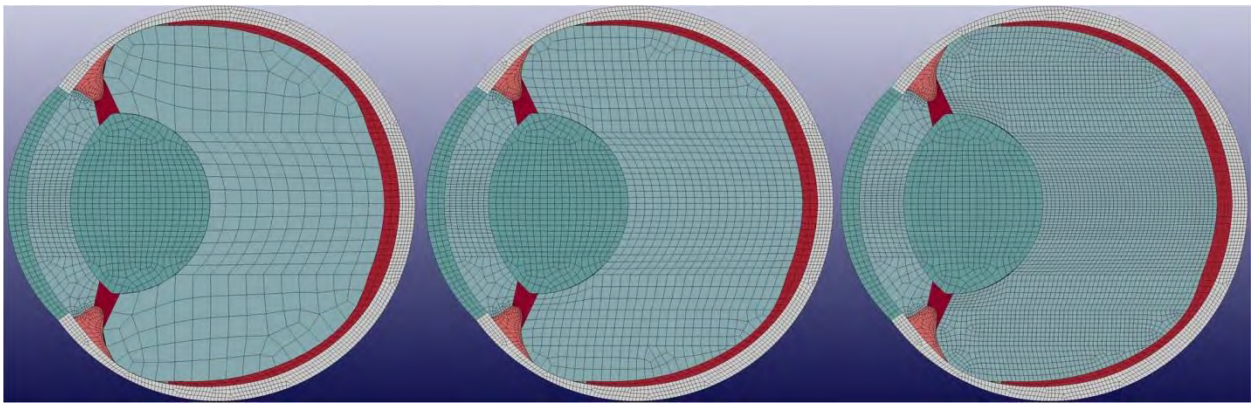

Figure 35. Eye model showing included components and 1 mm, 0.5 mm, and 0.25 mm mesh

Meshed parts were exported from CUBIT in the LS-DYNA (LSTC, Livermore, CA) keyword file format. The individual parts were imported and assembled in the LSPREPOST software. Contacts were defined for each part to part contact. The lens to zonules, zonules to ciliary body, ciliary body to sclera, and sclera to cornea were attached sequentially using *CONTACT_TIED_SURFACE_TO_SURFACE. This type ties the nodes and outer segments of the two parts together at the contact interface so that the displacements of adjacent tissues must be equal. Failure of the contact was not modeled at these attachments, as none was expected based on the concurrent physical experiments and previous experiments described in the literature. Contacts between the vitreous and all other structures, retina and all other structures, and aqueous and all other structures were modeled using *CONTACT_AUTOMATIC_ SURFACE_TO_ SURFACE_TIEBREAK. This contact type allows a failure criterion to be defined specifically for when normal stress or shear stress at the contact junction reaches a user-defined threshold, above which, the contact releases in the area where the stress value was exceeded. Due to a lack of knowledge on the specific failure thresholds for these junctions in the physical eye, the failure values were set to a level believed to be above reported physiological failure levels of the tissues, with the exception of the retina-to-sclera junction. This contact interface was varied experimentally to obtain a failure level that corresponded to retinal detachments observed in the physical experiments. Liu et al. (2013) used a value of 340 ± 78 Pa for the retinal adhesive force. This was used as the initial value in the present model.

The eye was modeled in a rigid holder filled with gelatin, mimicking the experimental setup used in the porcine blast experiments. Rigid boundary conditions and material were used for the holder. The gelatin contact with the holder was tied, as the contacting surfaces of the gelatin and holder did not exhibit relative motion in the physical experiments. Contact between the gelatin and sclera was specified using *CONTACT_AUTOMATIC_SURFACE_TO_SURFACE,with translation allowed between the surfaces. The model including porcine eye structures, ridged holder, and gelatin contained 64,460 elements for a characteristic element size of 1 mm. Blast loading was applied to the exposed forward facing surfaces of the eye and gelatin using

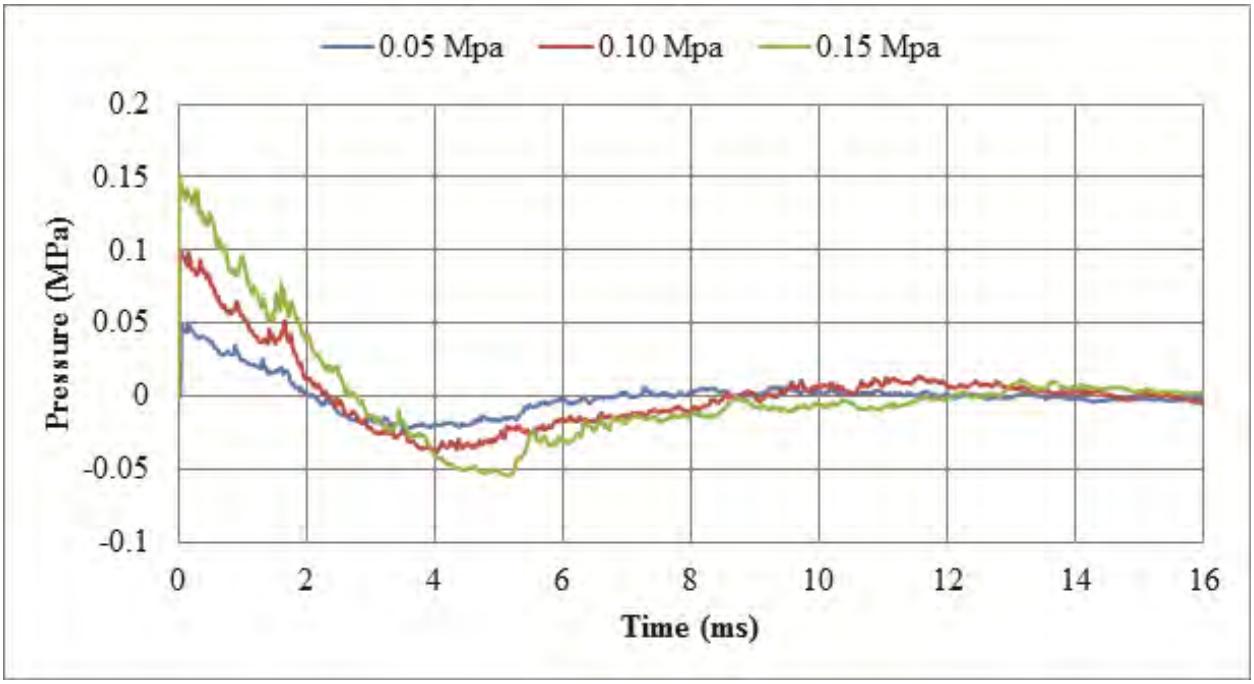

Figure 36. Pressure time histories for three levels of blast used in Porcine Eye FEA model

*LOAD_SEGMENT_SET. Static pressure time history recorded in the physical experiments was used. Three cases were represented and defined as peak overpressures of 0.05 MPa, 0.10 MPa, and 0.15 MPa (Figure 36).

Tests of the model with various types of constitutive models for cornea and sclera (linear, viscoelastic, plastic) found little difference in response, with the dominant variable always the stiffness of the tissue. Therefore, linear elastic models were chosen to represent the cornea and sclera. The stiffness of the cornea and sclera was iterated from starting values based on the work of Rossi et al. (2012) and Esposito et al. (2013). Final values were chosen based on matching the experimental BB impact data of the Delori et al. (1969) experiments. The aqueous humor was modeled using a linear fluid model available in LS-DYNA. Because of the relatively small deformations of the blast loading and resultant lack of fluid flow, this model was felt to be appropriate and returned acceptable results. The aqueous is compositionally similar to a saline solution and therefore is not expected to exhibit complex rheological behavior. The vitreous humor was modeled with a viscoelastic definition, using properties described by Rossi et al. (2012). The remaining tissues; chorioretina, zonules, ciliary body, and lens were modeled as linear elastic with values taken from various sources in the literature (Table 12). The compressibility of the chorioretina (as indicated by Poisson's ratio) was found to have a significant effect on the model under blast loading. Sigal et al. (2005) reported a range of 0.4 to 0.49 for this property. Using a value of 0.47 (i.e. slightly compressible), the model exhibited more overall deformation and suggested significant compression of the chorioretina. With a Poisson's ratio of 0.49 (i.e. largely incompressible) in the chorioretina the model exhibited a different response than with the 0.47 (largely

Table 12. Material Properties Used in the Porcine Eye FEA Model

PartName	Density (g/mm^3)	Youngs Modulus (Mpa)	Bulk Modulus (Mpa)	Poissons Ratio	Source of Material Properties
Aqueous	0.0010	-	2200	-	Rossi 2012
Choroid	0.0010	0.05	-	0.47	Sigal 2004
Ciliary	0.0016	11	-	0.45	Power 2001
Cornea	0.0014	12	-	0.487	Rossi 2011
Gelatin	0.0010	-	2260	-	Power 2001
Lens	0.0011	1.5	-	0.499	Stitzel 2002
Retina	0.0010	0.05	-	0.47	Sigal 2004
Sclera	0.0014	28	-	0.49	Rossi 2011
Vitreous	0.0010	-	2000	-	Rossi 2012
Zonules	0.0010	5	-	0.45	Stitzel 2002

compressible) and for that reason results are included for models with chorioretina with both values, which will be referred to as compressible and incompressible.

A mesh sensitivity study was performed to determine the ideal balance of mesh size and computational accuracy. Versions of the model were created with 1 mm mesh, 0.5 mm mesh, and 0.25 mm mesh. The 0.15 MPa blast level with 0.47 Poisson's ratio retina was used due to the larger deformation of the mesh in the compressible model. Various measurements, including corneal apex displacement, pressure at the center of the vitreous, and stress at the macula area of the retina, were compared between the three mesh sizes (Figure 37). A Grid Convergence Index (GCI) assessment was performed for peak values of the corneal apex displacement, vitreous pressure, and pressure at the macula (Table 13). The GCI method gives the rate of convergence of the solution as mesh size decreases and predicts the range of error in which the exact solution falls within 95% confidence intervals. This methodology is especially useful for cases such as this where the exact solution is not known. It should be noted that GCI predicts the exact solution of the ideal mesh size of the model; it does not account for material properties, material models, geometry or the many other variables possible in a FEA model. The same three metrics were also evaluated over a time history using the L_2 norm relative error. This method computes the average error between two curves, taken as vectors x and y, by taking the error at each point.

$$L_2 = \sqrt{\frac{\sum(x-y)^2}{\sum(x)^2}}$$

The L_2 norm is sensitive to small fluctuations in the data if they happen to be out of synch. The nature of the data in this experiment includes high frequency noise in some measurements and the relative error between different mesh sizes can be moderate, while the overall shape of the curve is fairly well matched. The 0.25 mm mesh was used

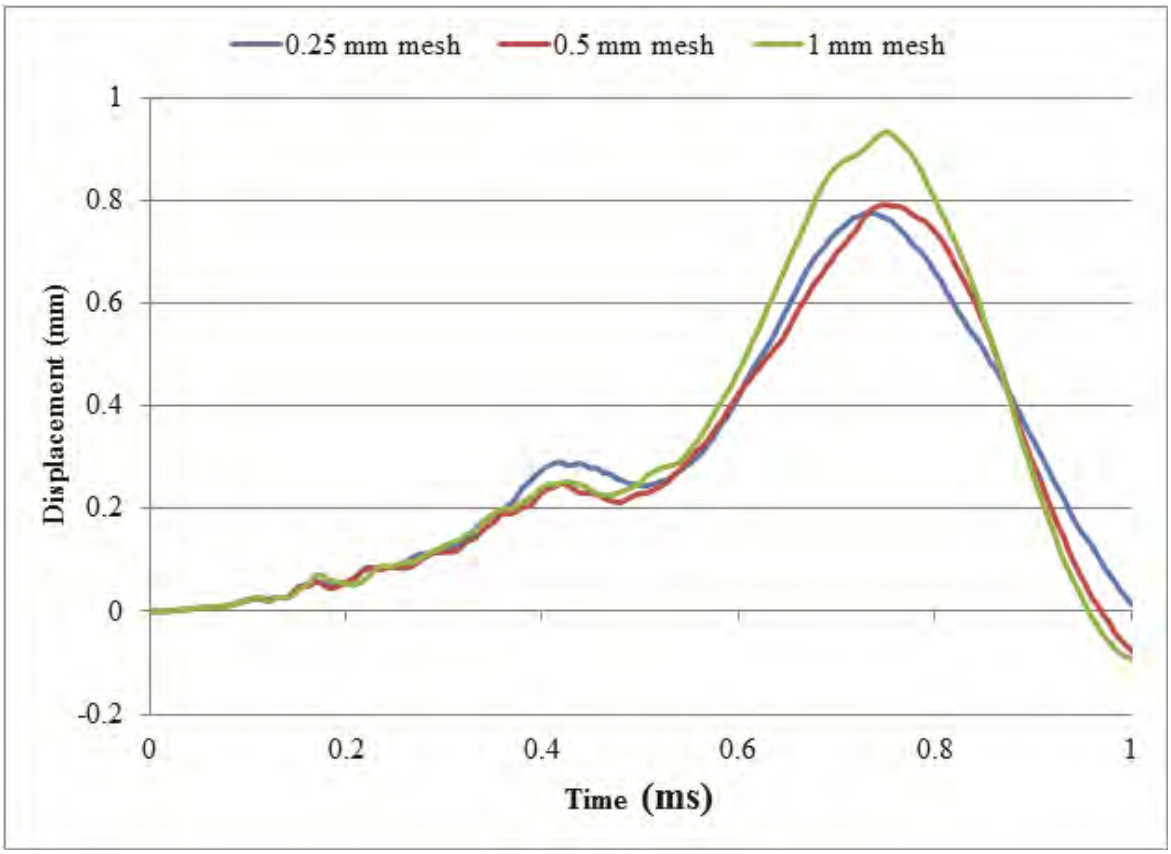

Figure 37. Corneal displacement history of three mesh sizes for peak blast pressure of 0.15 MPa

Table 13. Results of Mesh Sensitivity Study

Metric	0.25 mm mesh	0.5 mm mesh	1 mm mesh	p (rate of converge)	predicted solution	GCI	L_2 Norm 0.5 mm Mesh*	L_2 Norm 1.0 mm Mesh*
Corneal Apex Displacement (mm)	0.7762	0.7919	0.9332	1.48	0.7674	0.01417	10.8	19.7
Vitreous Pressure (Mpa)	0.1499	0.1487	0.1453	0.97	0.1511	0.01038	11.5	12.5
Retina Stress (Mpa)	0.0284	0.0276	0.0265	0.66	0.0298	0.06074	10.3	12.0

***Percent change in value relative to L_2 norm for 0.25 mm mesh (smallest mesh size)**

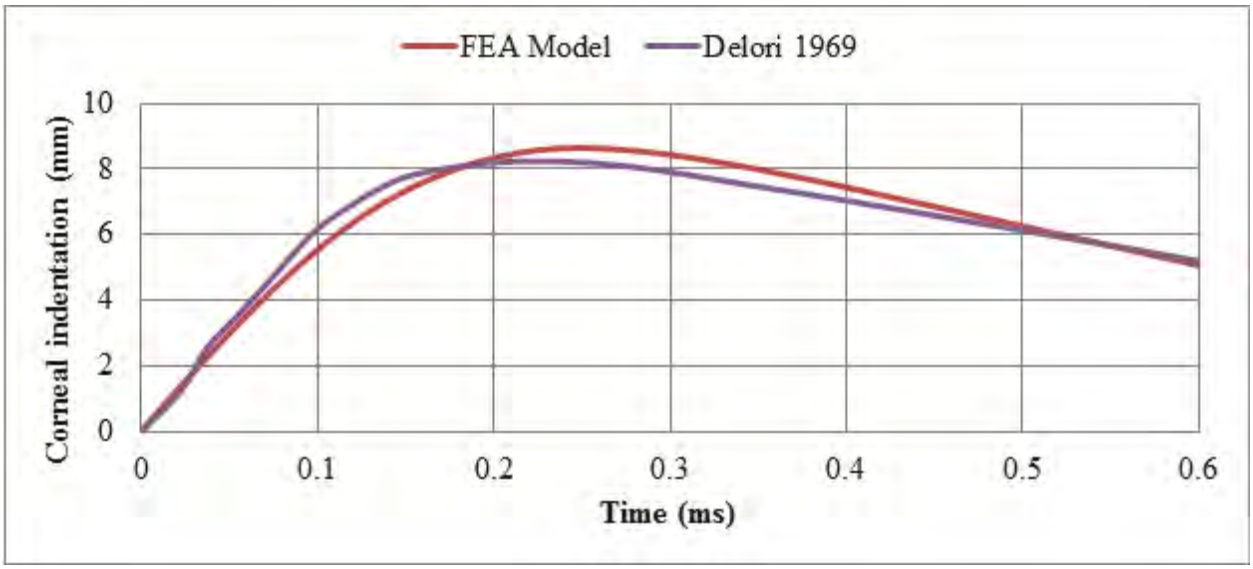

Figure 38. Corneal Indentation for FEA model and Delori et al. (1969) experimental data.

as the baseline for this analysis. The results of the L_2 norm analysis showed a slight decrease in the normalized error between the 0.5 mm mesh and 1.0 mm mesh (Table 13). The small amount of error between the 0.5 mm mesh and GCI predicted exact value was acceptable given the shorter run times. Therefore, the 0.5 mm mesh was deemed sufficiently dense to reproduce the key features of both primary blast and blunt impact in the porcine eye model. All subsequent results are reported based on this mesh.

2.11.2 LS-DYNA Model Validation

Validation of the model was performed against projectile impact studies, namely the 1969 study by Delori in which porcine eyes were impacted with BBs. BB impact subjects the eye to much more extreme deformation with higher stress and strain than the low level blast used in this study. The impact FEA model showed similar rate pressure reflections within the eye, albeit at higher levels than the blast model. This projectile study was used because the data is much more complete than that of existing blast studies, giving time histories of various external deformation parameters. Current blast experiments, including the concurrent SLOT project only offer binary measurements of whether or not an injury occurred. The Delori experimental setup was duplicated as closely as possible within the computational modeling environment. A 4.5 mm diameter, 0.345 gram BB impacted the center of the cornea at a velocity of 62.3 m/s. Indentation of the cornea, equatorial variation, and longitudinal variation of the globe were measured versus time and compared to the data reported by Delori. Model predictions were highly correlated with the experimental data (Figure 38). L_2 norms were 5.5% for corneal displacement, 2.2% for equatorial variation, and 9.7% for longitudinal variation.

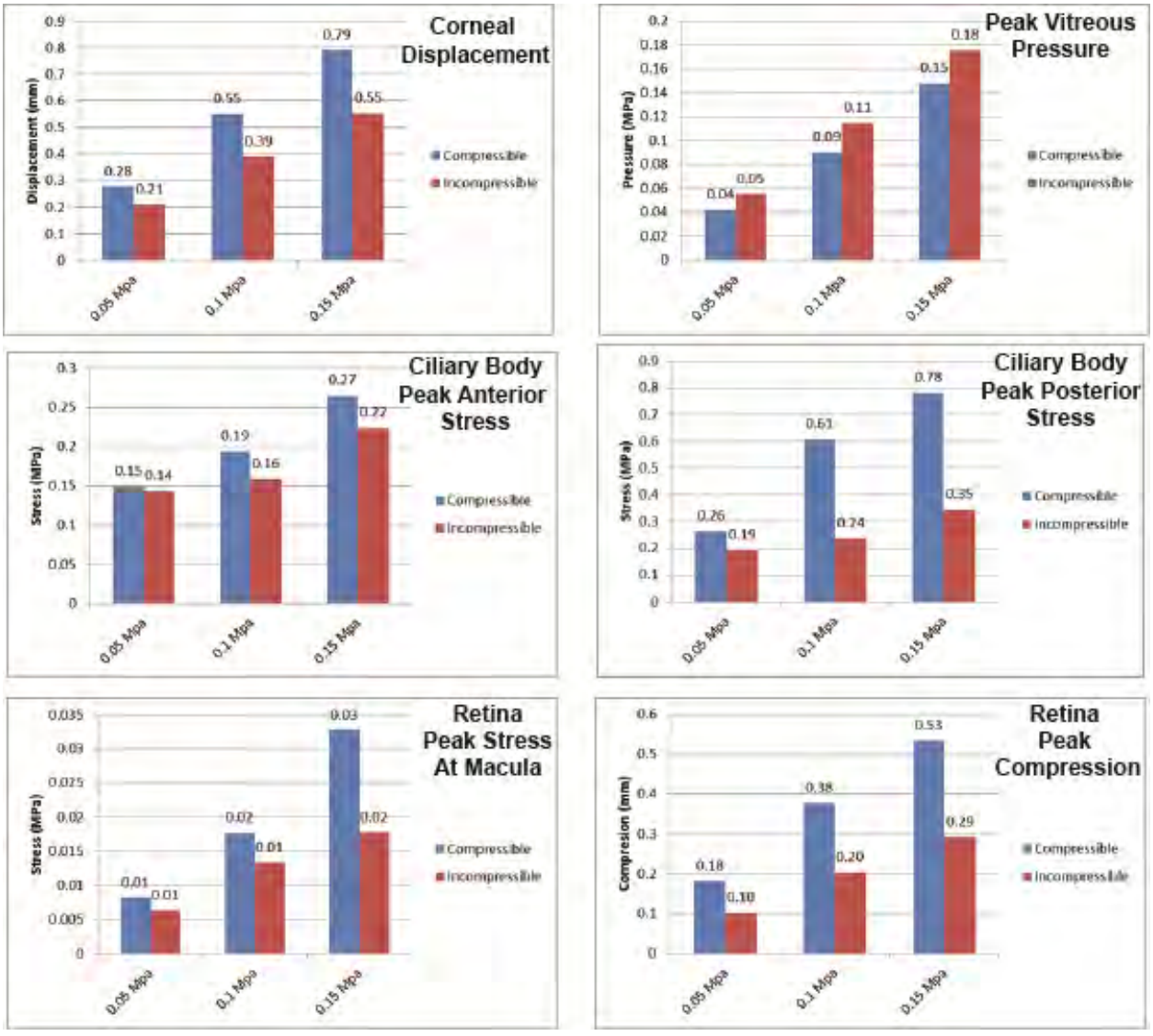

Figure 39. LS-DYNA Porcine Eye Model predictions for peak blast overpressure of 0.05 MPa, 0.10 MPa, and 0.15 MPa.

2.11.3 Model Predictions Compared to Experimentally Observed Trauma

For the range of primary blast overpressure used in the porcine eye experiments, the LS-DYNA model predicts that stress, pressure, and displacement will increase with higher levels of blast overpressure. Measurements included corneal apex displacement, pressure near the center of the vitreous, stress at the anterior and posterior surface of the ciliary body, stress and compression at the macula of the retina, and stress in the sclera (Figure 39). These metrics were selected to allow correlation with observable responses in the physical experiments. Corneal apex displacement can be visually

observed in the high speed video of the physical tests, though quantitative measurement is limited by spatial resolution. Stress in the ciliary body was of interest due to the number of angle injuries observed in the physical experiments. Scleral and retinal measurements of stress were also performed due to commonly observed damage in these regions during physical experiments. In the compressible retina model, all stress and displacement measures were lower than those for the incompressible retina model at all levels of blast. For pressure measurements this was reversed, with the less compressible model displaying higher pressure in the vitreous.

The response of the model to the blast was initial longitudinal compression and rearward displacement with equatorial expansion. The compression chiefly involved the anterior chamber, lens, and vitreous moving rearward while the posterior sclera remained largely in place. Following maximum compression, the model rebounded back toward its original shape while undergoing complex oscillations. Using the full positive and negative phase of the blast data, the model would avulse from the gelatin. Complete avulsion of the eye from the gelatin was observed in a number of the physical experiments at the 0.15 MPa blast level. Internally, the individual components of the model oscillated at different frequencies according to mass and stiffness. Overall displacement of the cornea at the highest level of blast, 0.15 MPa, was on the order of 1 mm, in agreement with high speed video of the physical blast experiments.

The model showed increased levels of stress in areas of injury found in the SLOT physical experiments, namely the ciliary body (angle), sclera, and retina (Figure 39a). The highest levels of stress were found in the sclera in the region of the vitreous base. These values ranged up to 1 MPa, and were approximately 75% higher for the compressible retina model than the incompressible model. The peak stress in this area was coincident in time with the initial compression phase of the eyeball over the first 1 ms of the simulation. The areas of maximum stress were found in the thinnest section of the sclera, adjacent to the vitreous base, centered longitudinally at the vitreous base attachment (Figure 40c). This section of the sclera acts as a hinge between the anterior and posterior chambers, which displayed relative differential movement in the model. The attachment of the relatively massive vitreous places additional stress on this area as it resonates out of phase with the movement of the sclera. The stress concentration in this area correlated well with the equatorial location of scleral delamination observed in the physical experiments (Figure 40c).

The next highest levels of stress were found in the ciliary body at its posterior surface, ranging up to 0.8 MPa (Figure 40b). The stress in this region was induced by differential movement with the attached vitreous, occurring later in time compared to the nearby stress in the sclera, coincident with the initial rebound of the anterior chamber following its rearward displacement at the onset of the blast wave. Again, the level of regional stress was decreased in the incompressible retina model. The anterior surface of the ciliary body returned stress levels up to 0.27 MPa when subjected to the most severe blast. The source of this stress appeared to be fluctuating pressure in the aqueous humor.

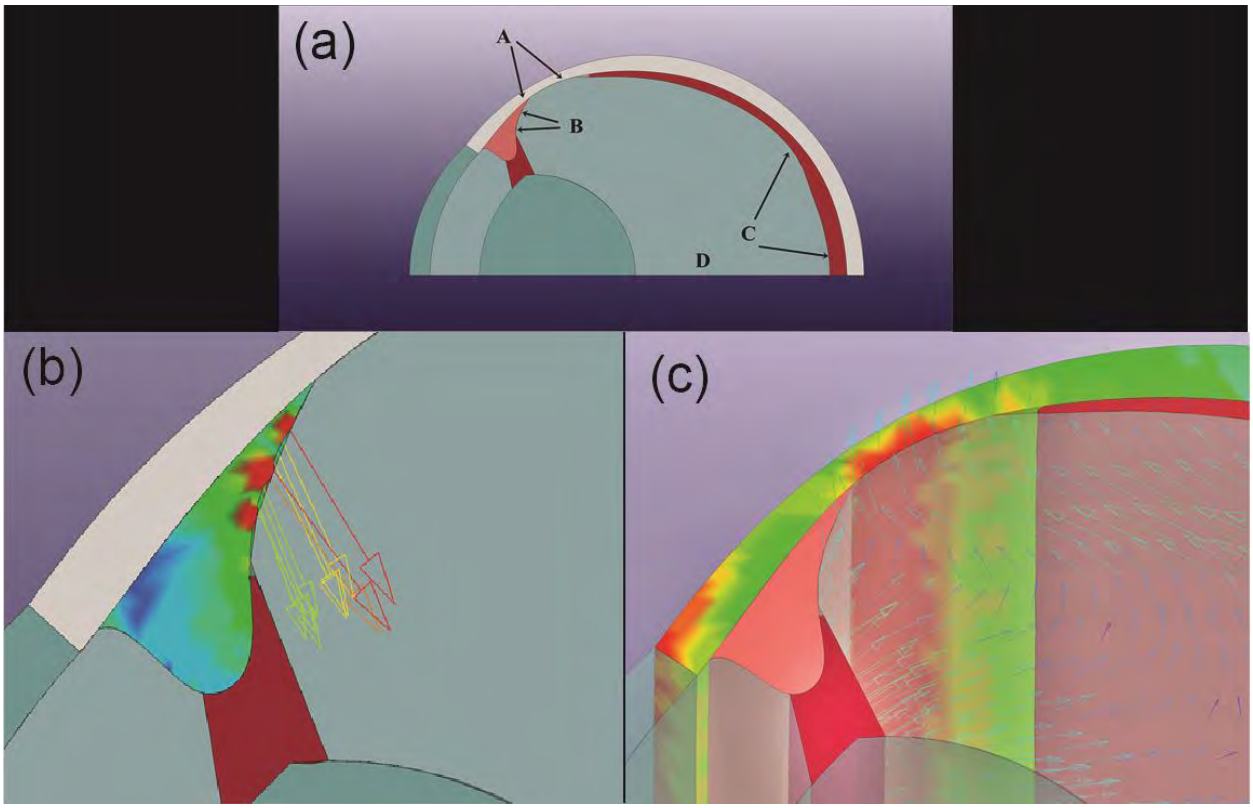

Figure 40. (a) The model showed increased levels of stress in areas of injury found in the SLOT physical experiments, namely the ciliary body (angle), sclera, and retina. Arrows show instantaneous movement of (b) vitreous relative to ciliary body, and (c) vitreous relative to zonules and sclera.

Angle recession and cyclodialysis were the most common findings in the physical experiments. The model suggests a possible mechanism for these injuries as the ciliary muscles are pulled on by the vitreous from behind at the same time the anterior portion of the sclera to which the ciliary muscles are attached rebounds forward. This finding merits follow on work with a more detailed description of the individual ciliary muscles and zonules. Material property testing of the ciliary muscles and their adhesion to the vitreous and sclera would benefit this effort.

Rearward displacement of the vitreous compressed the retina between the vitreous and the sclera. This compression occurred with both the compressible and incompressible retina material properties. The maximum compression of the retina predicted by the compressible model was a 62% decrease in thickness at the retinal apex, with 33% compression in the incompressible retina model. For the highest level of blast, peak pressure on the retina was 0.36 MPa in the incompressible model and 0.30 MPa for the compressible model. Stress levels in the retina were an order of magnitude lower than the pressure, 0.02 to 0.03 MPa. Retinal detachments were among the most serious injuries in the porcine blast experiments. The model indicates a coup-contre-

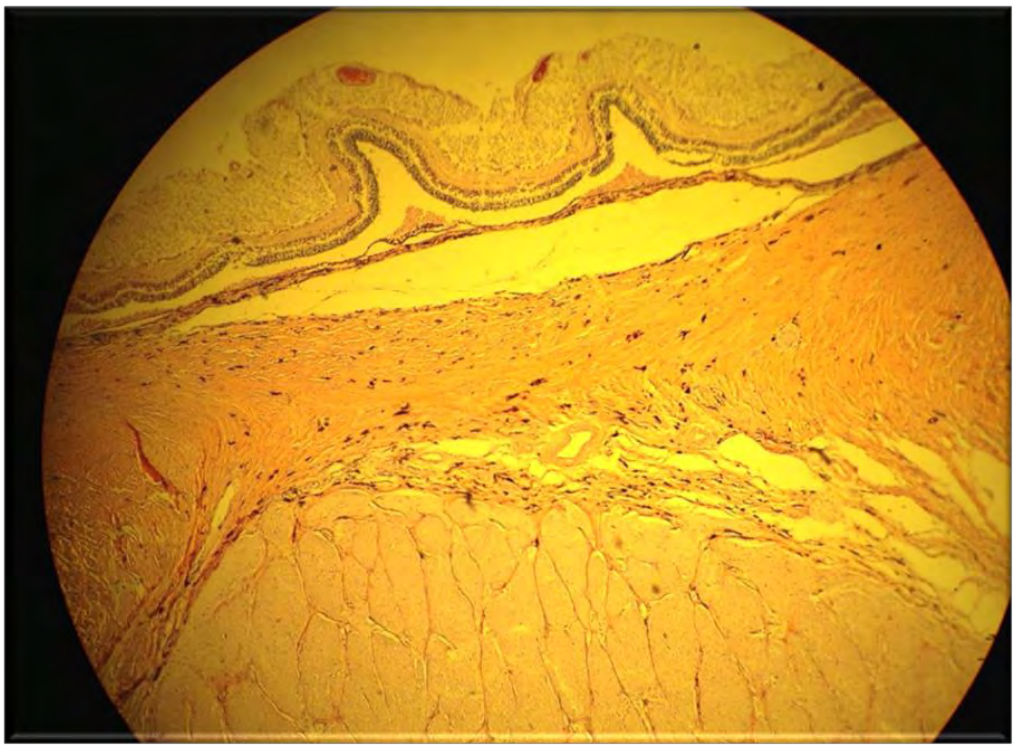

Figure 41. Retinal detachment in region of blood vessel observed during one of the porcine blast experiments

coup mechanism of injury to the retina due to the movement of the vitreous. The findings on retinal dynamics merit further work with more detail. It is known that the retina is non-homogenous, with blood vessels throughout it. Histopathology suggests that the junction between the different material properties of the retina and blood vessel is susceptible to the initiation of a retinal detachment (Figure 41). The optic nerve head presents the same type of discontinuity, along with the tethering effect of the optic nerve. Though modeling these very thin tissues would be computationally intensive it may be possible to create smaller sub models based on the overall loading conditions determined with the present whole-eye model.

Differential movement of internal structures, particularly the vitreous was shown to be a likely mechanism of injury to the retina, sclera, and ciliary body. The vitreous accounts for more than 50 percent of the mass of the eyeball, is largely incompressible, and is strongly attached to the sclera and ciliary body over a relatively small area. These characteristics contribute to the stresses imposed by the movement of the vitreous on smaller and more delicate structures of the eye. The characteristics of the retina, mainly the compressibility, play a role in determining the magnitude of movement of the vitreous and in turn the amount of stress at the sclera and ciliary body. The model shows that loading by sub-lethal levels of blast overpressure is capable of causing internal injury to the eye, warranting careful examination of the eyes of those exposed to survivable blast.

2.11.4 Limitations of the FEA Model

Dynamic FEA models of soft tissue structures are subject to certain limitations. The primary limitation is the lack of material properties derived specifically for use in a computational model intended to simulate high loading rates. Though the material models are capable of simulating rate effects and anisotropy, few tissues are characterized this way, particularly for the extremely rapid loading imposed by blast. Though care was taken to ensure the model had a coherent response when compared to physical experiments, the addition of more detailed and specific material properties would significantly improve the model. Secondarily, the eye contains many small structures such as the zonules, blood vessels, iris, lamina cribosa, et cetera. These structures are of interest when characterizing certain injuries. However, modeling them with FEA as part of a larger overall model of the eye would require extremely fine mesh, leading to a very computationally expensive model. Finally the internal contacts between tissues in the eye have not been characterized and are therefore not well defined in the FEA model. The connection between the vitreous and retina in particular is not well quantified. The dynamics of the model in this work show that any connection between the vitreous and retina would induce traction force on the retina, contributing to retinal detachments.

2.11.5 CTH

CTH modeling efforts focused on modeling blast wave generation in the shock tube. The objective was to investigate the initial loading conditions required to generate Friedlander waveforms similar to those observed in the porcine eye experiments, i.e., sharp shock front with correct peak pressure and pulse width. Unlike LS-DYNA where the pressure-time history can be directly input to the program, CTH must generate the waveform as part of the computation. In this case, a volume of high pressure air is placed in the upstream end of the shock tube and allowed to propagate toward the open end of the shock tube. This is analogous to pressurizing the shock tube's driver section and allowing the aluminum disk to rupture. As air propagates down the tube, a shock front or Friedlander waveform develops (Figure 42).

Due to symmetry, a 2-D geometrical model was deemed adequate for simulating the performance of the shock tube. Each computational cell was 0.25 x 0.25 cm in size resulting in a total of 164,000 cells. An embedded tabular equation of state model (SESAME table) was used to simulate the air, and the shock tube is modeled as a rigid (impermeable, non-moveable) material. In the initial trials the correct pulse width (~ 2 ms) was consistently achieved for a number of peak pressures, but the negative pressure phase (see Figure 2) was not achieved. However, through trial and error we were able to replicate this by using a sound speed absorbing boundary condition (condition 1 in CTH) at the open end of the tube. The choice of this particular boundary condition was not an obvious choice, as our first inclination was to allow the air to exit the open end (condition 2 in CTH). However, this did not consistently produce the desired negative pressure phase, and on occasion caused the computation to terminate

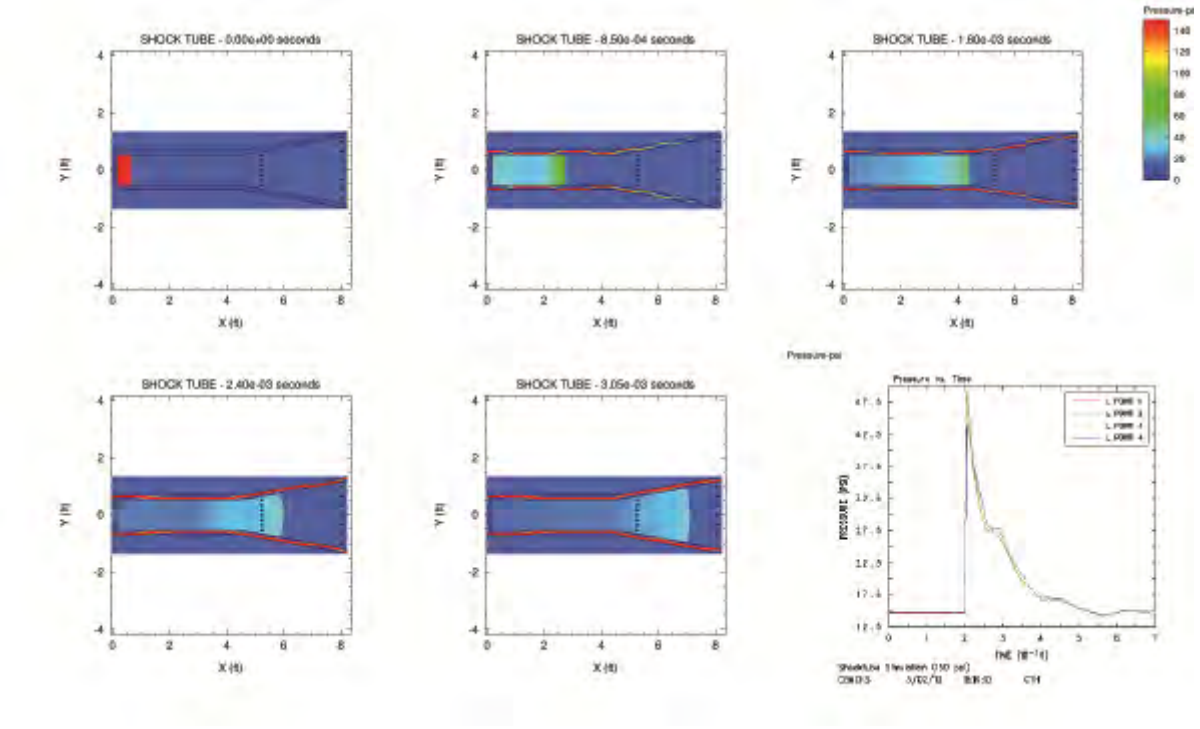

Figure 42. CTH simulation of the shock tube. The simulation is started by placing a volume of high pressure air at the upstream end and allowing it to propagate down the tube. The shock front (Friedlander waveform) develops at the open end.

early due to mass balance errors. CTH assumes mass conservation in the calculations, so letting mass exit the computational grid sometimes results in non-convergence during iteration.

The next series of CTH computations placed an eye-orbit mimic model at the open end of the tube in a configuration similar to that employed in the porcine eye experiments (Figure 43). The eye-orbit mimic assembly was held in place with a rigid tube that was fixed in place (not allowed to move in the computations) and extended out the open end of the tube. Due to the rotational symmetry of the eye, an axisymmetric model was utilized with the eye centerline as the axis of rotation. The small thickness of the ocular tissues (e.g., sclera ~ 1 mm) required a much more refined grid than was used in the shock tube simulations. A grid size of 0.20 x 0.20 cm was chosen to ensure at least 5 computational cells across the scleral thickness. This resulted in approximately 1.4 million computational cells with run times in excess of 1 week.

Dimensional and geometric details of the eye and orbit were taken predominately from a single reference; Wolff's Anatomy of the Eye and Orbit, 8th Edition (Bron et al., 2001). The structures important to modeling dynamic response and trauma were identified as the cornea, aqueous humor, iris, zonule, lens, vitreous, sclera, retina, and and choroid (Figure 43b). The sclera, retina, and choroid have been combined into a

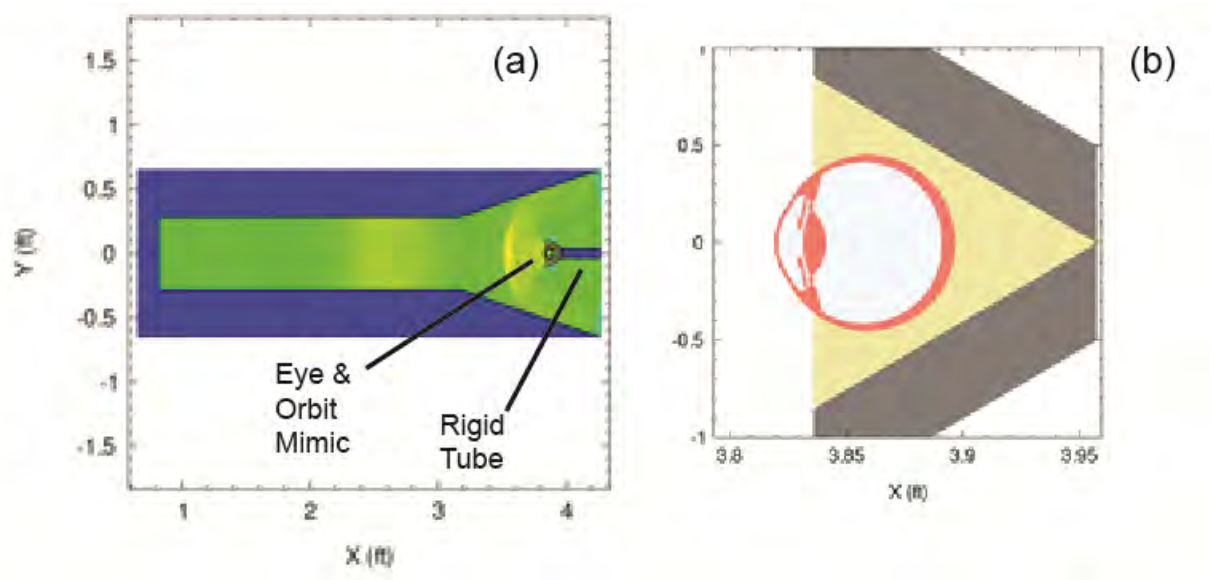

Figure 43. (a) CTH model of the shock tube with eye-orbit mimic included. The eye-orbit assembly is held in place by a rigid tube that is not allowed to move during the computations. (b) Close up of the eye-orbit mimic model. Note that gelatin is placed between the eye and orbit mimic to simulate the extraocular muscles.

Table 14. Mechanical Properties of the Ocular Tissues

	Density kg/m^3	Young's Modulus (Pa)	Poisson's Ratio	Sound Speed (m/s)	Yield Stress (Pa)	Failure Stress (Pa)	Heat Capacity J/(kg-K)	Guneisen Parameter	Up-Us Slope
Optic nerve	1400	6.56E+06	0.49	1540	1.50E+03		3664	0.1	2
Retina	1400	5.20E+03					3664	0.1	2
Dura	1400	3.58E+08	0.47	1540	9.40E+06	9.49E+06	3664	0.1	2
Lens	1079	6.89E+06	0.49	1540		1.75E+07	3664	0.1	2
Cornea	1400	1.24E+08	0.42	1540	9.40E+06	9.45E+06	3664	0.1	2
Iris	1400	1.24E+08	0.42	1540	9.40E+06	9.45E+06	3664	0.1	2
Ciliary Body	1400	3.58E+08	0.47	1540	9.40E+06	9.49E+06	3664	0.1	2
Zonule	1000	3.58E+08		1540			3664	0.1	2
Sclera	1400	3.58E+08	0.47	1540	9.40E+06	9.49E+06	3664	0.1	2
Choroid	1400	3.58E+08	0.47	1540	9.40E+06	9.49E+06	3664	0.1	2
Aqueous Humor	1003	--	--	1503	--	--	3664	0.1	2
Vitreous	1009	1.54E+05	0.49	1528	1.0E+1	1.57E+05	3664	0.1	2
Orbital Bone	1610	9.81E+10	0.35	2503	1.57E+08	1.57E+08	1256	0.1	2

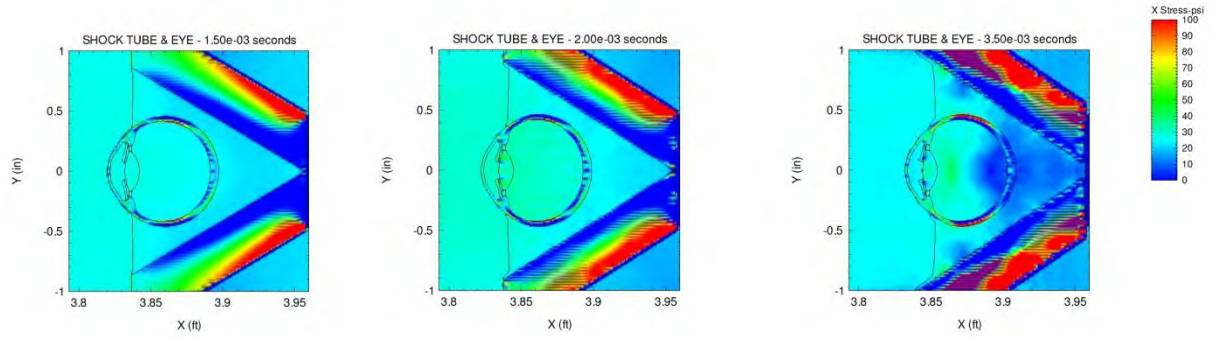

Figure 43. CTH simulation of 151 kPa peak pressure showing development of low level stress (~ 100 psi) in the mid-sclera regions of the eye. CTH simulations have shown that in early times stress is concentrated in the cornea, but propagates to the scleral regions at late times

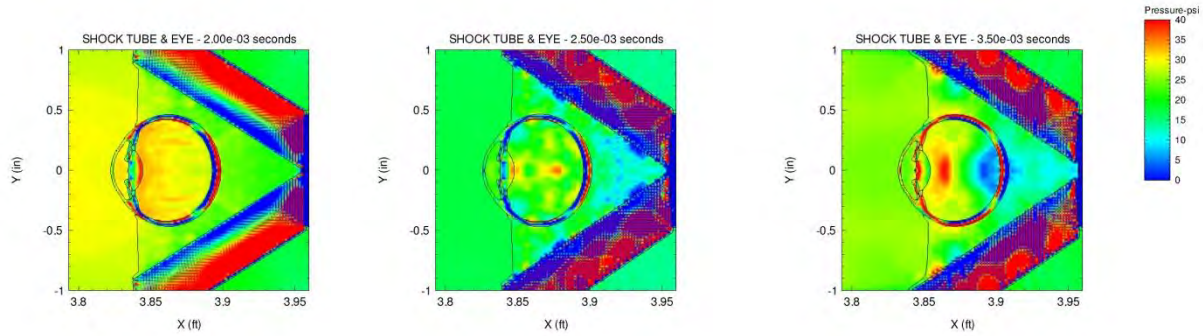

Figure 44. CTH simulation at 151 kPa peak pressure showing pressure reflection off posterior. Our research has suggested that such reflections may be responsible for retinal detachments.

single scleral shell as modeling the individual layers is not practical in CTH (due to their thinness). However, it has been shown in previous work that deformation and strain partitioning can be adequately modeled using a single scleral shell approach.

Representative mechanical properties of the ocular tissues used in the CTH model are presented in Table 14. The heat capacity, Gűneisen Parameter, and Up-Us slope (slope of Hugoniot curve) of all tissues were taken to be those of water. This assumption was considered reasonable as human tissue is thought to contain considerable water either in solution or suspension. In the simple model the retina, choroid, and sclera were modeled as a single membrane using the scleral properties. To simulate material response, a Mie-Grűneisen equation of state and a modified Johnson-Cooke constitutive model were used for each tissue.

A number of CTH calculations at the various blast pressure conditions observed in the porcine experiments are currently underway. Consistent with experimental

observations, peak blast pressures in the 48 kPa to 151 kPa range are producing low levels of stress and strain in the eyes, mostly in the corneal and scleral region (Figure 43). In early times (associated with blast wave arrival) stress is concentrated in the cornea, but propagates to the mid- and posterior scleral regions in late times. The propagating stress may be due to a minor flattening of the globe from pressure loading or simply a response to interior pressure wave propagation. In most of the simulations pressure reflections off the posterior can be observed (Figure 44). Our previous research with blunt impact events suggests that such reflections may contribute to retinal detachments.

3. KEY RESEARCH ACCOMPLISHMENTS

- Completion of 85 shock tube experiments on porcine eye specimens. Detailed procedures for preparation and blast testing of porcine eye specimens were developed and validated.

- Completion of pathology (including assessment of trauma types and levels) on 55 porcine eye specimens (42 blast exposures and 13 controls). The pathology assessment relied on post-blast screening using ultrasound techniques (UBM and B-scan), supplemented by limited dissection and histopathology. The ultrasound techniques provided clear information about the chorioretina (pre- and post-impact), but were unable to adequately resolve trauma in the angle region. Although dissection and histopathology helped resolve trauma in the angle region, the potential for artifact was present.

- Development of rigorous control procedures that allowed estimation of the relative effects of shipping, handling, mounting, preparation, tissue degradation, and re-pressurization of the globe in development of injuries not related to primary blast. These controls were included in every blast test performed.

- Development of a scoring methodology on a per-tissue basis that allowed for interpretation in the framework of the OTCS zone-based scoring system.

- Development of trauma risk curves for a number of sub-globe-rupture trauma categories.

- Development of a numerical model of overall visual incapacitation based on tissue-specific injury scores. The model was correlated with the blast characteristics of a typical improvised explosive device (IED), and predictions of level of incapacitation vs, distance from detonation point made.

- Completion of numerical simulations using software packages CTH and LS-DYNA. The LS-DYNA simulations were particularly fruitful in revealing mechanical response that contributes to chorioretinal trauma, namely oscillatory compression and tension on the retina during wave propagation through the eye.

Separation of the vitreous and retina, as observed in the simulations, may contribute to retinal detachments.

- Optic nerve specimens have been successfully cut and mounted in preparation for imaging using the Matrix Assisted Laser Desorption Ionization (MALDI) technique. The sections were mounted on the ITO slides from a methanol layer, and appear to have attached well on to the slides after evaporation of the methanol. Trauma-related proteins will be identified by the homology of the measured m/z spectra with protein sequences published in the UniProt database

- Development, submission, and approval of animal use protocol for *in vivo* rabbit blast exposures (A-14-007, approved by ISR IUCAC and the USAMRMC Animal Care and Use Review Office).

- Completion of 17 *in vivo* rabbit blast experiments with collection of blood and aqueous fluid sample for biomarker study.

- Completion of pre- and post-blast imaging on 17 rabbits including (1) Direct Ophthalmoscope, (2) Slit Lamp, (3) Fundus photography, (4) OCT (retinal), (5) HRT Corneal Conformal, and (7) Ultrasound (UBM, B-scan).

- Identification of potential trauma-related biomarkers of use in ocular trauma studies of the *in vivo* rabbit blast experiments.

4. REPORTABLE OUTCOMES

Two abstracts/posters were presented by the team at the 2013 ARVO Meeting in Seattle:

(1) A Computational Models for Investigation of Ocular Trauma Due to Primary Blast
(2) Primary Blast-Induced Ocular Trauma Modulated by Peak Pressure

Two abstracts/posters were presented by the team at the 2014 ARVO Meeting in Orlando:

(1) Computational Modeling of Internal Eye Injury due to Primary Blast
(2) The Identification of Trauma-Related Biomarkers Following Blast Injuries to the Eye

Four abstracts/posters were presented by the team at the 2015 ARVO Meeting in Denver:

(1) Effects of *in vivo* Isolated Low-level Primary Blast Overpressure in Dutch Belted Rabbit: Corneal and Retinal Tomographic Responses

(2) Simulations of Porcine Eye Exposure to Primary Blast Insult
(3) Risk of Injury to Ocular Tissues from Primary Blast Overpressure Exposure
(4) Biomarker Detection in Rabbits Following Primary Blast Using Luminex Bead-Based Assays

One abstract/poster was presented by the team at the Biomedical Engineering Society (BMES) Annual Meeting, September 25-28, 2013 in Seattle:

(1) Primary Blast-Induced Ocular Trauma

Three abstracts/posters were presented by the team at the Biomedical Engineering Society (BMES) annual meeting scheduled for October 22-25, 2014 in San Antonio, Texas:

(1) Blast Induced Traumatic Brain Injury: Detection through Immunocytochemistry and MALDI
(2) A Computational Model of the Porcine Eye
(3) Primary Blast Influences Incidence and Severity of Ocular Injury in a Porcine Eye Model

A paper titled *"Anatomical manifestations of primary ocular trauma observed in a post-mortem porcine model*" has been published in the journal *Investigative Ophthalmology and Visual Science* (2014; 55:1124-1132).

A paper titled "Simulations of Porcine Eye Exposure to Primary Blast Insult" has been accepted for publication in the journal *Translational Vision Science & Technology.*

A paper titled " Low-Level Primary Blast Causes Acute Ocular Trauma in Rabbits" has been submitted to the journal *Neurotrauma*.

Four Master's Degree theses have been completed by graduate students at UTSA under the supervision of SLOT team members and funded by the VRP Grant:

(1) Daniel Sherwood, Determining the probability of ocular trauma from survivable primary blast. [Master's Thesis], University of Texas at San Antonio, 2014.

(2) Richard Watson, A computational model of the porcine eye for investigation of primary blast. [Master's Thesis], University of Texas at San Antonio,2014.

(3) Kristin Jones, Assessment of acute ocular trauma in rabbits following sub-lethal primary blast exposure: [Master's Thesis], University of Texas at San Antonio,2015.

(4) Jessica Hernandez, Ocular trauma-induced changes in aqueous and plasma biomarker expression levels: [Master's Thesis], University of Texas at San Antonio,2015.

5. CONCLUSIONS

Blast experiments on enucleated porcine eye specimens and *in vivo* rabbits were conducted at the ISR Shock Tube Laboratory (STL) located at Joint Base San Antonio, Fort Sam Houston,TX. Although the magnitude of blast waves generated by the shock tube were below the whole body lethal criteria as predicted by Bowen et al. (1968), it none the less produced a broad array of closed-globe injuries, many of which would seriously compromise visual function and have both immediate and lifelong adverse effects. The experimental techniques and injury characterization methodologies offered an objective assessment as to which injuries were due solely to primary blast exposure (in the absence of blast-driven fragments and debris). Thus, the data generated in in this study has significantly increased our understanding of primary blast-induced ocular injury.

A notable strength of this study was the evaluation of the blast trauma using complimentary methods including UBM, B-scan, gross dissection and histopathology. Specifically, our results show that ultrasound scans give clear information about the chorioretina (pre- and post-impact) while dissection can result in artifact. Conversely, the ultrasound methods were unable to resolve angle recession while histological sections gave more reliable information regarding anterior segment damage. Pre-blast imaging each eye using ultrasound allowed exclusion of eyes that would otherwise contribute artifacts and improved confidence that any damage to the eye observed after blast exposure was due only to the primary blast effects (rather than preparation or other factors). In combination, these modalities assist in identifying intraocular injuries that could have lifelong adverse effects.

Previous blunt impact studies conducted with paintballs on enucleated pig eyes found ocular damage generally increases from minor angle recession to globe rupture over an impact energy range of 2-13.5 Joules (Sponsel et al., 2011). The present study found a similarly increasing trend in ocular damage with increasing blast energy (reflected specific impulse), but globe rupture was not observed, and globe distortion and movement were far less than in the paintball study. This may be due to several factors such as the lower energies associated with the blast, simultaneous compression of the periorbita, and distribution of the energy over the entire exposed surface rather than concentrating the load at the point of projectile impact. None the less, we observed a range in ocular injury severity including angle recession, internal scleral delamination, cyclodialysis, peripheral chorioretinal detachments and radial peripapillary retinal detachments. Petras et al., (1997) observed a similar trend in rats exposed to overpressures of 104 to 173 kPa. The most frequently observed injuries were angle recession and chorioretinal detachments, while the most severely damaged tissues were the sclera (delaminations) and retina (detachments). Some non-exposed control eyes exhibited damage to the angle, choroid and retina that was clearly not due to blast exposure. This may indicate continual degradation of the porcine eyes after the pre-screening ultrasound was performed, damage inflicted to the eye due to the presence of the gelatin, and/or other artifacts of the preparation. Still, incidence and severity of damage in the blast exposed eyes was significantly correlated with the reflected specific

impulse indicating that blast wave exposure alone (i.e., without fragments or other projectiles) caused the damage.

Porcine eyes were exposed to 6 peak reflected blast overpressure levels of approximately 35, 85, 115, 135, 155, and 230 kPa, and reflected specific impulses of approximately 26, 55, 85, 115, 130, and 210 Pa-s, respectively. Using terminology consistent with the Ocular Trauma Classification Score (OTCS, Pieramici et al., 1997), the majority of porcine ocular blast injuries were lamellar injuries. Probability of injury (angle recession, cyclodialysis, peripheral chorioretinal detachments, radial peripapillary retinal detachments, and internal scleral delamination) was found to increase with reflected specific impulse in Zone 1 (external surface) and Zone 3 (internal posterior segment), while no significant correlation was found in Zone 2 (interior anterior segment). Again, no full-thickness openings of the eyewall (scleral rupture) were observed in any of the eyes tested. Porcine eyes are known to have a higher mechanical strength than human eyes (Kennedy et al., 2007), suggesting that blast conditions that produce injuries in porcine eyes will likely induce more serious injuries in the human eye. Thus, the injury data generated from porcine eyes should be considered as a conservative estimate of injuries which might occur in human eyes under the same primary blast conditions.

During the *in vivo* rabbit blast experiments, rabbits were exposed to single peak reflected blast overpressure levels of approximately 55 kPa, 85 kPa, and 130 kPa, and reflected specific impulses of approximately 60, 100, and 160 Pa-s, respectively. An extensive imaging series was conducted on each rabbit before and after blast exposure to identify and characterize any blast-induced ocular trauma. The imaging included (1) Direct Ophthalmoscope, (2) Slit Lamp, (3) Fundus photography, (4) OCT (retinal), (5) HRT Corneal Confocal imaging, and (7) Ultrasound (UBM, B-scan) on both OD & OS eyes. Slit lamp images were used to observe any surface corneal damage as well as sphincter ruptures that could be present post-blast. No iris sphincter ruptures were observed in slit lamp images. B-scan and UBM images appeared normal with no indication of retinal detachment. Thicknesses of the cornea and inner retinal layers increased significantly with specific impulse immediately and 48 hours after blast exposure, providing new *in vivo* evidence of tissue damage due to primary blast. Clinically significant changes in corneal thickness arose immediately and were sustained through 48 hours, suggesting possible disruption of endothelial function. In addition results reveal an overall increase in the nerve fiber layer thickness after blast. The results reveal that survivable (non-lethal) primary blast overpressure can cause significant ocular damage in actively perfused living eyes. Likely clinical outcomes are decreased visual acuity (due to increased corneal light scattering), and retinal swelling with potential for subsequent detachment. However, because our study only examined rabbits up to 48 hours post blast, whether or not these injuries eventually repair themselves was not determined.

It is noteworthy that isolated primary blast was able to produce ocular compromise in the living rabbit eye at levels of overpressure typically much lower than those employed in the ex vivo porcine eyes. The repeated measures ANOVA results from OCT sectorial

analysis of the exposed rabbit eyes revealed an overall increase in the nerve fiber layer (μm) after blast (p-value = 0.008). This retinal thickening was confirmed upon masked histopathologic analysis to be associated with significant disruption of the innermost Mueller cell membranes, cells that traverse the retina and sequester the nerve fiber layer axons segmentally into the so-called inner limiting membrane. This disruptive inner retinal damage increased in extent with increasing blast overpressure. Such disruption would be expected to be associated with immediate and protracted compromise of retinal signal transmission to the optic nerve. Corneal edema was also observed subjectively in slit lamp images confirmed with HRT tomography measurements. This edema was generally mild (~10%) but arose rapidly at all blast levels and was sustained through the study follow-up interval, suggesting that normal endothelial cell mediated recovery was compromised. Even without the aforementioned more serious retinal damage, this level of corneal thickening would be expected to immediately decrease visual acuity by a factor of 3, sufficient to compromise the functional viability of any warfighter. The blast overpressure levels used in all the rabbit studies would be expected to be readily survivable at any distance >25 feet. Thus, it appears that primary blast can cause ocular compromise of both practical and clinical significance, independent of any schrapnel, head and body acceleration/deceleration phenomena, heat, toxicity, or post-impact infection or inflammation.

Aqueous and blood plasma samples were drawn from each of the blast-exposed and control rabbits in order to evaluate the release of trauma-related biomarkers into the injured eye and the host circulatory system. Samples were taken at intervals of pre-blast (baseline) as well as 3, 24, and 48 hours post blast. Immunoassays of protein markers were carried out using Luminex technology, bead-based multiplexed assays using two magnetic bead millipore kits; (1) Milliplex Rat Cytokine/Chemokine Panel (RECYMAG65K27PMX), and (2) Milliplex Human Neurological Disorders Panel (HND1MAG-39K). In the Human Neurological assay panel both NGF-β and NSE in the blood plasma were significantly correlated with blast specific impulse, but for aqueous humor samples, no biomarkers showed significant correlations. In the Rat Cytokine assay panel G-CSF in the aqueous humor along with Eotaxin, MIP-1a, Il-4, IL-13, IL-12(p)70, MCP-1, LiX, and MIP-2 in the blood plasma were significantly correlated with blast specific impulse.

The computational eye models provided the opportunity to visualize the interior structures of a surrogate eye during the extreme dynamics of a blast event and provided insight into mechanisms of primary blast injury. Of particular interest was the response of the LS-DYNA model at the interface of the vitreous and retina. A series of snapshots of the model progressing forward in time revealed motion of the vitreous as it encountered the retina, compressing it and the choroid against the sclera. This compression is followed by rebound of the vitreous away from the retina. Given the reported tensile strength of the choroid and retina, this finding indicates a high likelihood of damage to the retina via the interaction with the vitreous in both tension and compression. The degree of compression of the retina was related to the peak blast overpressure, with maximum compression occurring at the highest blast overpressures.

Statistical analysis of the physical experiments also showed increasing risk of retinal injury with the higher blast overpressures.

Differential movement of internal structures, particularly relative to the vitreous was shown to be a likely mechanism of injury to the retina, sclera, and ciliary body. The vitreous accounts for more than 50 percent of the mass of the eyeball. It is largely incompressible and strongly attached to the retina and ciliary body over a relatively small area. These characteristics contribute to the stresses imposed by the movement of the vitreous on the smaller and more delicate structures of the eye. The characteristics of the retina, mainly its compressibility, play a role in determining the magnitude of movement of the vitreous and in turn the amount of stress at the sclera and ciliary body. Consistent with the experimental findings, the computational modeling also revealed that blast loading at sub lethal levels is capable of causing internal injury to the eye, warranting careful examination of the eyes of those exposed to survivable blast.

A simplified predictive model for soldier ocular incapacitation risk was developed by combining tissue risk data into three broad ocular integrity categories (1) optical integrity, (2) neurophysiological integrity, and (3) structural Integrity. The model is based largely on the *ex vivo* porcine eye experiments and tissue-specific injury scores with predictions plotted against reflected specific impulse. Additional military and clinical input will be needed to map this incapacitation score to a metric for mission readiness, but the model can predict acute or chronic concerns if the blast characteristics of the weapon or scenario are known, specifically the reflected specific impulse. To place the results in a more recognizable context a commonly encountered blast scenario was analyzed and the associated incapacitation model predictions outlined. For this illustrative example we chose to simulate the blast of a standard US M107 155mm artillery projectile. This projectile is very similar to a Soviet 152mm artillery projectile which was commonly used as an improvised explosive device (IED) against American soldiers and Marines in Iraq and Afghanistan. The model predicts the likelihood of incapacitation in each category as a function of distance from the detonation point. For example, the model predicts that for distances of less than 20 feet from the detonation point (of the 155 mm projectile) half of all exposed personnel will experience 100% total ocular incapacitation, decreasing to approximately 80% total incapacitation at 30 feet, and 45% total ocular incapacitation at 40 feet.

The results of our controlled porcine experiments and numerical simulations provide a sobering new revelation as to the ocular risks from the isolated effects of primary blast. Unfortunately, the implications for human blast victims are even worse. The pig eye is thicker and stronger than the human eye, with a strength factor estimated as twofold higher according to experimental studies carried out for automotive impact (Kennedy et al., 2006). Thus, the proportion of human eyes sustaining severe incapacitation at any non-lethal (whole body) distance from the detonation point would likely be substantially greater than predicted by our data, and the distances at which incapacitation could arise would likely be significantly further than those determined experimentally using the pig model.

Although the abattoir-fresh porcine eye model remains a relatively inexpensive and efficient model for study, its general relationship to human ocular injury levels needs to be more carefully examined, especially for blast. Further controlled blast studies with preserved eye bank human donor eyes would be one option for determining the extent of this difference. Extrapolation by innovative use of computer modeling is also an option, but may be limited due to a general lack of knowledge about tissue response in dynamic blast environments. It is hoped that future research funding can be made available for basic research aimed at tissue property characterization and development of high fidelity tissue constitutive models. Another practical approach would be to perform a forensic review of daily accident/battlefield incident reports for survivors of documented explosions. The distance from the explosive device is typically recorded, and the unit designations and specific personnel involvement is also typically a matter of record. Overpressure effects of primary blast are minimally affected by the position of non-enclosing barriers or body attitude. Thus knowing the distance of a group of exposed warfighters from a blast may be sufficient information for a productive analysis. Unit designations could be matched with available VA records of survivors, and comprehensive ophthalmological examinations could be carried out to characterize and quantify the nature and extent of any longstanding ocular injury.

6. REFERENCES

Asejczyk-Widlicka M., Pierscionek B. K., 2008, The elasticity and rigidity of the outer coats of the eye, *Brittish Journal of Ophthalmology*, 92:1415-1418.

Bandyopadhyay S, Hennes H, Gorelick MH, Wells RG, WalshKelly, CM.,2005, Serum neuron-specific enolase as a predictor of short-term outcome in children with closed traumatic brain injury, *Academic Emergency Medicine*, 12, 732:738.

Bowen, I.G., Fletcher, E.R., and Richmond, D.R., 1968, Estimate of Man's tolerance to direct effects of air blast: Defense Atomic Support Agency Report, DASA 2113, 44 p.

Bron, A.J., Tripathi, R.C., and Tripathi, B.J., 1997, *Wolff's Anatomy Of The Eye And Orbi, 8th Edition,* Hodder Arnold Publishers, London, 736 p.

Burd, H.J., Judeg, S.J., and Cross, J.A., 2002, Numerical modeling of the accommodating lens, *Vision Research*, 42: 2235-2251.

Chen, I.-Fang. et al., 2013, Anti-nociceptive effect of IL-12p40 in a rat model of neuropathic pain. *Science Direct*, 62(3): 401-406.

Choong, M. et al., 2004, LIX: A chemokine with a role in hematopoietic stem cells maintenance. *Science Direct*, 25(6): 239-245.

Collett, D., 2003, *Modeling Binary Data*: Chapman & Hall, New York, 228 p.

Covaceuszach, S., Capsoni, S., Ugolini, G., Spirito, F., Vignone, D., Cattaneo, A., 2009, Development of a non-invasive NGF-based therapy for Alzheimer's disease. *Currente. Alzheimer Research*. 6:158-170.

Delori, F., Pomerantzeff, O., and Cox, M.S., 1969, Deformation of the globe under high-speed impact, Its relation to contusion injuries*: Investigative Ophthalmology and Visual Science*, 8:290-301.

Duke-Elder S, 1954, Concussion injuries, Text-book of Ophthalmology, Vol VI: Injuries, Henry Kimpton, London: 5751-5961.

Duma, S.M., Ng, T.P., Kennedy, E.A., Stitzel, J.D., Hering, I.P., and Kuhn, F.,2005, Determination of significant parameters for eye injury risk from projectiles, *Journal of Trauma*, 59,: 960-964.

Duma S, and Kennedy, E., 2011, Final Report: Eye Injury Risk Functions for Human and FOCUS Eyes: Hyphema, Lens Dislocation and Retinal Damage: USAMRMC report W81XWH-05-2-0055, 66 p.

Esposito, L., Clemente, C., Bonora, N., Rossi, T., and, 2013, Modeling human eye under blast loading, Computer Methods in Biomechanics and Biomedical Engineering, http//www.dx.doi.org/10.1080/10255842.2013.779684.

Fortea, J. (2014). Cerebrospinal fluid β-amyloid and phospho-tau biomarker interactions affecting brain structure in preclinical Alzheimer disease, *Annals of Neurology,* 76(2):223-30.

Gardner, J. et al., 2014, G-CSF drives a posttraumatic immune program that protects the host from infection, *The Journal of Immunology,* 192:2405-2417

Gray, W., Weiss, C.E., Sponsel, W. E, 2008b, Computational and experimental study of paintball impact ocular trauma, *Proceedings 24th International Symposium on Ballistics*, 1260-1267.

Gray, W., Sponsel, W.E., Scribbick, F.W., Stern, A.R., Weiss, C.E., Groth, S.L.,and Walker, J.D., 2011, Numerical modeling of paintball impact ocular trauma: Identification of progressive injury mechanisms, *Investigative Ophthalmology and Visual Science*, 52: 7506-7513.

Haschek, W., Rousseaux, C., Wallig, M., 2013, *Haschek and Rousseaux's Handbook of Toxicologic Pathology*, 3rd ed, Elsevier, Amsterdam, 2963 p.

Hines-Beard, J., Marchetta, J., Gordon, S., Chaum,E., Geisert, E, and Rex, T., 2012, A mouse model of ocular blast injury that induces closed globe anterior and posterior pole damage, *Experimental Eye Research*, 99: 63-70.

Hyek-Choi, J., Greene, W., and Johnson, A., 2014, Pathophysiology of blast-induced ocular trauma in rats after repeated exposure to low-level blast overpressure, *Clinical and Experimental Ophthalmology,* 43 (3): 239-246

Kennedy, E.A., Voorhies, K.D., Herring, J.P., Rath, A.L., and Duma, S.M., 2004, Prediction of severe eye injuries in automobile accidents static and dynamic rupture of the eye, *Annu Proc Assoc Adv Automot Med*, 48: 165-179.

Kennedy, E.A., Ng, T.P., McNally, C., Stitzel, J.D., and Duma, S.M., 2006, Risk functions for human and porcine eye rupture based on projectile characteristics of blunt objects, Stapp Car Crash Journal, 50: 651-671.

Kennedy, E.A., McNally, C., and Duma, S.M., 2007, Experimental techniques for measuring the biomechanical response of the eye during impact, *Biomedical Science Instrumentation*, 43: 7-12.

Kennedy, E.A., and Duma, S.M., 2008, The effects of the extraocular muscles on eye impact force-deflection and globe rupture response, *Journal of Biomechanics*, 41: 3297-3302.

Lawrence, D., 2002, Intranasal delivery could be used to administer drugs directly to the Brain, *Lancet*, 359: 1674.

Liu, X., Wang, L., Wang, C. et al., 2013. Mechanism of traumatic retinal detachment in blunt impact: a finite element study, *Journal of Biomechanics,* 46: 1321–1327.

Mader, T.H., Carroll, R.D., Slade, C.S., George, R.K., Ritchey, J.P., and Neville, S.P. 2006, Ocular war injuries of the Iraq insurgency, January-September 2006. *Ophthalmology,* 113: 97-104.

Needham, C.E, 2010, Blast Waves in *Shockwave and High Pressure Phenomena. Springer. 859 p.*

Olsen, T.W., Sanderson, S., Feng, X., and Hubbard, W.C., 2002, Porcine sclera: thickness and surface area, *Investigative Ophthalmology and Visual Science*, 43(8): 2529–2532.

Panzer, M.B., Myers, B.S., and Bass, C.R., 2013, Mesh considerations for finite element blast modelling in biomechanics, *Computer Methods in Biomechanics and Biomedical Engineering, 16*: 612–621.

Petras, J.M., Bauman, R.A., and Elsayed, N.M., 1997, Visual system degeneration induced by blast overpressure, *Toxicology,* 121: 41-49.

Pieramici, D., Sternberg, P. Aaberg, T.M et al, 1997, A system for classifying mechanical injuries of the eye (globe), *American Journal of Ophthalmology*, 123: 820-831.

Power, E.,D., 2001, A nonlinear finite element model of the human eye to investigate ocular injuries from night vision goggles, [Thesis] Virginia Polytechnic Institute and State University, Blacksburg,Virginia, 147 p.

Proud, W.G., Goldein, H.T., Esmail, S., and Willianson, D.M., 2009, A review of wound ballistics literature: the human body and injury processes: Security and Use of Innovative Technologies Against Terrorism (Teixeria-Das et al., Editors), Universidade de Aveiro, 67-82.

Qiushi, L., et al., 2014, Intranasal Nerve Growth Factor Attenuates Tau Phosphorylation in Brain After Traumatic Brain Injury in Rats, *Journal of the Neurological Sciences, 345:* 48-55.

Richmond, D.R., and White, C. S., 1962, A tentative estimation of Man's tolerance to overpressures from air blast, Lovelace Foundation for Medical Education and Research, 34 p.

Richmond, D.R., Damon, E.G., Fletcher, E.R., Bowen, I.G., and White, C.S., 1966, The relationship between selected blast-wave parameters and the response of mammals exposed to air blast: Lovelace Foundation for Medical Education and Research, 36 p.

Richmond, D.R., Yelverton, J.T., Fletcher, E.R., and Phillips, Y.Y., 1985, Biologic response to complex blast wave: Ninth International Symposium MABS 9, Oxford, England (Los Alamos Report 20000926 077).

Reilly, M.A., Hamilton, P.D., Perry, G, and Ravi, N., 2009. Comparison of the behavior of natural and refilled porcine lenses in a robotic lens stretcher, *Experimental Eye Researc,* 88: 483–494.

Rossi T, Boccassini B, Esposito L, et al., 2012, Primary blast injury to the eye and orbit: finite element modeling, *Investigative Ophthalmology and Visual Science,* 53:8057-8066.

Sanchez, R., Martin, R., Ussa, F., and Fernandez-Bueno, I., 2011, The parameters of the porcine eyeball. *Graefe's Archive for Clinical and Experimental Ophthalmology,* 249: 475–482.

Sherwood D, Sponsel WE, Lund BJ et al. 2014, Anatomical manifestations of primary blast ocular trauma observed in postmortem porcine model: *Investigative Ophthalmology and Visual Science* , 55: 1124-1132.

Sigal, I.A., Flanagan, J.G., Tertinegg, I., and Ether, C.R., 2005, Factors influencing nerve head biomechanics, *Investigative Ophthalmology and Visual Science*, 46: 4189-4199.

Sponsel, W.E., Gray, W., Scribbick, F.W., Stern, A.R., Weiss, C.E., Groth, S.L.,and Walker, J.D., 2011, Blunt eye trauma: Empirical histopathologic paintball impact thresholds in fresh mounted porcine eyes, *Investigative Ophthalmology and Visual Science*, 52: 5157-5166.

Stuhmiller, J.H., 2008a, Blast Injury: Translating research into operational medicine, Textbook of Military Medicine, Borden Research Institute.

Stuhmiller, J.H., 2008b, Blast Injury: Translating research into operational medicine: Chapter 10, Ophthalmic Care of the Combat Causality, Textbook of Military Medicine, Borden Research Institute.

Stitzel JD, Duma SM, Cormier JM, Herring IP. 2002, A nonlinear finite element model of the eye with experimental validation for the prediction of globe rupture, *Stapp Car Crash J*, 46:81-102.

Stewart, C., 2006, Blast injuries: Preparing for the inevitable, *Emergency Medicine Practice*, 8: 1-28.

Thach, et al., 1999, Ocular injuries from paintball pellets, *Ophthalmology*, 106: 533-537.

Thach, et al., 2008, Severe eye injuries in the War in Iraq, 2003-2005, *Ophthalmology,* 115: 377-382.

Tian, L. et al., 2012, Intranasal Administration of Nerve Growth Factor Ameliorate β-amyloid Deposition after Traumatic Brain Injury in Rats, *Brain Research,1440: 47-55.*

Watson, R., Gray, W., Sponsel, W.E., Lund, B.J., Glickman, R.D. and Reilly, M.A., 2014, Simulations of Porcine Eye Exposure to Primary Blast Insult, *Translational Vision Science and Technology* (in press).

Weichel, E.D., Colyer, M.H., Baustista C., Bower, K.S., and French, L.M., 2009, Traumatic brain injury associated with combat ocular trauma, *Journal of Head Trauma Rehabilitation*, 24: 41-50.

Van Horn, D.L., Hynduak, R.A.,Edelhauser, H.F., McDonald, T.O., and DeSantos, L.M., 1977, Ultrastructural alterations associated with loss of transparency in Buphthahnic rabbits, *Experimental Eye Research*, 25:171-182.

Yang J, Caprioli RM., 2011, Matrix sublimation/recrystallization for imaging proteins by mass-spectrometry at high spatial resolution. *Analytical Chemistry*, 83:5728-5734.

Yoo L, Reed J, Shin A, et al. 2011, Characterization of ocular tissues using microindentation and hertzian viscoelastic models, *Investigative Ophthalmology and Visual Science*, 52: 3475-3482.

Zurek, J., Fedora, M., 2011, The Usefulness of S100B, NSE, GFAP, NF-H, secretagogin and Hsp70 as a Predictive Biomarker of Outcome in Children with Traumatic Brain Injury, Acta Neurochir (Wien),154(1):93-103;.

APPENDIX I

Summary of Porcine Blast Experiments and Observed Trauma

Experiment Set	20130110-1	20130110-2	20130110-3	20130117-3	20130117-4
Side-on Press (kPa)	49.3	99.6	152.4	47.4	119.2
Side-on Duration (ms)	2.15	2.44	2.67	2.23	2.56
Side-on Impulse (Pa-sec)	52.98	113	162.8	53.37	136.4
Reflected Pressure (kPa)	91.9	170.3	251.1	86	214.9
Reflected Impulse (Pa-s)	60.27	147.7	238.4	61.04	190.5
Reflected Duration (ms)	2.22	2.64	3.01	2.26	2.99
Reflected Min Pressure (kPa)	-23.3644	-33.4366	-40.1635	-23.6532	-35.6711
Reflected Neg. Phase Duration (ms)	16.8300	16.3500	15.8800	16.7450	16.0050
Reflected Neg. Impulse (Pa-s)	-0.0698	-0.0781	-0.0981	-0.0694	-0.0949
Reflected Pressure Difference (Pa)	115.3026	203.7023	290.8268	109.6784	250.3748
Injury (CIS) Score					
Angle	2	2	0	3	3
Anterior Chamber	0	0	0	0	0
Choroid	1	1	3	2	3
Cornea	0	0	0	0	0
Iris	0	0	0	0	0
Lamina Cribosa	0	0	0	0	1
Lens	0	0	0	0	0
Optic Nerve	0	0	0	0	1
Retina	0	1	3	0	3
Sclera	0	0	3	1	1
Zone 1	0	0	3	1	1
Zone 2	2	2	0	3	3
Zone 3	1	1	3	2	3

Experiment Set	20130117-2	20130117-6	20130124-2	20130124-6	20130124-7
Side-on Press (kPa)	134.3	23.8	82.8	21.8	138.9
Side-on Duration (ms)	2.58	2.12	2.35	2.16	2.68
Side-on Impulse (Pa-sec)	165.5	27.36	93.61	26.7	171.4
Reflected Pressure (kPa)	256.8	49.1	144.7	48.6	259.6
Reflected Impulse (Pa-s)	239.8	29.58	116.8	28.75	252.7
Reflected Duration (ms)	3.07	2.23	2.55	2.19	3.1
Reflected Min Pressure (kPa)	-42.8147	-11.8463	-29.7088	-11.2142	-42.5394
Reflected Neg. Phase Duration (ms)	15.9250	16.7550	16.4450	16.8050	13.8450
Reflected Neg. Impulse (Pa-s)	-0.0996	-0.0325	-0.0791	-0.0321	-0.1093
Reflected Pressure Difference (Pa)	299.0413	60.9561	174.3767	59.8595	301.5798
Injury (CIS) Score					
Angle	2	2	3	2	3
Anterior Chamber	0	0	3	0	0
Choroid	4	3	0	3	2
Cornea	0	0	0	0	0
Iris	0	3	0	0	0
Lamina Cribosa	4	2	0	2	0
Lens	0	0	0	0	0
Optic Nerve	3	0	0	2	0
Retina	4	3	0	3	4
Sclera	1	0	0	0	2
Zone 1	1	0	0	0	2
Zone 2	2	3	3	2	3
Zone 3	4	3	0	3	4

Experiment Set	20130131-2	20130131-3	20130131-4	20130131-7	20130207-8
Side-on Press (kPa)	99.8	136.6		147.2	137.8
Side-on Duration (ms)	2.43	2.49		2.72	2.5
Side-on Impulse (Pa-sec)	114.5	146.8		188.9	158.1
Reflected Pressure (kPa)	184.5	233.1	140.3	289.2	271.3
Reflected Impulse (Pa-s)	150.1	207.4	112.1	286.3	230.7
Reflected Duration (ms)	2.89	2.97	2.46	3.14	3.11
Reflected Min Pressure (kPa)	-33.3119	-37.0928	-28.6724	-37.6549	-36.6132
Reflected Neg. Phase Duration (ms)	16.3600	16.0200	16.5900	9.3150	15.8800
Reflected Neg. Impulse (Pa-s)	-0.0799	-0.0864	-0.0765	-0.1382	-0.0816
Reflected Pressure Difference (Pa)	217.8480	269.7364	168.9362	326.4579	307.9380
Injury (CIS) Score					
Angle	0	3	3	1	1
Anterior Chamber	0	0	0	0	2
Choroid	0	3	3	2	1
Cornea	0	0	0	0	0
Iris	0	0	0	0	0
Lamina Cribosa	0	0	1	0	1
Lens	0	0	0	0	0
Optic Nerve	0	0	1	0	1
Retina	0	4	3	1	1
Sclera	0	4	1	1	1
Zone 1	0	4	1	1	1
Zone 2	0	3	3	1	2
Zone 3	0	4	3	2	1

Experiment Set	20130307-5	20130307-6	20130307-7	20130328-2	20130328-7
Side-on Press (kPa)	50.2	78.1	42.3		46.3
Side-on Duration (ms)	2.08	2.26	2.07		2.07
Side-on Impulse (Pa-sec)	52.2	88.46	44.87		48.31
Reflected Pressure (kPa)	96.4	139.1	85.4	55.5	79.7
Reflected Impulse (Pa-s)	60.21	111.3	51.16	30.05	55.65
Reflected Duration (ms)	2.17	2.48	2.21	2.09	2.18
Reflected Min Pressure (kPa)	-23.2874	-28.9531	-18.5840	-12.0845	-22.3872
Reflected Neg. Phase Duration (ms)	16.8250	16.5150	16.8350	16.8900	16.8100
Reflected Neg. Impulse (Pa-s)	-0.0679	-0.0823	-0.0620	-0.0314	-0.0664
Reflected Pressure Difference (Pa)	119.6673	168.0294	103.9478	59.7272	102.0442
Injury (CIS) Score					
Angle	4	3	0	3	3
Anterior Chamber	0	2	3	0	0
Choroid	0	2	3	3	3
Cornea	0	0	0	0	0
Iris	4	2	0	0	0
Lamina Cribosa	1	0	0	0	1
Lens	0	0	2	0	0
Optic Nerve	1	0	3	0	1
Retina	0	1	4	3	3
Sclera	0	3	3	0	0
Zone 1	0	3	3	0	0
Zone 2	4	3	3	3	3
Zone 3	1	2	4	3	3

Experiment Set	20130405-1	20130405-2	20130405-5	20130405-6	20130606-1
Side-on Press (kPa)	126.1	113.1	90	70.4	140
Side-on Duration (ms)	2.5	2.42	2.39	2.32	2.79
Side-on Impulse (Pa-sec)	147.8	128.4	100.4	80.61	169.5
Reflected Pressure (kPa)	221.6	191	158.7	129	271.4
Reflected Impulse (Pa-s)	210.9	177.2	130.7	99.96	253.8
Reflected Duration (ms)	2.96	2.93	2.65	2.42	3.15
Reflected Min Pressure (kPa)	-35.1950	-35.1761	-30.8880	-27.6040	-38.8951
Reflected Neg. Phase Duration (ms)	13.5900	16.1400	16.4250	16.5800	15.8600
Reflected Neg. Impulse (Pa-s)	-0.0954	-0.0947	-0.0797	-0.0813	-0.0875
Reflected Pressure Difference (Pa)	256.8391	226.1374	189.5572	156.6039	310.3174
Injury (CIS) Score					
Angle	3	3	2	1	0
Anterior Chamber	0	0	0	0	0
Choroid	4	3	0	2	0
Cornea	0	0	0	0	0
Iris	2	2	0	0	0
Lamina Cribosa	0	0	0	1	0
Lens	2	3	0	0	0
Optic Nerve	3	3	3	1	0
Retina	4	4	3	2	0
Sclera	0	3	0	0	0
Zone 1	0	3	0	0	0
Zone 2	3	3	2	1	0
Zone 3	4	4	3	2	0

Experiment Set	20130606-3	20130606-4	20130606-5	20130606-6	20130613-1
Side-on Press (kPa)	117.3	101.2	78	37.6	147.5
Side-on Duration (ms)	2.55	2.47	2.39	2.23	2.79
Side-on Impulse (Pa-sec)	143.8	116.1	86.71	41.46	186.9
Reflected Pressure (kPa)	209.2	176	142	76.2	290
Reflected Impulse (Pa-s)	203.6	157.2	111.2	48.35	286
Reflected Duration (ms)	2.99	2.75	2.65	2.28	3.33
Reflected Min Pressure (kPa)	-39.8118	-35.4844	-31.0807	-19.7558	-39.2034
Reflected Neg. Phase Duration (ms)	16.0000	16.2450	16.4650	16.7400	15.7700
Reflected Neg. Impulse (Pa-s)	-0.0726	-0.0722	-0.0667	-0.0474	-0.0937
Reflected Pressure Difference (Pa)	249.0197	211.4690	173.0540	95.9084	328.7406
Injury (CIS) Score					
Angle	4	2	3	1	1
Anterior Chamber	0	0	0	0	0
Choroid	2	4	2	2	3
Cornea	0	0	0	0	0
Iris	0	0	0	0	0
Lamina Cribosa	0	0	0	0	2
Lens	0	3	0	0	0
Optic Nerve	0	2	0	0	2
Retina	2	4	2	2	3
Sclera	0	3	0	0	3
Zone 1	0	3	0	0	3
Zone 2	4	3	3	1	1
Zone 3	2	4	2	2	3

Experiment Set	20130613-2	20130613-4	20130613-5	20130620-1	20130620-2
Side-on Press (kPa)	135.2	116.1	98.5	155.3	122.9
Side-on Duration (ms)	2.61	2.58	2.48	2.9	2.53
Side-on Impulse (Pa-sec)	164.7	143.3	116.8	190	144.1
Reflected Pressure (kPa)	248.9	215	172.6	307.8	221.2
Reflected Impulse (Pa-s)	242.3	203.2	157.1	291.7	206.8
Reflected Duration (ms)	3.05	2.97	2.72	3.35	3.02
Reflected Min Pressure (kPa)	-39.0984	-36.2242	-35.7049	-40.1466	-36.6132
Reflected Neg. Phase Duration (ms)	15.5000	16.0200	16.2750	9.8700	15.9950
Reflected Neg. Impulse (Pa-s)	-0.0859	-0.0708	-0.0738	-0.1428	-0.0696
Reflected Pressure Difference (Pa)	288.0321	251.1956	208.2900	347.9001	257.8210
Injury (CIS) Score					
Angle	1	4	2	2	1
Anterior Chamber	0	0	0	0	0
Choroid	2	2	4	2	3
Cornea	0	0	0	0	0
Iris	3	0	0	0	0
Lamina Cribosa	3	0	0	0	1
Lens	0	0	0	0	0
Optic Nerve	3	1	3	0	3
Retina	3	2	4	2	3
Sclera	1	0	3	0	4
Zone 1	1	0	3	0	4
Zone 2	3	4	2	2	1
Zone 3	3	2	4	2	3

Experiment Set	20130620-5	20130620-6	20130801-2	20130801-3	20130801-4
Side-on Press (kPa)	101.8	77.7	60.3	88.28	87.14
Side-on Duration (ms)	2.47	2.3	3.488	3.743	3.617
Side-on Impulse (Pa-sec)	119	86.54	120.5	178.5	173.6
Reflected Pressure (kPa)	174.6	138.3	88.84	140.5	139.7
Reflected Impulse (Pa-s)	160.9	110.7	162.4	264.3	256.3
Reflected Duration (ms)	2.74	2.64	4.05	4.56	4.4
Reflected Min Pressure (kPa)	-35.7706	-30.3375	-29.3487	-35.2429	-34.7990
Reflected Neg. Phase Duration (ms)	16.2500	16.5050	14.9650	8.2800	8.6000
Reflected Neg. Impulse (Pa-s)	-0.0709	-0.0678	-0.0808	-0.1316	-0.1263
Reflected Pressure Difference (Pa)	210.0074	168.6588	118.1852	175.7263	174.4499
Injury (CIS) Score					
Angle	0	0	4	3	1
Anterior Chamber	0	0	0	0	0
Choroid	0	1	4	2	4
Cornea	0	0	0	0	0
Iris	0	0	3	0	0
Lamina Cribosa	0	2	3	1	0
Lens	0	0	0	0	0
Optic Nerve	0	2	4	1	3
Retina	0	1	4	2	4
Sclera	0	1	0	0	0
Zone 1	0	1	0	0	0
Zone 2	0	0	4	3	1
Zone 3	0	2	4	2	4

Experiment Set	20130801-5	20130801-7
Side-on Press (kPa)	85.12	87.31
Side-on Duration (ms)	3.568	3.614
Side-on Impulse (Pa-sec)	171.5	177.8
Reflected Pressure (kPa)	141.5	134.3
Reflected Impulse (Pa-s)	252.3	263
Reflected Duration (ms)	4.56	4.494
Reflected Min Pressure (kPa)	-33.3844	-35.1478
Reflected Neg. Phase Duration (ms)	8.3800	8.4500
Reflected Neg. Impulse (Pa-s)	-0.1258	-0.1330
Reflected Pressure Difference (Pa)	174.9168	169.4886
Injury (CIS) Score		
Angle	1	2
Anterior Chamber	0	0
Choroid	1	3
Cornea	0	0
Iris	0	0
Lamina Cribosa	2	0
Lens	0	0
Optic Nerve	2	0
Retina	1	3
Sclera	0	3
Zone 1	0	3
Zone 2	1	2
Zone 3	2	3

APPENDIX II

Summary of xMap Biomarker Detection Data

Human Neurological Aqueous Panel

Animal	Exposure	Refl. Impulse kPa-ms	UCHL1(Park) pg/ml			NGF-b pg/ml		
			Baseline	24 hr	48 hr	Baseline	24hr	48 hr
4170	Control1	0	<0.13↓	<0.13↓	<0.13↓	0.64	2.41	3.64
4169	LB1	58	N/A	0.18	N/A	1.73	2.68	7.33
4171	LB2	57.3	N/A	<0.13↓	N/A	1.89	2.25	8.75
4172	Control2	0	<0.13↓	N/A	<0.13↓	1.56	1.37	3.19
4173	LB3	56.9	N/A	<0.13↓	<0.13↓	6.55	4.18	2.68
4174	Control3	0	<0.13↓	<0.13↓	<0.13↓	1.23	2.18	9.26
4206	Control4	0	0.41	<0.13↓	<0.13↓	3.55	2.55	3.14
4205	LB4	57.1	N/A	N/A	0.2	3.48	2.82	10.28
4208	Control5	0	<0.13↓	<0.13↓	<0.13↓	2.22	1.47	2.36
4207	LB5	56	N/A	<0.13↓	<0.13↓	N/A	2.08	4.11
4210	LB6	59.3	N/A	N/A	N/A	N/A	2.78	6.46
4224	MLB1	100.5	<0.13↓	<0.13↓	<0.13↓	1.25	2.48	2.73
4225	MLB2	104.3	<0.13↓	<0.13↓	<0.13↓	2.27	2.64	6.29
4226	MLB3	96.5	<0.13↓	<0.13↓	<0.13↓	1.4	2.41	7.03
4251	HB	157	<0.13↓	<0.13↓	<0.13↓	1.3	2.13	3.55
4229	MLB6	97.9	<0.13↓	<0.13↓	<0.13↓	1.52	1.85	5.06
4228	MLB5	97.1	N/A	<0.13↓	<0.13↓	3.5	2.5	6.81
4250	HB	141.6	<0.13↓	<0.13↓	<0.13↓	1.47	3.41	8.1
4247	HB	156.6	<0.13↓	N/A	N/A	N/A	1.85	3.41
4248	HB3	141.6	16.75	<0.19↓	N/A	2.67	2.16	2.67
4249	HB4	158	<0.19↓	N/A	<0.19↓	1.83	2	3.77
4252	HB	158.5	<0.13↓	<0.13↓	<0.13↓	1.99	4.09	5.5

Human Neurological Aqueous Panel

Animal	Exposure	Reflected Impulse kPa-ms	DJ-1 (Park 7) pg/ml			a-SYN pg/ml		
			Baseline	24 hr	48 hr	Baseline	24 hr	48 hr
4170	Control1	0	<1.23↓	<1.23↓	<1.23↓	<0.07↓	<0.07↓	<0.07↓
4169	LB1	58	<1.23↓	<1.23↓	<1.23↓	<0.07↓	<0.07↓	<0.07↓
4171	LB2	57.3	N/A	<1.23↓	<1.23↓	<0.07↓	<0.07↓	<0.07↓
4172	Control2	0	<1.23↓	<1.23↓	<1.23↓	<0.07↓	<0.07↓	<0.07↓
4173	LB3	56.9	<1.23↓	N/A	<1.23↓	<0.07↓	<0.07↓	<0.07↓
4174	Control3	0	<1.23↓	<1.23↓	<1.23↓	<0.07↓	<0.07↓	<0.07↓
4206	Control4	0	<1.23↓	<1.23↓	<1.23↓	<0.07↓	<0.07↓	<0.07↓
4205	LB4	57.1	N/A	<1.23↓	<1.23↓	<0.07↓	<0.07↓	<0.07↓
4208	Control5	0	<1.23↓	<1.23↓	<1.23↓	<0.07↓	<0.07↓	<0.07↓
4207	LB5	56	N/A	<1.23↓	<1.23↓	N/A	<0.07↓	<0.07↓
4210	LB6	59.3	N/A	<1.23↓	<1.23↓	N/A	<0.07↓	<0.07↓
4224	MLB1	100.5	<1.23↓	<1.23↓	<1.23↓	<0.07↓	<0.07↓	<0.07↓
4225	MLB2	104.3	<1.23↓	<1.23↓	<1.23↓	<0.07↓	<0.07↓	<0.07↓
4226	MLB3	96.5	<1.23↓	<1.23↓	<1.23↓	<0.07↓	<0.07↓	<0.07↓
4251	HB	157	<1.23↓	<1.23↓	<1.23↓	<0.07↓	<0.07↓	<0.07↓
4229	MLB6	97.9	<1.23↓	<1.23↓	<1.23↓	<0.07↓	<0.07↓	<0.07↓
4228	MLB5	97.1	N/A	<1.23↓	<1.23↓	<0.07↓	<0.07↓	<0.07↓
4250	HB	141.6	<1.23↓	<1.23↓	<1.23↓	<0.07↓	<0.07↓	<0.07↓
4247	HB	156.6	N/A	<1.23↓	3.2	N/A	<0.07↓	<0.07↓
4248	HB3	141.6	<2.04	<2.04	<2.04	<.10	<.10	<.10
4249	HB4	158	<2.04	9.37	<2.04	<.10	<.10	<.10
4252	HB	158.5	<1.23↓	<1.23↓	<1.23↓	<0.07↓	<0.07↓	<0.07↓

Human Neurological Aqueous Panel

Animal	Exposure	Reflected Impulse kPa-ms	NSE pg/ml			Tau (total) pg/ml		
			Baseline	24 hr	48 hr	Baseline	24 hr	48 hr
4170	Control1	0	7.07	9.17	11.76	<0.01↓	<0.01↓	<0.01↓
4169	LB1	58	10.44	15.61	14.21	0.25	<0.01↓	0.04
4171	LB2	57.3	10.76	12.1	11.71	0.02	<0.01↓	0.1
4172	Control2	0	10.08	12.53	12.77	<0.01↓	0.11	<0.01↓
4173	LB3	56.9	18.1	15.7	15.77	<0.01↓	<0.01↓	<0.01↓
4174	Control3	0	10.03	11.07	11.77	<0.01↓	<0.01↓	<0.01↓
4206	Control4	0	13.55	15.54	12.67	<0.01↓	<0.01↓	<0.01↓
4205	LB4	57.1	12.43	12.02	12.63	0.27	0.15	<0.01↓
4208	Control5	0	8.99	10.34	9	<0.01↓	<0.01↓	<0.01↓
4207	LB5	56	N/A	9.65	10.49	N/A	<0.01↓	<0.01↓
4210	LB6	59.3	N/A	12.23	13.93	N/A	0.1	<0.01↓
4224	MLB1	100.5	10.86	9.9	9.7	<0.01↓	<0.01↓	<0.01↓
4225	MLB2	104.3	14.92	13.49	14.25	<0.01↓	<0.01↓	<0.01↓
4226	MLB3	96.5	10.99	10.35	10.5	<0.01↓	<0.01↓	<0.01↓
4251	HB	157	11.52	8.45	11.68	<0.01↓	<0.01↓	<0.01↓
4229	MLB6	97.9	9.48	10.48	8.76	<0.01↓	<0.01↓	<0.01↓
4228	MLB5	97.1	7.36	8.19	9.79	0.18	<0.01↓	<0.01↓
4250	HB	141.6	13.05	14.74	13.44	<0.01↓	<0.01↓	<0.01↓
4247	HB	156.6	N/A	9.72	11.71	N/A	<0.01↓	<0.01↓
4248	HB3	141.6	7.46	8.53	7.93	0.06	<.02	0.06
4249	HB4	158	7.56	7.31	7.78	<.02	<.02	<.02
4252	HB	158.5	12.12	12.76	12.32	<0.01↓	<0.01↓	<0.01↓

Human Neurological Aqueous Panel

Animal	Exposure	Reflected Impulse kPa-ms	Phospho-Tau (Thr231) pg/ml		
			Baseline	24 hr	48 hr
4170	Control1	0	<0.19↓	<0.19↓	<0.19↓
4169	LB1	58	<0.19↓	<0.19↓	<0.19↓
4171	LB2	57.3	<0.19↓	<0.19↓	<0.19↓
4172	Control2	0	<0.19↓	N/A	<0.19↓
4173	LB3	56.9	<0.19↓	0.3	<0.19↓
4174	Control3	0	<0.19↓	<0.19↓	<0.19↓
4206	Control4	0	<0.19↓	<0.19↓	<0.19↓
4205	LB4	57.1	0.79	N/A	0.49
4208	Control5	0	<0.19↓	<0.19↓	<0.19↓
4207	LB5	56	N/A	<0.19↓	<0.19↓
4210	LB6	59.3	N/A	<0.19↓	<0.19↓
4224	MLB1	100.5	<0.19↓	0.45	<0.19↓
4225	MLB2	104.3	<0.19↓	<0.19↓	<0.19↓
4226	MLB3	96.5	<0.19↓	<0.19↓	<0.19↓
4251	HB	157	<0.19↓	<0.19↓	<0.19↓
4229	MLB6	97.9	<0.19↓	2.01	<0.19↓
4228	MLB5	97.1	N/A	<0.19↓	<0.19↓
4250	HB	141.6	<0.19↓	<0.19↓	<0.19↓
4247	HB	156.6	N/A	<0.19↓	<0.19↓
4248	HB3	141.6	25.16	<.18	0.24
4249	HB4	158	0.19	<.18	<.18
4252	HB	158.5	<0.19↓	<0.19↓	0.31

Human Neurological Plasma Panel

Animal	Exposure	Refl. Impulse kPa-ms	UCHL1 (PARK5) pg/ml				NGF-b pg/ml			
			B-line	3 hr	24 hr	48 hr	B-line	3 hr	24 hr	48 hr
4169	LB1	0	0.21	1.22	0.88	0.41	1.62	4.15	8.81	5.72
4170	Control1	58		2.05	1.78			7.14	3.95	
4171	LB2	57.3		0.75	0.47	0.18		1.12	<0.34↓	<0.34↓
4172	Control2	0	0.2				0.94			
4173	LB3	56.9				0.28				3.06
4174	Control3	0	0.13	0.46	0.5		2.17	2.82	2.75	
4205	LB4	0		0.39	0.95	2.6		1.44	2.08	3.24
4206	Control4	57.1	0.35				1.92			
4207	LB5	0	0.19		0.44	0.08	1.49		1.07	1.76
4208	Control5	56		0.58				1.62		
4210	LB6	59.3		0.55	0.66	0.27		2.21	2.46	2.35
4224	MLB1	100.5	0.09		0.66	0.23	1.62		4	9.03
4225	MLB2	104.3	0.16	0.76	0.89	0.38	1.26	1.44	0.8	1.07
4226	MLB3	96.5	0.21	0.2	0.4	0.36	<0.34↓	<0.34↓	1.07	0.61
4228	MLB5	157	0.41	0.55	0.98	0.41	2.08	1.46	2.03	4.6
4229	MLB6	97.9	0.27	0.59	0.53	0.54	<0.34↓	<0.34↓	<0.34↓	<0.34↓
4251	HB2	97.1	0.16	0.65		0.49	1.85	1.01		1.4
4247	HB1	141.6	0.33	0.63	0.54	0.2	0.84	0.94	1.07	1.81
4250	HB5	156.6	0.38	0.5	0.41	0.38	1.85	0.71	1.67	1.07
4248	HB3	141.6	<.19	0.26	0.58	0.23	<.82	<.82	0.94	<.82
4249	HB4	158	<.19	0.24	0.3	<.19	1.58	1.65	2.67	2.5
4252	HB6	158.5	0.19	0.3	0.15	0.07	1.03	1.62	0.8	0.71

Human Neurological Plasma Panel

Animal	Exposure	Refl. Impulse kPa-ms	DJ-1 (PARK7) pg/ml				a-SYN pg/ml			
			B-line	3 hr	24 hr	48 hr	B-line	3 hr	24 hr	48 hr
4169	LB1	0	1.38	4.37	3.91	0.71	<0.04↓	<0.04↓	<0.04↓	<0.04↓
4170	Control1	58		10.8	5.72			<0.04↓	<0.04↓	
4171	LB2	57.3		2.83	1.89	0.89		<0.04↓	<0.04↓	<0.04↓
4172	Control2	0	1.72				<0.04↓			
4173	LB3	56.9				1.28				<0.04↓
4174	Control3	0	0.64	1.73	3.37		<0.04↓	<0.04↓	<0.04↓	
4205	LB4	0		1.98	2.96	35.37		<0.04↓	0.09	<0.04↓
4206	Control4	57.1	2.42				<0.04↓			
4207	LB5	0	1.51		3.33	<0.50↓	<0.04↓		<0.04↓	<0.04↓
4208	Control5	56		1.33				<0.04↓		
4210	LB6	59.3		1.84	2.38	0.69		<0.04↓	<0.04↓	<0.04↓
4224	MLB1	100.5	<0.50↓		3.27	1.13	<0.04↓		<0.04↓	<0.04↓
4225	MLB2	104.3	0.54	3.81	4.31	2.08	<0.04↓	<0.04↓	<0.04↓	<0.04↓
4226	MLB3	96.5	1.73	0.88	1.25	0.82	<0.04↓	<0.04↓	<0.04↓	<0.04↓
4228	MLB5	157	<0.50↓	2.28	3.74	2.36	<0.04↓	<0.04↓	<0.04↓	<0.04↓
4229	MLB6	97.9	<0.50↓	1.23	1.2	1.85	<0.04↓	<0.04↓	<0.04↓	<0.04↓
4251	HB2	97.1	1.84	3.78		3.21	0.09	0.11		0.07
4247	HB1	141.6	1.74	2.48	4.23	1.25	<0.04↓	<0.04↓	<0.04↓	<0.04↓
4250	HB5	156.6	1.49	1.18	3.96	1.26	<0.04↓	<0.04↓	0.13	<0.04↓
4248	HB3	141.6	<2.04	3.54	3.6	4.14	<.10	<.10	<.10	<.10
4249	HB4	158	2.1	6.43	7.37	2.55	<.10	<.10	<.10	<.10
4252	HB6	158.5	<0.50↓	1.13	1.01	<0.50↓	0.12	0.05	<0.04↓	<0.04↓

Human Neurological Plasma Panel

Animal	Exposure	Refl. Impulse kPa-ms	NSE pg/ml				Tau (total) pg/ml			
			B-line	3 hr	24 hr	48 hr	B-line	3 hr	24 hr	48 hr
4169	LB1	0	1.82	5.42	6	5.21	<0.02↓	<0.02↓	<0.02↓	<0.02↓
4170	Control1	58		4.91	4.91			<0.02↓	<0.02↓	
4171	LB2	57.3		7.34	7.75	6.02		<0.02↓	<0.02↓	<0.02↓
4172	Control2	0	2.18				<0.02↓			
4173	LB3	56.9				5.39				<0.02↓
4174	Control3	0	0.38	1.28	1.54		<0.02↓	<0.02↓	<0.02↓	
4205	LB4	0		5.31	5.78	5.75		<0.02↓	0.1	<0.02↓
4206	Control4	57.1	3.18				<0.02↓			
4207	LB5	0	4.25		4.88	3.15	<0.02↓		<0.02↓	<0.02↓
4208	Control5	56		2.57				<0.02↓		
4210	LB6	59.3		4.07	5.5	4.33		<0.02↓	<0.02↓	<0.02↓
4224	MLB1	100.5	4.53		6.16	5.11	<0.02↓		<0.02↓	<0.02↓
4225	MLB2	104.3	4.45	5.3	5.46	4.45	<0.02↓	<0.02↓	<0.02↓	<0.02↓
4226	MLB3	96.5	3.98	5.26	6.27	4.92	<0.02↓	<0.02↓	<0.02↓	<0.02↓
4228	MLB5	157	2.97	3.67	4.65	4.44	<0.02↓	<0.02↓	<0.02↓	<0.02↓
4229	MLB6	97.9	<0.12↓	<0.12↓	0.54	0.34	<0.02↓	<0.02↓	<0.02↓	<0.02↓
4251	HB2	97.1	3.62	6.09		5.09	<0.02↓	<0.02↓		<0.02↓
4247	HB1	141.6	4.56	6.42	4.65	4.95	<0.02↓	<0.02↓	<0.02↓	<0.02↓
4250	HB5	156.6	3.2	5.27	6.33	3.93	<0.02↓	<0.02↓	<0.02↓	<0.02↓
4248	HB3	141.6	5.06	6.91	10.95	7.89	<0.02↓	<0.02↓	<0.02↓	<0.02↓
4249	HB4	158	1.23	1.32	2.16	1.58	0.02	<0.02↓	0.02	0.02
4252	HB6	158.5	3.39	4.57	4.59	3.77	0.13	0.12	0.04	0.05

Human Neurological Plasma Panel

Animal	Exposure	Reflecgted Impulse kPa-ms	Phospho-Tau (Thr231) pg/ml			
			Baseline	3 hr	24 hr	48 hr
4169	LB1	0	<0.19↓	1.17	0.89	0.47
4170	Control1	58		0.46	0.34	
4171	LB2	57.3		0.3	<0.19↓	<0.19↓
4172	Control2	0	0.27			
4173	LB3	56.9				0.23
4174	Control3	0	<0.19↓	<0.19↓	<0.19↓	
4205	LB4	0		0.44	0.57	2.38
4206	Control4	57.1	0.31			
4207	LB5	0	0.27		0.46	0.28
4208	Control5	56		0.69		
4210	LB6	59.3		0.58	0.62	0.41
4224	MLB1	100.5	<0.19↓		<0.19↓	<0.19↓
4225	MLB2	104.3	<0.19↓	0.8	0.34	0.48
4226	MLB3	96.5	<0.19↓	0.61	0.3	0.41
4228	MLB5	157	<0.19↓	<0.19↓	<0.19↓	<0.19↓
4229	MLB6	97.9	0.28	<0.19↓	0.32	0.59
4251	HB2	97.1	0.21	0.78		0.76
4247	HB1	141.6	0.29	0.79	0.37	0.4
4250	HB5	156.6	<0.19↓	0.39	0.47	0.21
4248	HB3	141.6	0.29	0.48	0.51	0.41
4249	HB4	158	0.2	0.47	0.52	0.3
4252	HB6	158.5	0.69	0.68	0.55	0.46

Rat Aqueous Panel

Animal	Exposure	Reflected Impulse kPa-ms	G-CSF pg/ml			Eotaxin pg/ml		
			Baseline	24 hr	48 hr	Baseline	24 hr	48 hr
4170	Control1	0		10.62			5.75	
4169	LB1	58	9.83	12.19	6.69	5.04	6.83	5.75
4171	LB2	57.3	12.97	17.61	5.52	<2.94↓	5.52	<2.94↓
4172	Control2	0	9.83	<1.53↓	12.97	3.45	5.97	3.45
4173	LB3	56.9	9.04	15.3	2.54	<2.94↓	11.86	<2.94↓
4174	Control3	0	17.61	5.91	11.4	5.52	<2.94↓	3.45
4206	Control4	0	<1.53↓	3.63	9.04	<2.94↓	<2.94↓	<2.94↓
4205	LB4	57.1	2.19	9.83	9.04	<2.94↓	<2.94↓	<2.94↓
4208	Control5	0	12.97	14.53	16.84	5.97	5.28	5.52
4207	LB5	56	12.19	10.62	14.53	8.9	3.45	5.04
4210	LB6	59.3	20.65	8.26	8.26	10.38	<2.94↓	<2.94↓
4224	MLB1	100.5	16.84	9.83	9.83	5.97	<2.94↓	5.04
4225	MLB2	104.3	12.58	6.69	<1.53↓	4.01	<2.94↓	<2.94↓
4226	MLB3	96.5	16.84	9.83	8.26	5.04	4.01	<2.94↓
4251	HB	157	14.53	3.63	9.83	3.74	<2.94↓	5.52
4229	MLB6	97.9	5.91	12.97	5.91	4.28	9.74	<2.94↓
4228	MLB5	97.1	9.83	<1.53↓	5.91	3.45	<2.94↓	<2.94↓
4250	HB	141.6	8.26	22.15	<1.53↓	<2.94↓	4.01	<2.94↓
4247	HB	156.6	10.62	10.62	<1.53↓	5.97	5.52	<2.94↓
4248	HB3	141.6	4.42	7.85	5.65	13.4	<4.86	<4.86
4249	HB4	158	6.51	6.07	6.07	<4.86	7.09	<4.86
4252	HB	158.5	7.47	7.47	2.19	4.54	<2.94↓	<2.94↓

Rat Aqueous Panel

Animal	Exposure	Reflected Impulse kPa-ms	GM-CSF pg/ml			IL-1a pg/ml		
			Baseline	24 hr	48 hr	Baseline	24 hr	48 hr
4170	Control1	0		85.11			<6.35↓	
4169	LB1	58	61.53	22.44	N/A	6.41	6.41	6.41
4171	LB2	57.3	N/A	91.33	30.74	<6.35↓	17.15	<6.35↓
4172	Control2	0	<6.88↓	45.84	60.43	<6.35↓	<6.35↓	<6.35↓
4173	LB3	56.9	68.09	87.19	27.19	<6.35↓	<6.35↓	<6.35↓
4174	Control3	0	80.91	44.69	15.3	20.05	<6.35↓	6.41
4206	Control4	0	38.93	41.24	30.74	<6.35↓	<6.35↓	<6.35↓
4205	LB4	57.1	76.68	41.24	<6.88↓	<6.35↓	<6.35↓	<6.35↓
4208	Control5	0	N/A	70.25	55.99	<6.35↓	17.15	12.23
4207	LB5	56	N/A	48.11	48.11	<6.35↓	<6.35↓	10.21
4210	LB6	59.3	93.39	N/A	30.74	18.6	<6.35↓	<6.35↓
4224	MLB1	100.5	76.68	49.25	109.56	12.23	<6.35↓	<6.35↓
4225	MLB2	104.3	55.99	48.11	<6.88↓	12.23	<6.35↓	<6.35↓
4226	MLB3	96.5	58.22	50.38	72.4	12.23	<6.35↓	<6.35↓
4251	HB	157	55.99	22.44	17.67	30.47	<6.35↓	<6.35↓
4229	MLB6	97.9	93.39	144.32	97.48	<6.35↓	11.55	<6.35↓
4228	MLB5	97.1	48.11	N/A	22.44	<6.35↓	N/A	<6.35↓
4250	HB	141.6	<6.88↓	N/A	97.48	<6.35↓	<6.35↓	<6.35↓
4247	HB	156.6	N/A	N/A	N/A	<6.35↓	<6.35↓	<6.35↓
4248	HB3	141.6	6237	47.69	<6.85	<10.50	<10.50	<10.50
4249	HB4	158	36.08	N/A	30.94	<10.50	<10.50	<10.50
4252	HB	158.5	<6.88↓	101.54	48.11	<6.35↓	<6.35↓	<6.35↓

Rat Aqueous Panel

Animal	Exposure	Reflected Impulse kPa-ms	Leptin pg/ml			MIP-1a pg/ml		
			Baseline	24 hr	48 hr	Baseline	24 hr	48 hr
4170	Control1	0		<7.06↓			<1.21↓	
4169	LB1	58	<7.06↓	41.34	N/A	<1.21↓	<1.21↓	<1.21↓
4171	LB2	57.3	N/A	<7.06↓	<7.06↓	<1.21↓	<1.21↓	<1.21↓
4172	Control2	0	<7.06↓	27.43	<7.06↓	<1.21↓	<1.21↓	<1.21↓
4173	LB3	56.9	<7.06↓	<7.06↓	<7.06↓	<1.21↓	<1.21↓	<1.21↓
4174	Control3	0	<7.06↓	<7.06↓	<7.06↓	<1.21↓	<1.21↓	<1.21↓
4206	Control4	0	<7.06↓	<7.06↓	<7.06↓	<1.21↓	<1.21↓	<1.21↓
4205	LB4	57.1	<7.06↓	<7.06↓	<7.06↓	<1.21↓	<1.21↓	<1.21↓
4208	Control5	0	<7.06↓	<7.06↓	<7.06↓	<1.21↓	<1.21↓	<1.21↓
4207	LB5	56	<7.06↓	18.96	<7.06↓	<1.21↓	<1.21↓	<1.21↓
4210	LB6	59.3	<7.06↓	N/A	<7.06↓	<1.21↓	<1.21↓	<1.21↓
4224	MLB1	100.5	<7.06↓	<7.06↓	<7.06↓	<1.21↓	<1.21↓	<1.21↓
4225	MLB2	104.3	<7.06↓	<7.06↓	<7.06↓	<1.21↓	<1.21↓	<1.21↓
4226	MLB3	96.5	<7.06↓	<7.06↓	<7.06↓	<1.21↓	<1.21↓	<1.21↓
4251	HB	157	<7.06↓	<7.06↓	<7.06↓	<1.21↓	<1.21↓	<1.21↓
4229	MLB6	97.9	<7.06↓	<7.06↓	76.67	<1.21↓	<1.21↓	<1.21↓
4228	MLB5	97.1	N/A	N/A	<7.06↓	<1.21↓	<1.21↓	<1.21↓
4250	HB	141.6	<7.06↓	N/A	<7.06↓	<1.21↓	<1.21↓	<1.21↓
4247	HB	156.6	N/A	86.48	N/A	<1.21↓	<1.21↓	<1.21↓
4248	HB3	141.6	6076	<3.91	<3.91	<.68	<.68	<.68
4249	HB4	158	<3.91	N/A	<3.91	<.68	<.68	<.68
4252	HB	158.5	<7.06↓	N/A	<7.06↓	<1.21↓	<1.21↓	<1.21↓

Rat Aqueous Panel

Animal	Exposure	Reflected Impulse kPa-ms	IL-4 pg/ml			IL-1b pg/ml		
			Baseline	24 hr	48 hr	Baseline	24 hr	48 hr
4170	Control1	0		4.85			<1.08↓	
4169	LB1	58	2.39	7.36	23.91	<1.08↓	<1.08↓	N/A
4171	LB2	57.3	<2.27↓	12.32	<2.27↓	5.77	<1.08↓	<1.08↓
4172	Control2	0	<2.27↓	<2.27↓	<2.27↓	<1.08↓	<1.08↓	<1.08↓
4173	LB3	56.9	<2.27↓	23.35	<2.27↓	<1.08↓	<1.08↓	<1.08↓
4174	Control3	0	6.1	<2.27↓	<2.27↓	<1.08↓	<1.08↓	<1.08↓
4206	Control4	0	<2.27↓	<2.27↓	<2.27↓	<1.08↓	<1.08↓	<1.08↓
4205	LB4	57.1	<2.27↓	<2.27↓	<2.27↓	<1.08↓	<1.08↓	<1.08↓
4208	Control5	0	4.85	5.48	7.36	N/A	<1.08↓	<1.08↓
4207	LB5	56	<2.27↓	2.39	6.1	<1.08↓	<1.08↓	<1.08↓
4210	LB6	59.3	13.53	<2.27↓	<2.27↓	<1.08↓	N/A	<1.08↓
4224	MLB1	100.5	6.1	<2.27↓	6.1	<1.08↓	<1.08↓	<1.08↓
4225	MLB2	104.3	<2.27↓	<2.27↓	<2.27↓	<1.08↓	<1.08↓	<1.08↓
4226	MLB3	96.5	2.39	2.39	<2.27↓	<1.08↓	<1.08↓	<1.08↓
4251	HB	157	<2.27↓	<2.27↓	<2.27↓	<1.08↓	<1.08↓	<1.08↓
4229	MLB6	97.9	3.6	8.62	<2.27↓	<1.08↓	3.67	3.36
4228	MLB5	97.1	<2.27↓	<2.27↓	<2.27↓	<1.08↓	<1.08↓	<1.08↓
4250	HB	141.6	<2.27↓	9.86	<2.27↓	<1.08↓	<1.08↓	<1.08↓
4247	HB	156.6	<2.27↓	<2.27↓	<2.27↓	N/A	N/A	N/A
4248	HB3	141.6	12.13	5.44	<.84	761.69	<.60	<.60
4249	HB4	158	3.49	<.84	3.49	<.60	<.60	<.60
4252	HB	158.5	4.85	<2.27↓	<2.27↓	<1.08↓	3.88	<1.08↓

Rat Aqueous Panel

Animal	Exposure	Refl. Impulse kPa-ms	IL-2 pg/ml			IL-6 pg/ml		
			Baseline	24 hr	48 hr	Baseline	24 hr	48 hr
4170	Control1	0		<5.81↓			<296.84↓	
4169	LB1	58	<5.81↓	9.19	<5.81↓	<296.84↓	<296.84↓	<296.84↓
4171	LB2	57.3	<5.81↓	12.4	<5.81↓	<296.84↓	<296.84↓	<296.84↓
4172	Control2	0	<5.81↓	<5.81↓	<5.81↓	<296.84↓	<296.84↓	<296.84↓
4173	LB3	56.9	<5.81↓	9.19	<5.81↓	<296.84↓	<296.84↓	<296.84↓
4174	Control3	0	10.8	<5.81↓	<5.81↓	<296.84↓	<296.84↓	<296.84↓
4206	Control4	0	<5.81↓	<5.81↓	<5.81↓	<296.84↓	<296.84↓	<296.84↓
4205	LB4	57.1	<5.81↓	<5.81↓	<5.81↓	<296.84↓	<296.84↓	<296.84↓
4208	Control5	0	<5.81↓	9.19	<5.81↓	<296.84↓	<296.84↓	<296.84↓
4207	LB5	56	<5.81↓	<5.81↓	<5.81↓	<296.84↓	<296.84↓	<296.84↓
4210	LB6	59.3	<5.81↓	<5.81↓	<5.81↓	<296.84↓	<296.84↓	<296.84↓
4224	MLB1	100.5	12.4	<5.81↓	<5.81↓	<296.84↓	<296.84↓	<296.84↓
4225	MLB2	104.3	<5.81↓	<5.81↓	<5.81↓	<296.84↓	<296.84↓	<296.84↓
4226	MLB3	96.5	7.59	<5.81↓	<5.81↓	<296.84↓	<296.84↓	<296.84↓
4251	HB	157	5.99	<5.81↓	<5.81↓	<296.84↓	<296.84↓	<296.84↓
4229	MLB6	97.9	<5.81↓	<5.81↓	<5.81↓	<296.84↓	<296.84↓	<296.84↓
4228	MLB5	97.1	<5.81↓	N/A	<5.81↓	<296.84↓	N/A	<296.84↓
4250	HB	141.6	<5.81↓	<5.81↓	<5.81↓	<296.84↓	<296.84↓	<296.84↓
4247	HB	156.6	8.39	<5.81↓	<5.81↓	<296.84↓	<296.84↓	<296.84↓
4248	HB3	141.6	11.59	3.64	4.68	469.41	<296.84↓	<296.84↓
4249	HB4	158	<3.21	4.15	<3.21	<296.84↓	<296.84↓	<296.84↓
4252	HB	158.5	<5.81↓	<5.81↓	<5.81↓	<296.84↓	323.61	<296.84↓

Rat Aqueous Panel

Animal	Exposure	Refl. Impulse kPa-ms	EGF pg/ml			IL-13 pg/ml		
			Baseline	24 hr	48 hr	Baseline	24 hr	48 hr
4170	Control1	0		<0.13↓			<2.27↓	
4169	LB1	58	<0.13↓	<0.13↓	<0.13↓	<2.27↓	<2.27↓	<2.27↓
4171	LB2	57.3	<0.13↓	<0.13↓	<0.13↓	<2.27↓	<2.27↓	<2.27↓
4172	Control2	0	<0.13↓	<0.13↓	<0.13↓	<2.27↓	<2.27↓	<2.27↓
4173	LB3	56.9	<0.13↓	<0.13↓	<0.13↓	<2.27↓	3.57	<2.27↓
4174	Control3	0	<0.13↓	<0.13↓	<0.13↓	<2.27↓	<2.27↓	<2.27↓
4206	Control4	0	<0.13↓	<0.13↓	<0.13↓	<2.27↓	<2.27↓	<2.27↓
4205	LB4	57.1	<0.13↓	<0.13↓	<0.13↓	<2.27↓	<2.27↓	<2.27↓
4208	Control5	0	<0.13↓	<0.13↓	<0.13↓	<2.27↓	<2.27↓	<2.27↓
4207	LB5	56	<0.13↓	<0.13↓	<0.13↓	<2.27↓	<2.27↓	<2.27↓
4210	LB6	59.3	<0.13↓	<0.13↓	<0.13↓	<2.27↓	<2.27↓	<2.27↓
4224	MLB1	100.5	<0.13↓	<0.13↓	<0.13↓	<2.27↓	<2.27↓	<2.27↓
4225	MLB2	104.3	<0.13↓	<0.13↓	<0.13↓	<2.27↓	<2.27↓	<2.27↓
4226	MLB3	96.5	<0.13↓	<0.13↓	<0.13↓	<2.27↓	<2.27↓	<2.27↓
4251	HB	157	<0.13↓	<0.13↓	<0.13↓	<2.27↓	<2.27↓	<2.27↓
4229	MLB6	97.9	<0.13↓	<0.13↓	<0.13↓	<2.27↓	<2.27↓	<2.27↓
4228	MLB5	97.1	<0.13↓	N/A	<0.13↓	<2.27↓	<2.27↓	<2.27↓
4250	HB	141.6	<0.13↓	<0.13↓	<0.13↓	<2.27↓	<2.27↓	<2.27↓
4247	HB	156.6	<0.13↓	<0.13↓	<0.13↓	<2.27↓	<2.27↓	<2.27↓
4248	HB3	141.6	<.06	<.06	<.06	<3.79	<3.79	<3.79
4249	HB4	158	<.06	<.06	<.06	<3.79	<3.79	<3.79
4252	HB	158.5	<0.13↓	<0.13↓	<0.13↓	<2.27↓	<2.27↓	<2.27↓

Rat Aqueous Panel

Animal	Exposure	Refl. Impulse kPa-ms	IL-10 pg/ml			IL-12p70 pg/ml		
			Baseline	24 hr	48 hr	Baseline	24 hr	48 hr
4170	Control1	0		<2.08↓			15.46	
4169	LB1	58	<2.08↓	10.16	N/A	15.46	10.54	27.28
4171	LB2	57.3	N/A	<2.08↓	<2.08↓	15.46	16.68	10.54
4172	Control2	0	<2.08↓	<2.08↓	<2.08↓	10.54	<5.83↓	15.46
4173	LB3	56.9	<2.08↓	<2.08↓	<2.08↓	13.01	35.08	17.89
4174	Control3	0	<2.08↓	<2.08↓	<2.08↓	24.98	<5.83↓	10.54
4206	Control4	0	<2.08↓	<2.08↓	<2.08↓	<5.83↓	<5.83↓	15.46
4205	LB4	57.1	<2.08↓	<2.08↓	<2.08↓	<5.83↓	17.89	10.54
4208	Control5	0	7.31	<2.08↓	<2.08↓	17.89	22.65	17.89
4207	LB5	56	N/A	5.37	<2.08↓	6.84	17.89	22.65
4210	LB6	59.3	11.31	N/A	<2.08↓	21.47	<5.83↓	<5.83↓
4224	MLB1	100.5	<2.08↓	<2.08↓	<2.08↓	15.46	24.98	15.46
4225	MLB2	104.3	<2.08↓	<2.08↓	<2.08↓	15.46	10.54	<5.83↓
4226	MLB3	96.5	<2.08↓	<2.08↓	<2.08↓	20.28	17.89	6.84
4251	HB	157	<2.08↓	<2.08↓	<2.08↓	24.98	8.07	13.01
4229	MLB6	97.9	N/A	6.75	<2.08↓	<5.83↓	17.89	19.09
4228	MLB5	97.1	N/A	N/A	<2.08↓	<5.83↓	<5.83↓	<5.83↓
4250	HB	141.6	<2.08↓	N/A	19.97	<5.83↓	17.89	19.09
4247	HB	156.6	3.52	<2.08↓	N/A	<5.83↓	15.46	<5.83↓
4248	HB3	141.6	3321	<2.14	<2.14	<10.36	<10.36	10.69
4249	HB4	158	<2.14	<2.14	<2.14	10.69	<10.36	14.5
4252	HB	158.5	2.77	<2.08↓	<2.08↓	11.78	13.01	<5.83↓

Rat Aqueous Panel

Animal	Exposure	Reflected Impulse kPa-ms	INFy pg/ml			IL-5 pg/ml		
			Baseline	24 hr	48 hr	Baseline	24 hr	48 hr
4170	Control1	0		9.85			<4.26↓	
4169	LB1	58	<6.68↓	<6.68↓	<6.68↓	<4.26↓	24.48	<4.26↓
4171	LB2	57.3	<6.68↓	11	<6.68↓	39.74	<4.26↓	<4.26↓
4172	Control2	0	<6.68↓	<6.68↓	<6.68↓	<4.26↓	<4.26↓	<4.26↓
4173	LB3	56.9	<6.68↓	72.08	<6.68↓	<4.26↓	58.51	7.21
4174	Control3	0	11	<6.68↓	<6.68↓	<4.26↓	7.21	7.21
4206	Control4	0	<6.68↓	<6.68↓	<6.68↓	<4.26↓	<4.26↓	<4.26↓
4205	LB4	57.1	<6.68↓	<6.68↓	<6.68↓	<4.26↓	<4.26↓	<4.26↓
4208	Control5	0	<6.68↓	19.23	<6.68↓	7.21	13.93	13.93
4207	LB5	56	<6.68↓	<6.68↓	8.73	7.21	<4.26↓	<4.26↓
4210	LB6	59.3	8.73	<6.68↓	<6.68↓	7.21	<4.26↓	<4.26↓
4224	MLB1	100.5	14.49	<6.68↓	<6.68↓	<4.26↓	19.58	19.58
4225	MLB2	104.3	<6.68↓	<6.68↓	<6.68↓	<4.26↓	<4.26↓	<4.26↓
4226	MLB3	96.5	<6.68↓	<6.68↓	<6.68↓	<4.26↓	<4.26↓	<4.26↓
4251	HB	157	9.85	<6.68↓	<6.68↓	<4.26↓	<4.26↓	<4.26↓
4229	MLB6	97.9	<6.68↓	<6.68↓	<6.68↓	<4.26↓	<4.26↓	<4.26↓
4228	MLB5	97.1	<6.68↓	<6.68↓	<6.68↓	<4.26↓	58.51	<4.26↓
4250	HB	141.6	<6.68↓	<6.68↓	<6.68↓	<4.26↓	7.21	<4.26↓
4247	HB	156.6	<6.68↓	<6.68↓	<6.68↓	<4.26↓	<4.26↓	<4.26↓
4248	HB3	141.6	10.64	7.43	5.43	<6.18	7.41	<6.18
4249	HB4	158	3.6	33.8	7.43	7.41	47.52	10.51
4252	HB	158.5	<6.68↓	<6.68↓	<6.68↓	<4.26↓	<4.26↓	<4.26↓

Rat Aqueous Panel

Animal	Exposure	Reflected Impulse kPa-ms	IL-17A pg/ml			IL-18 pg/ml		
			Baseline	24 hr	48 hr	Baseline	24 hr	48 hr
4170	Control1	0		4.14			<6.72↓	
4169	LB1	58	<3.29↓	11.44	3.7	<6.72↓	<6.72↓	<6.72↓
4171	LB2	57.3	28.22	7.29	<3.29↓	<6.72↓	<6.72↓	<6.72↓
4172	Control2	0	<3.29↓	<3.29↓	<3.29↓	<6.72↓	<6.72↓	<6.72↓
4173	LB3	56.9	<3.29↓	11.21	<3.29↓	<6.72↓	<6.72↓	<6.72↓
4174	Control3	0	<3.29↓	<3.29↓	<3.29↓	<6.72↓	<6.72↓	<6.72↓
4206	Control4	0	<3.29↓	<3.29↓	<3.29↓	<6.72↓	<6.72↓	<6.72↓
4205	LB4	57.1	<3.29↓	<3.29↓	<3.29↓	<6.72↓	<6.72↓	<6.72↓
4208	Control5	0	5.92	4.14	<3.29↓	<6.72↓	<6.72↓	<6.72↓
4207	LB5	56	9.13	<3.29↓	<3.29↓	<6.72↓	<6.72↓	<6.72↓
4210	LB6	59.3	6.15	<3.29↓	<3.29↓	<6.72↓	<6.72↓	<6.72↓
4224	MLB1	100.5	5.02	<3.29↓	<3.29↓	<6.72↓	<6.72↓	<6.72↓
4225	MLB2	104.3	<3.29↓	<3.29↓	<3.29↓	<6.72↓	<6.72↓	<6.72↓
4226	MLB3	96.5	3.7	<3.29↓	<3.29↓	<6.72↓	<6.72↓	<6.72↓
4251	HB	157	4.36	<3.29↓	<3.29↓	<6.72↓	<6.72↓	<6.72↓
4229	MLB6	97.9	4.58	8.21	5.02	<6.72↓	<6.72↓	<6.72↓
4228	MLB5	97.1	<3.29↓	N/A	<3.29↓	<6.72↓	8.76	<6.72↓
4250	HB	141.6	<3.29↓	<3.29↓	<3.29↓	<6.72↓	<6.72↓	<6.72↓
4247	HB	156.6	13.29	11.91	<3.29↓	<6.72↓	<6.72↓	<6.72↓
4248	HB3	141.6	3287	4.74	<2.15	<8.95	<8.95	<8.95
4249	HB4	158	3.81	<2.15	3.81	<8.95	<8.95	<8.95
4252	HB	158.5	<3.29↓	<3.29↓	<3.29↓	<6.72↓	<6.72↓	<6.72↓

Rat Aqueous Panel

Animal	Exposure	Reflected Impulse kPa-ms	MCP-1 pg/ml			IP-10 pg/ml		
			Baseline	24 hr	48 hr	Baseline	24 hr	48 hr
4170	Control1	0		<17.09↓			<1.47↓	
4169	LB1	58	<17.09↓	<17.09↓	<17.09↓	<1.47↓	N/A	<1.47↓
4171	LB2	57.3	<17.09↓	<17.09↓	<17.09↓	7.93	<1.47↓	<1.47↓
4172	Control2	0	<17.09↓	<17.09↓	<17.09↓	<1.47↓	<1.47↓	<1.47↓
4173	LB3	56.9	<17.09↓	<17.09↓	<17.09↓	<1.47↓	N/A	<1.47↓
4174	Control3	0	<17.09↓	<17.09↓	<17.09↓	<1.47↓	<1.47↓	<1.47↓
4206	Control4	0	<17.09↓	<17.09↓	<17.09↓	<1.47↓	<1.47↓	<1.47↓
4205	LB4	57.1	<17.09↓	<17.09↓	<17.09↓	<1.47↓	<1.47↓	<1.47↓
4208	Control5	0	<17.09↓	<17.09↓	<17.09↓	<1.47↓	<1.47↓	<1.47↓
4207	LB5	56	<17.09↓	<17.09↓	<17.09↓	N/A	<1.47↓	<1.47↓
4210	LB6	59.3	<17.09↓	<17.09↓	<17.09↓	12.4	N/A	2.71
4224	MLB1	100.5	<17.09↓	<17.09↓	<17.09↓	<1.47↓	<1.47↓	<1.47↓
4225	MLB2	104.3	<17.09↓	<17.09↓	<17.09↓	<1.47↓	<1.47↓	<1.47↓
4226	MLB3	96.5	<17.09↓	<17.09↓	<17.09↓	<1.47↓	<1.47↓	<1.47↓
4251	HB	157	<17.09↓	<17.09↓	<17.09↓	<1.47↓	<1.47↓	<1.47↓
4229	MLB6	97.9	<17.09↓	<17.09↓	<17.09↓	11.85	<1.47↓	<1.47↓
4228	MLB5	97.1	<17.09↓	<17.09↓	<17.09↓	N/A	N/A	<1.47↓
4250	HB	141.6	<17.09↓	<17.09↓	<17.09↓	<1.47↓	N/A	<1.47↓
4247	HB	156.6	<17.09↓	<17.09↓	<17.09↓	N/A	<1.47↓	<1.47↓
4248	HB3	141.6	<34.35	<34.35	<34.35	1156	<1.20	<1.20
4249	HB4	158	<34.35	56.41	<34.35	<1.20	N/A	2.23
4252	HB	158.5	<17.09↓	<17.09↓	57.82	<1.47↓	N/A	<1.47↓

Rat Aqueous Panel

Animal	Exposure	Reflected Impulse kPa-ms	GRO/KC/CINC- pg/ml			VEGF pg/ml		
			Baseline	24 hr	48 hr	Baseline	24 hr	48 hr
4170	Control1	0		67.49			6.01	
4169	LB1	58	77.72	54.16	<8.92↓	9.25	<2.70↓	<2.70↓
4171	LB2	57.3	70.96	17.87	20.92	<2.70↓	8.71	<2.70↓
4172	Control2	0	41.08	<8.92↓	70.96	<2.70↓	<2.70↓	7.9
4173	LB3	56.9	29.83	148.98	56.66	<2.70↓	4.65	<2.70↓
4174	Control3	0	90.57	20.92	38.33	<2.70↓	<2.70↓	<2.70↓
4206	Control4	0	<8.92↓	38.33	46.43	<2.70↓	<2.70↓	<2.70↓
4205	LB4	57.1	43.78	38.33	<8.92↓	<2.70↓	<2.70↓	<2.70↓
4208	Control5	0	79.92	47.74	61.55	<2.70↓	<2.70↓	<2.70↓
4207	LB5	56	111.34	20.92	32.71	<2.70↓	<2.70↓	<2.70↓
4210	LB6	59.3	70.96	<8.92↓	<8.92↓	<2.70↓	<2.70↓	<2.70↓
4224	MLB1	100.5	66.32	41.08	55.41	<2.70↓	<2.70↓	<2.70↓
4225	MLB2	104.3	60.34	54.16	<8.92↓	<2.70↓	<2.70↓	<2.70↓
4226	MLB3	96.5	59.12	32.71	28.38	2.79	<2.70↓	<2.70↓
4251	HB	157	59.12	40.05	<8.92↓	<2.70↓	<2.70↓	<2.70↓
4229	MLB6	97.9	20.92	49.05	29.83	<2.70↓	<2.70↓	<2.70↓
4228	MLB5	97.1	29.83	26.91	<8.92↓	<2.70↓	7.9	<2.70↓
4250	HB	141.6	17.87	23.93	<8.92↓	<2.70↓	<2.70↓	<2.70↓
4247	HB	156.6	96.71	<8.92↓	<8.92↓	<2.70↓	<2.70↓	<2.70↓
4248	HB3	141.6	78.63	42.01	22.6	<3.64	10.66	<3.64
4249	HB4	158	51.48	35.27	26.5	<3.64	<3.64	<3.64
4252	HB	158.5	<8.92↓	<8.92↓	<8.92↓	<2.70↓	<2.70↓	<2.70↓

Rat Aqueous Panel

Animal	Exposure	Refl. Impulse kPa-ms	Fractalkine pg/ml			LIX pg/ml		
			Baseline	24 hr	48 hr	Baseline	24 hr	48 hr
4170	Control1	0		<1.18↓			<16.87↓	
4169	LB1	58	<1.18↓	<1.18↓	<1.18↓	<16.87↓	<16.87↓	<16.87↓
4171	LB2	57.3	<1.18↓	<1.18↓	<1.18↓	<16.87↓	<16.87↓	<16.87↓
4172	Control2	0	<1.18↓	<1.18↓	<1.18↓	<16.87↓	<16.87↓	<16.87↓
4173	LB3	56.9	<1.18↓	<1.18↓	<1.18↓	<16.87↓	<16.87↓	<16.87↓
4174	Control3	0	<1.18↓	<1.18↓	<1.18↓	<16.87↓	<16.87↓	<16.87↓
4206	Control4	0	<1.18↓	<1.18↓	<1.18↓	<16.87↓	<16.87↓	<16.87↓
4205	LB4	57.1	1.65	<1.18↓	<1.18↓	<16.87↓	<16.87↓	<16.87↓
4208	Control5	0	<1.18↓	<1.18↓	<1.18↓	<16.87↓	<16.87↓	<16.87↓
4207	LB5	56	<1.18↓	<1.18↓	<1.18↓	<16.87↓	<16.87↓	<16.87↓
4210	LB6	59.3	<1.18↓	<1.18↓	<1.18↓	<16.87↓	<16.87↓	<16.87↓
4224	MLB1	100.5	<1.18↓	<1.18↓	<1.18↓	<16.87↓	<16.87↓	<16.87↓
4225	MLB2	104.3	<1.18↓	<1.18↓	<1.18↓	<16.87↓	<16.87↓	<16.87↓
4226	MLB3	96.5	<1.18↓	<1.18↓	<1.18↓	<16.87↓	<16.87↓	<16.87↓
4251	HB	157	<1.18↓	<1.18↓	<1.18↓	<16.87↓	<16.87↓	<16.87↓
4229	MLB6	97.9	2.74	2.64	<1.18↓	<16.87↓	<16.87↓	<16.87↓
4228	MLB5	97.1	N/A	9.62	<1.18↓	<16.87↓	42.06	<16.87↓
4250	HB	141.6	<1.18↓	2.94	<1.18↓	<16.87↓	<16.87↓	<16.87↓
4247	HB	156.6	<1.18↓	<1.18↓	<1.18↓	<16.87↓	<16.87↓	<16.87↓
4248	HB3	141.6	406.31	<.66	<.66	<24.28	<24.28	<24.28
4249	HB4	158	<.66	N/A	<.66	<24.28	<24.28	<24.28
4252	HB	158.5	<1.18↓	<1.18↓	<1.18↓	<16.87↓	<16.87↓	<16.87↓

Rat Aqueous Panel

Animal	Exposure	Refl. Impulse kPa-ms	MIP-2 pg/ml			TNF-a pg/ml		
			Baseline	24 hr	48 hr	Baseline	24 hr	48 hr
4170	Control1	0		54.82			<1.50↓	
4169	LB1	58	49.43	41.81	45.69	<1.50↓	<1.50↓	<1.50↓
4171	LB2	57.3	59.98	56.57	24.7	<1.50↓	<1.50↓	<1.50↓
4172	Control2	0	45.69	<14.16↓	37.79	<1.50↓	<1.50↓	<1.50↓
4173	LB3	56.9	24.7	37.79	27	<1.50↓	<1.50↓	<1.50↓
4174	Control3	0	56.57	14.92	33.61	<1.50↓	<1.50↓	<1.50↓
4206	Control4	0	<14.16↓	24.7	29.25	<1.50↓	<1.50↓	<1.50↓
4205	LB4	57.1	14.92	19.92	14.92	<1.50↓	<1.50↓	<1.50↓
4208	Control5	0	37.79	49.43	24.7	<1.50↓	<1.50↓	<1.50↓
4207	LB5	56	29.25	29.25	37.79	<1.50↓	<1.50↓	<1.50↓
4210	LB6	59.3	49.43	19.92	<14.16↓	<1.50↓	<1.50↓	<1.50↓
4224	MLB1	100.5	63.3	33.61	19.92	<1.50↓	<1.50↓	<1.50↓
4225	MLB2	104.3	33.61	19.92	<14.16↓	<1.50↓	<1.50↓	<1.50↓
4226	MLB3	96.5	72.78	29.25	14.92	<1.50↓	<1.50↓	<1.50↓
4251	HB	157	35.73	17.45	14.92	<1.50↓	<1.50↓	<1.50↓
4229	MLB6	97.9	19.92	37.79	<14.16↓	<1.50↓	<1.50↓	<1.50↓
4228	MLB5	97.1	37.79	14.92	<14.16↓	<1.50↓	<1.50↓	<1.50↓
4250	HB	141.6	29.25	19.92	<14.16↓	<1.50↓	<1.50↓	<1.50↓
4247	HB	156.6	19.92	19.92	<14.16↓	<1.50↓	<1.50↓	<1.50↓
4248	HB3	141.6	29.68	43.66	29.68	<1.08	<1.08	<1.08
4249	HB4	158	51.76	23.95	43.66	<1.08	1.66	<1.08
4252	HB	158.5	45.69	14.92	14.92	<1.50↓	<1.50↓	<1.50↓

Rat Aqueous Panel

Animal	Exposure	Reflected Impulse kPa-ms	RANTES pg/ml		
			Baseline	24 hr	48 hr
4170	Control1	0		<2.49↓	
4169	LB1	58	<2.49↓	<2.49↓	<2.49↓
4171	LB2	57.3	<2.49↓	<2.49↓	<2.49↓
4172	Control2	0	<2.49↓	<2.49↓	<2.49↓
4173	LB3	56.9	<2.49↓	<2.49↓	<2.49↓
4174	Control3	0	<2.49↓	<2.49↓	<2.49↓
4206	Control4	0	<2.49↓	<2.49↓	<2.49↓
4205	LB4	57.1	<2.49↓	<2.49↓	<2.49↓
4208	Control5	0	<2.49↓	<2.49↓	<2.49↓
4207	LB5	56	<2.49↓	<2.49↓	<2.49↓
4210	LB6	59.3	<2.49↓	N/A	<2.49↓
4224	MLB1	100.5	<2.49↓	<2.49↓	<2.49↓
4225	MLB2	104.3	<2.49↓	<2.49↓	<2.49↓
4226	MLB3	96.5	<2.49↓	<2.49↓	<2.49↓
4251	HB	157	<2.49↓	<2.49↓	<2.49↓
4229	MLB6	97.9	<2.49↓	<2.49↓	<2.49↓
4228	MLB5	97.1	<2.49↓	N/A	<2.49↓
4250	HB	141.6	<2.49↓	<2.49↓	<2.49↓
4247	HB	156.6	<2.49↓	<2.49↓	N/A
4248	HB3	141.6	2105	<4.47	<4.47
4249	HB4	158	<4.47	<4.47	<4.47
4252	HB	158.5	<2.49↓	<2.49↓	<2.49↓

Rat Plasma Panel

Animal	Exposure	Refl. Impulse kPa-ms	G-CSF pg/ml				Eotaxin pg/ml			
			B-line	3 hr	24 hr	48 hr	B-line	3 hr	24 hr	48 hr
4169	LB1	0		<2.68↓	<2.68↓			<3.04↓	<3.04↓	
4170	Control1	58			<2.68↓				<3.04↓	
4171	LB2	57.3		<2.68↓	<2.68↓	7		<3.04↓	3.99	11.85
4172	Control2	0	<2.68↓				<3.04↓			
4173	LB3	56.9				<2.68↓				14.4
4174	Control3	0	<2.68↓	5.67	6		<3.04↓	<3.04↓	<3.04↓	
4205	LB4	0		<2.68↓	<2.68↓	<2.68↓		<3.04↓	<3.04↓	<3.04↓
4206	Control4	57.1	<2.68↓				6.64			
4207	LB5	0	<2.68↓		<2.68↓	<2.68↓	<3.04↓		<3.04↓	<3.04↓
4208	Control5	56		3.74				9.83		
4210	LB6	59.3		<2.68↓	<2.68↓	<2.68↓		<3.04↓	<3.04↓	<3.04↓
4224	MLB1	100.5	3.74		11.8	<2.68↓	<3.04↓		7.06	<3.04↓
4225	MLB2	104.3	<2.68↓	<2.68↓	<2.68↓	<2.68↓	<3.04↓	<3.04↓	<3.04↓	<3.04↓
4226	MLB3	96.5	<2.68↓	3.43	4.69	9.04	<3.04↓	6.42	19.69	11.26
4228	MLB5	157	<2.68↓	3.13	<2.68↓	<2.68↓	<3.04↓	<3.04↓	<3.04↓	3.13
4229	MLB6	97.9	<2.68↓	<2.68↓	<2.68↓	<2.68↓	<3.04↓	<3.04↓	<3.04↓	10.33
4251	HB2	97.1	<2.68↓	<2.68↓		<2.68↓	<3.04↓	<3.04↓		<3.04↓
4247	HB1	141.6	<2.68↓	<2.68↓	<2.68↓	<2.68↓	7.06	3.71	3.71	<3.04↓
4250	HB5	156.6	<2.68↓	<2.68↓	<2.68↓	<2.68↓	<3.04↓	<3.04↓	<3.04↓	<3.04↓
4248	HB3	141.6	<2.34	<2.34	<2.34	<2.34	<4.86	<4.86	<4.86	<4.86
4249	HB4	158	<2.34	<2.34	<2.34	<2.34	<4.86	<4.86	<4.86	<4.86
4252	HB6	158.5	15.95	32.17	10.42	28.86	16.4	15.25	14.89	12

Rat Plasma Panel

Animal	Exposure	Reflected Impulse kPa-ms	GM-CSF pg/ml				IL-1a pg/ml			
			Baseline	3 hr	24 hr	48 hr	Baseline	3 hr	24 hr	48 hr
4169	LB1	0		29.79	14.8			<6.49↓	<6.49↓	
4170	Control1	58			62.99				<6.49↓	
4171	LB2	57.3		36.18	41.44	62.99		<6.49↓	<6.49↓	16.69
4172	Control2	0	8.55				<6.49↓			
4173	LB3	56.9				16.93				<6.49↓
4174	Control3	0	27.65	48.73	37.23		<6.49↓	<6.49↓	<6.49↓	
4205	LB4	0		31.93	52.85	39.34		7.21	<6.49↓	<6.49↓
4206	Control4	57.1	116.4				11.23			
4207	LB5	0	54.89		22.29	21.21	<6.49↓		<6.49↓	<6.49↓
4208	Control5	56		211.83				18.39		
4210	LB6	59.3		16.93	40.39	32.99		<6.49↓	<6.49↓	<6.49↓
4224	MLB1	100.5	23.36		50.79	13.74	<6.49↓		7.21	<6.49↓
4225	MLB2	104.3	40.39	20.14	54.89	23.36	<6.49↓	<6.49↓	<6.49↓	<6.49↓
4226	MLB3	96.5	40.39	38.29	60.98	57.94	<6.49↓	<6.49↓	28.37	6.74
4228	MLB5	157	56.93	58.96	27.65	36.18	<6.49↓	<6.49↓	<6.49↓	<6.49↓
4229	MLB6	97.9	<6.50↓	8.55	48.73	76.85	<6.49↓	<6.49↓	<6.49↓	15.57
4251	HB2	97.1	44.58	36.18		38.29	<6.49↓	<6.49↓		<6.49↓
4247	HB1	141.6	72.93	50.79	38.29	25.51	11.23	<6.49↓	<6.49↓	<6.49↓
4250	HB5	156.6	29.79	21.21	44.58	14.8	<6.49↓	<6.49↓	<6.49↓	<6.49↓
4248	HB3	141.6	18.82	19.44	28.8	9.82	<10.50	<10.50	<10.50	<10.50
4249	HB4	158	<6.85	<6.85	<6.85	<6.85	<10.50	<10.50	<10.50	<10.50
4252	HB6	158.5	364.83	365.55	306.65	376.92	153.54	119.44	111.9	99.6

Rat Plasma Panel

Animal	Exposure	Reflected Impulse kPa-ms	Leptin pg/ml				MIP-1a pg/ml			
			Baseline	3 hr	24 hr	48 hr	Baseline	3 hr	24 hr	48 hr
4169	LB1	0		<7.46↓	<7.46↓			<1.07↓	<1.07↓	
4170	Control1	58			<7.46↓				<1.07↓	
4171	LB2	57.3		<7.46↓	<7.46↓	<7.46↓		<1.07↓	<1.07↓	<1.07↓
4172	Control2	0	<7.46↓				<1.07↓			
4173	LB3	56.9				<7.46↓				<1.07↓
4174	Control3	0	<7.46↓	<7.46↓	<7.46↓		<1.07↓	<1.07↓	<1.07↓	<1.07↓
4205	LB4	0		<7.46↓	<7.46↓	<7.46↓		<1.07↓	<1.07↓	<1.07↓
4206	Control4	57.1	53.17				2.4			
4207	LB5	0	<7.46↓		<7.46↓	<7.46↓	1.2		<1.07↓	<1.07↓
4208	Control5	56		92.57				1.09		
4210	LB6	59.3		<7.46↓	<7.46↓	<7.46↓		<1.07↓	<1.07↓	<1.07↓
4224	MLB1	100.5	<7.46↓		<7.46↓	<7.46↓	<1.07↓		2.07	<1.07↓
4225	MLB2	104.3	<7.46↓	<7.46↓	<7.46↓	<7.46↓	<1.07↓	<1.07↓	<1.07↓	<1.07↓
4226	MLB3	96.5	<7.46↓	<7.46↓	<7.46↓	<7.46↓	<1.07↓	<1.07↓	2.55	<1.07↓
4228	MLB5	157	<7.46↓	<7.46↓	<7.46↓	<7.46↓	1.2	<1.07↓	<1.07↓	<1.07↓
4229	MLB6	97.9	<7.46↓	<7.46↓	<7.46↓	<7.46↓	<1.07↓	<1.07↓	<1.07↓	1.81
4251	HB2	97.1	<7.46↓	<7.46↓		<7.46↓	<1.07↓	<1.07↓		<1.07↓
4247	HB1	141.6	<7.46↓	<7.46↓	<7.46↓	<7.46↓	6.03	4.13	<1.07↓	<1.07↓
4250	HB5	156.6	118.2	105.02	128.64	96.23	5.02	<1.07↓	6.7	<1.07↓
4248	HB3	141.6	<3.91	<3.91	<3.91	<3.91	2.33	1.83	1.98	2.18
4249	HB4	158	<3.91	<3.91	<3.91	<3.91	<.68	<.68	<.68	<.68
4252	HB6	158.5	1973	1915	1379	1445	6.07	6.33	5.25	7.34

Rat Plasma Panel

Animal	Exposure	Reflected Impulse kPa-ms	IL-4 pg/ml				IL-1b pg/ml			
			Baseline	3 hr	24 hr	48 hr	Baseline	3 hr	24 hr	48 hr
4169	LB1	0		<1.96↓	<1.96↓			<1.36↓	<1.36↓	
4170	Control1	58			2.88				<1.36↓	
4171	LB2	57.3		<1.96↓	<1.96↓	<1.96↓		<1.36↓	<1.36↓	<1.36↓
4172	Control2	0	5.54				<1.36↓			
4173	LB3	56.9				<1.96↓				<1.36↓
4174	Control3	0	<1.96↓	6.67	<1.96↓		<1.36↓	<1.36↓	<1.36↓	
4205	LB4	0		<1.96↓	16.16	<1.96↓		<1.36↓	<1.36↓	<1.36↓
4206	Control4	57.1	<1.96↓				10.66			
4207	LB5	0	11.38		<1.96↓	<1.96↓	<1.36↓		<1.36↓	<1.36↓
4208	Control5	56		<1.96↓				25.93		
4210	LB6	59.3		6.67	<1.96↓	<1.96↓		<1.36↓	<1.36↓	<1.36↓
4224	MLB1	100.5	<1.96↓		3.38	<1.96↓	<1.36↓		<1.36↓	<1.36↓
4225	MLB2	104.3	<1.96↓	<1.96↓	<1.96↓	<1.96↓	<1.36↓	<1.36↓	<1.36↓	<1.36↓
4226	MLB3	96.5	<1.96↓	9.01	54.23	30.14	<1.36↓	<1.36↓	<1.36↓	<1.36↓
4228	MLB5	157	13.77	<1.96↓	<1.96↓	2.88	<1.36↓	<1.36↓	<1.36↓	<1.36↓
4229	MLB6	97.9	<1.96↓	<1.96↓	3.38	18.54	<1.36↓	<1.36↓	<1.36↓	<1.36↓
4251	HB2	97.1	<1.96↓	<1.96↓		<1.96↓	<1.36↓	<1.36↓		<1.36↓
4247	HB1	141.6	<1.96↓	5.54	<1.96↓	<1.96↓	1.8	<1.36↓	<1.36↓	<1.36↓
4250	HB5	156.6	<1.96↓	<1.96↓	<1.96↓	<1.96↓	<1.36↓	<1.36↓	<1.36↓	<1.36↓
4248	HB3	141.6	5.44	2.74	2.32	<.87	<.60	<.60	<.60	<.60
4249	HB4	158	<.87	<.87	<.87	<.87	<.60	<.60	<.60	<.60
4252	HB6	158.5	67.09	68.05	46.48	41.17	484.29	470.37	306.58	371.6

Rat Plasma Panel

Anin.	Exposure	Refl. Impulse kPa-ms	IL-2 pg/ml				IL-6 pg/ml			
			B-line	3 hr	24 hr	48 hr	B-line	3 hr	24 nr	48 hr
4169	LB1	0		<7.31↓	<7.31↓			<296.84↓	<296.84↓	
4170	Control1	58			<7.31↓				<296.84↓	
4171	LB2	57.3		<7.31↓	<7.31↓	8.82		<296.84↓	<296.84↓	<296.84↓
4172	Control2	0	<7.31↓				<296.84↓			
4173	LB3	56.9				<7.31↓				<296.84↓
4174	Control3	0	<7.31↓	<7.31↓	<7.31↓		<296.84↓	<296.84↓	<296.84↓	
4205	LB4	0		<7.31↓	<7.31↓	<7.31↓		<296.84↓	<296.84↓	<296.84↓
4206	Control4	57.1	17.4				<296.84↓			
4207	LB5	0	11.17		<7.31↓	<7.31↓	<296.84↓		<296.84↓	<296.84↓
4208	Control5	56		9.6				<296.84↓		
4210	LB6	59.3		<7.31↓	<7.31↓	<7.31↓		<296.84↓	<296.84↓	<296.84↓
4224	MLB1	100.5	<7.31↓		<7.31↓	<7.31↓	<296.84↓		<296.84↓	<296.84↓
4225	MLB2	104.3	<7.31↓	<7.31↓	<7.31↓	<7.31↓	<296.84↓	<296.84↓	<296.84↓	<296.84↓
4226	MLB3	96.5	<7.31↓	<7.31↓	<7.31↓	11.17	<296.84↓	<296.84↓	<296.84↓	<296.84↓
4228	MLB5	157	30.17	26.49	<7.31↓	<7.31↓	<296.84↓	<296.84↓	<296.84↓	<296.84↓
4229	MLB6	97.9	<7.31↓	<7.31↓	<7.31↓	<7.31↓	<296.84↓	<296.84↓	<296.84↓	<296.84↓
4251	HB2	97.1	35.22	25		21.99	<296.84↓	<296.84↓		<296.84↓
4247	HB1	141.6	49.03	23.5	<7.31↓	<7.31↓	<296.84↓	<296.84↓	<296.84↓	<296.84↓
4250	HB5	156.6	14.29	<7.31↓	44.97	<7.31↓	<296.84↓	<296.84↓	<296.84↓	<296.84↓
4248	HB3	141.6	12.12	10.21	6.83	<3.21	<296.84↓	<296.84↓	<296.84↓	<296.84↓
4249	HB4	158	<3.21	<3.21	<3.21	<3.21	<296.84↓	<296.84↓	<296.84↓	<296.84↓
4252	HB6	158.5	46.33	63.36	33.79	53.02	892.59	722.96	738.93	862.67

Rat Plasma Panel

Animal	Exposure	Refl. Impulse kPa-ms	EGF pg/ml				IL-13 pg/ml			
			B-line	3 hr	24 hr	48 hr	B-line	3 hr	24 hr	48 hr
4169	LB1	0		<0.12↓	<0.12↓			4.69	4.63	
4170	Control1	58			<0.12↓				6.35	
4171	LB2	57.3		<0.12↓	<0.12↓	<0.12↓		<2.17↓	2.45	17.07
4172	Control2	0	<0.12↓				<2.17↓			
4173	LB3	56.9				<0.12↓				<2.17↓
4174	Control3	0	<0.12↓	<0.12↓	<0.12↓		<2.17↓	9.23	<2.17↓	
4205	LB4	0		<0.12↓	<0.12↓	<0.12↓		<2.17↓	8.08	<2.17↓
4206	Control4	57.1	<0.12↓				10.38			
4207	LB5	0	<0.12↓		<0.12↓	<0.12↓	<2.17↓		5.77	<2.17↓
4208	Control5	56		<0.12↓				6.92		
4210	LB6	59.3		<0.12↓	<0.12↓	<0.12↓		<2.17↓	5.77	<2.17↓
4224	MLB1	100.5	<0.12↓		<0.12↓	<0.12↓	<2.17↓		9.23	<2.17↓
4225	MLB2	104.3	<0.12↓	<0.12↓	<0.12↓	<0.12↓	<2.17↓	<2.17↓	<2.17↓	<2.17↓
4226	MLB3	96.5	<0.12↓	<0.12↓	<0.12↓	<0.12↓	<2.17↓	<2.17↓	13.21	27.41
4228	MLB5	157	<0.12↓	<0.12↓	<0.12↓	<0.12↓	3.52	8.08	<2.17↓	11.52
4229	MLB6	97.9	<0.12↓	<0.12↓	<0.12↓	<0.12↓	<2.17↓	<2.17↓	8.08	14.88
4251	HB2	97.1	<0.12↓	<0.12↓		<0.12↓	4.63	<2.17↓		<2.17↓
4247	HB1	141.6	<0.12↓	<0.12↓	<0.12↓	<0.12↓	8.66	6.92	5.2	2.45
4250	HB5	156.6	0.2	<0.12↓	0.47	<0.12↓	<2.17↓	<2.17↓	3.52	<2.17↓
4248	HB3	141.6	<.06	0.09	<.06	<.06	<3.79	<3.79	<3.79	<3.79
4249	HB4	158	<.06	<.06	<.06	<.06	<3.79	<3.79	<3.79	<3.79
4252	HB6	158.5	0.36	0.23	<0.12↓	<0.12↓	51.05	62.45	44.79	37.77

Rat Plasma Panel

Animal	Exposure	Refl. Impulse kPa-ms	IL-10 pg/ml				IL-12p70 pg/ml			
			B-line	3 hr	24 hr	48 hr	B-line	3 hr	24 hr	48 hr
4169	LB1	0		<4.07↓	<4.07↓			6.38	6.77	
4170	Control1	58			<4.07↓				10.71	
4171	LB2	57.3		<4.07↓	<4.07↓	<4.07↓		<4.76↓	<4.76↓	10.71
4172	Control2	0	6.83				17.26			
4173	LB3	56.9				<4.07↓				<4.76↓
4174	Control3	0	<4.07↓	<4.07↓	<4.07↓		<4.76↓	14.14	<4.76↓	
4205	LB4	0		15.16	5.98	<4.07↓		<4.76↓	12.48	<4.76↓
4206	Control4	57.1	41.29				34.85			
4207	LB5	0	<4.07↓		<4.07↓	<4.07↓	<4.76↓		<4.76↓	<4.76↓
4208	Control5	56		93.89				22.88		
4210	LB6	59.3		<4.07↓	5.14	<4.07↓		<4.76↓	21.53	<4.76↓
4224	MLB1	100.5	<4.07↓		6.4	<4.07↓	<4.76↓		39.13	<4.76↓
4225	MLB2	104.3	<4.07↓	<4.07↓	<4.07↓	<4.07↓	<4.76↓	<4.76↓	<4.76↓	<4.76↓
4226	MLB3	96.5	<4.07↓	<4.07↓	<4.07↓	<4.07↓	<4.76↓	25.46	32.62	45.17
4228	MLB5	157	5.98	<4.07↓	<4.07↓	<4.07↓	6.77	<4.76↓	<4.76↓	17.26
4229	MLB6	97.9	<4.07↓	<4.07↓	<4.07↓	<4.07↓	<4.76↓	<4.76↓	25.46	34.85
4251	HB2	97.1	<4.07↓	<4.07↓		<4.07↓	<4.76↓	<4.76↓		8.83
4247	HB1	141.6	8.93	<4.07↓	<4.07↓	<4.07↓	18.73	15.73	6.77	21.53
4250	HB5	156.6	11.02	<4.07↓	<4.07↓	<4.07↓	<4.76↓	<4.76↓	20.15	<4.76↓
4248	HB3	141.6	4.99	<2.14	<2.14	<2.14	<10.36	<10.36	<10.36	<10.36
4249	HB4	158	<2.14	<2.14	<2.14	<2.14	<10.36	<10.36	<10.36	<10.36
4252	HB6	158.5	1410	1234	913.27	981.95	75.23	84.28	63.16	76

Rat Plasma Panel

Animal	Exposure	Refl. Impulse kPa-ms	INFy pg/ml				IL-5 pg/ml			
			B-line	3 hr	24 hr	48 hr	B-line	3 hr	24 hr	48 hr
4169	LB1	0		<7.29↓	<7.29↓			<2.90↓	<2.90↓	
4170	Control1	58			<7.29↓				24.68	
4171	LB2	57.3		<7.29↓	<7.29↓	12.07		16.94	4.22	27.51
4172	Control2	0	<7.29↓				4.22			
4173	LB3	56.9				<7.29↓				<2.90↓
4174	Control3	0	<7.29↓	<7.29↓	<7.29↓		<2.90↓	4.22	8.05	
4205	LB4	0		<7.29↓	23.63	<7.29↓		<2.90↓	32.83	4.22
4206	Control4	57.1	18.71				30.23			
4207	LB5	0	30.62		<7.29↓	<7.29↓	65.38		61.95	56.54
4208	Control5	56		42.65				15.26		
4210	LB6	59.3		<7.29↓	24.62	<7.29↓		<2.90↓	21.7	<2.90↓
4224	MLB1	100.5	<7.29↓		<7.29↓	<7.29↓	9.92		34.09	15.26
4225	MLB2	104.3	<7.29↓	<7.29↓	<7.29↓	<7.29↓	<2.90↓	<2.90↓	<2.90↓	<2.90↓
4226	MLB3	96.5	<7.29↓	<7.29↓	94.34	50.6	<2.90↓	4.22	30.23	48.74
4228	MLB5	157	7.67	28.61	<7.29↓	14.86	<2.90↓	16.94	<2.90↓	32.83
4229	MLB6	97.9	<7.29↓	<7.29↓	7.67	23.63	<2.90↓	<2.90↓	21.7	32.83
4251	HB2	97.1	<7.29↓	<7.29↓		<7.29↓	<2.90↓	<2.90↓		21.7
4247	HB1	141.6	<7.29↓	<7.29↓	7.67	<7.29↓	38.92	8.05	<2.90↓	11.75
4250	HB5	156.6	<7.29↓	<7.29↓	<7.29↓	<7.29↓	8.05	<2.90↓	<2.90↓	<2.90↓
4248	HB3	141.6	9.29	5.67	7.95	<3.52	<6.18	8.97	12.76	<6.18
4249	HB4	158	<3.52	<3.52	<3.52	<3.52	<6.18	<6.18	<6.18	<6.18
4252	HB6	158.5	365.46	314.14	224.79	324.62	50.76	70.31	91.28	99.55

Rat Plasma Panel

Animal	Exposure	Refl. Impulse kPa-ms	IL-17A pg/ml				IL-18 pg/ml			
			B-line	3 hr	24 hr	48 hr	B-line	3 hr	24 hr	48 hr
4169	LB1	0		<3.96↓	<3.96↓			<6.57↓	<6.57↓	
4170	Control1	58			<3.96↓				<6.57↓	
4171	LB2	57.3		<3.96↓	<3.96↓	<3.96↓		<6.57↓	<6.57↓	10.24
4172	Control2	0	<3.96↓				<6.57↓			
4173	LB3	56.9				<3.96↓				<6.57↓
4174	Control3	0	<3.96↓	<3.96↓	<3.96↓		<6.57↓	<6.57↓	<6.57↓	
4205	LB4	0		<3.96↓	<3.96↓	<3.96↓		<6.57↓	14.57	<6.57↓
4206	Control4	57.1	<3.96↓				<6.57↓			
4207	LB5	0	22.73		10.95	16.99	13.47		<6.57↓	<6.57↓
4208	Control5	56		<3.96↓				20.75		
4210	LB6	59.3		<3.96↓	<3.96↓	<3.96↓		<6.57↓	<6.57↓	<6.57↓
4224	MLB1	100.5	<3.96↓		<3.96↓	<3.96↓	<6.57↓		8.17	<6.57↓
4225	MLB2	104.3	<3.96↓	<3.96↓	<3.96↓	<3.96↓	9.72	17.92	10.24	<6.57↓
4226	MLB3	96.5	<3.96↓	<3.96↓	5.15	7.49	<6.57↓	<6.57↓	42.15	15.68
4228	MLB5	157	<3.96↓	<3.96↓	<3.96↓	<3.96↓	9.2	9.2	<6.57↓	<6.57↓
4229	MLB6	97.9	<3.96↓	<3.96↓	<3.96↓	7.27	<6.57↓	<6.57↓	<6.57↓	10.24
4251	HB2	97.1	<3.96↓	5.57		<3.96↓	<6.57↓	<6.57↓		<6.57↓
4247	HB1	141.6	<3.96↓	<3.96↓	<3.96↓	<3.96↓	29.95	16.79	<6.57↓	<6.57↓
4250	HB5	156.6	<3.96↓	<3.96↓	<3.96↓	<3.96↓	60.71	35.76	49.13	10.24
4248	HB3	141.6	3.59	3.17	3.86	<2.15	<8.95	<8.95	<8.95	<8.95
4249	HB4	158	<2.15	<2.15	<2.15	<2.15	<8.95	<8.95	<8.95	<8.95
4252	HB6	158.5	53.96	47.4	24.83	49.53	63.01	66.47	24.18	51.45

Rat Plasma Panel

Animal	Exposure	Refl. Impulse kPa-ms	MCP-1 pg/ml				IP-10 pg/ml			
			B-line	3 hr	24 hr	48 hr	B-line	3 hr	24 hr	48 hr
4169	LB1	0		116.52	85.51			<1.37↓	<1.37↓	
4170	Control1	58			92.27				<1.37↓	
4171	LB2	57.3		95.53	22.27	85.51		<1.37↓	<1.37↓	<1.37↓
4172	Control2	0	<19.84↓				5.21			
4173	LB3	56.9				<19.84↓				<1.37↓
4174	Control3	0	<19.84↓	70.82	104.89		<1.37↓	<1.37↓	<1.37↓	
4205	LB4	0		<19.84↓	78.38	<19.84↓		5.66	3.51	<1.37↓
4206	Control4	57.1	165.13				5.44			
4207	LB5	0	85.51		<19.84↓	<19.84↓	<1.37↓		<1.37↓	<1.37↓
4208	Control5	56		54.05				21.04		
4210	LB6	59.3		<19.84↓	74.66	<19.84↓		<1.37↓	<1.37↓	<1.37↓
4224	MLB1	100.5	<19.84↓		98.72	54.05	<1.37↓		<1.37↓	<1.37↓
4225	MLB2	104.3	<19.84↓	49.42	<19.84↓	34.09	<1.37↓	<1.37↓	<1.37↓	<1.37↓
4226	MLB3	96.5	92.27	49.42	283.56	156.36	<1.37↓	<1.37↓	<1.37↓	<1.37↓
4228	MLB5	157	92.27	110.82	88.93	98.72	<1.37↓	<1.37↓	<1.37↓	<1.37↓
4229	MLB6	97.9	<19.84↓	<19.84↓	127.36	154.11	<1.37↓	<1.37↓	2.18	1.72
4251	HB2	97.1	44.57	78.38		85.51	<1.37↓	<1.37↓		<1.37↓
4247	HB1	141.6	110.82	92.27	54.05	54.05	4.67	1.57	<1.37↓	<1.37↓
4250	HB5	156.6	74.66	<19.84↓	49.42	<19.84↓	3.12	<1.37↓	2.65	<1.37↓
4248	HB3	141.6	<34.35	<34.35	<34.35	<34.35	1.57	1.69	1.43	<1.20
4249	HB4	158	<34.35	<34.35	<34.35	<34.35	<1.20	<1.20	<1.20	<1.20
4252	HB6	158.5	420.55	336.83	333.26	340.36	165.19	151.57	125.44	119.86

Rat Plasma Panel

Animal	Exposure	Refl. Impulse kPa-ms	GRO/KC/CINC- pg/ml				VEGF pg/ml			
			B-line	3 hr	24 hr	48 hr	B-line	3 hr	24 hr	48 hr
4169	LB1	0		124.03	109.11			<3.16↓	<3.16↓	
4170	Control1	58			149.94				<3.16↓	
4171	LB2	57.3		165.52	130.72	130.72		<3.16↓	<3.16↓	<3.16↓
4172	Control2	0	100.81				<3.16↓			
4173	LB3	56.9				53.13				<3.16↓
4174	Control3	0	28.63	59.5	34.29		<3.16↓	<3.16↓	<3.16↓	
4205	LB4	0		98.69	147.27	117.17		<3.16↓	<3.16↓	<3.16↓
4206	Control4	57.1	363.09				<3.16↓			
4207	LB5	0	96.55		85.58	27.2	<3.16↓		<3.16↓	<3.16↓
4208	Control5	56		708.59				<3.16↓		
4210	LB6	59.3		123.06	137.26	81.05		<3.16↓	<3.16↓	<3.16↓
4224	MLB1	100.5	90.03		130.72	91.13	<3.16↓		<3.16↓	<3.16↓
4225	MLB2	104.3	64.46	64.46	103.95	60.75	<3.16↓	<3.16↓	<3.16↓	<3.16↓
4226	MLB3	96.5	82.19	121.11	117.17	126.91	<3.16↓	<3.16↓	<3.16↓	<3.16↓
4228	MLB5	157	71.72	81.05	56.97	64.46	<3.16↓	4.54	<3.16↓	<3.16↓
4229	MLB6	97.9	35.68	41.19	82.19	83.33	<3.16↓	<3.16↓	<3.16↓	5.28
4251	HB2	97.1	59.5	94.4		41.19	<3.16↓	<3.16↓		<3.16↓
4247	HB1	141.6	70.53	75.26	92.22	77.59	11.56	3.21	<3.16↓	<3.16↓
4250	HB5	156.6	86.7	98.69	126.91	85.58	8.74	4.18	12.78	<3.16↓
4248	HB3	141.6	26.5	45.82	77.32	27.48	<3.64	<3.64	<3.64	<3.64
4249	HB4	158	<16.75	<16.75	<16.75	<16.75	<3.64	<3.64	<3.64	<3.64
4252	HB6	158.5	736.39	693.71	710.92	635.9	14.82	14.22	7.88	14.58

Rat Plasma Panel

Animal	Exposure	Refl. Impulse kPa-ms	Fractalkine pg/ml				LIX pg/ml			
			B-line	3 hr	24 hr	48 hr	B-line	3 hr	24 hr	48 hr
4169	LB1	0		<1.22↓	<1.22↓			98.83	89.37	
4170	Control1	58			1.53				111.73	
4171	LB2	57.3		<1.22↓	<1.22↓	4.14		115.75	113.75	204.87
4172	Control2	0	1.79				81.71			
4173	LB3	56.9				<1.22↓				144.25
4174	Control3	0	<1.22↓	<1.22↓	<1.22↓		<15.47↓	132.48	149.03	
4205	LB4	0		<1.22↓	2.22	<1.22↓		<15.47↓	199.03	<15.47↓
4206	Control4	57.1	3.79				164.01			
4207	LB5	0	3.27		<1.22↓	<1.22↓	191.79		<15.47↓	<15.47↓
4208	Control5	56		3.27				168.25		
4210	LB6	59.3		<1.22↓	<1.22↓	<1.22↓		103.28	147.46	24.66
4224	MLB1	100.5	<1.22↓		3.01	<1.22↓	43.02		201.39	19.23
4225	MLB2	104.3	<1.22↓	<1.22↓	<1.22↓	<1.22↓	24.66	73.43	<15.47↓	54.38
4226	MLB3	96.5	<1.22↓	<1.22↓	3.44	3.96	<15.47↓	123.44	464.66	194.23
4228	MLB5	157	3.27	3.09	<1.22↓	3.35	171.02	134.22	61.18	171.02
4229	MLB6	97.9	<1.22↓	<1.22↓	1.36	2.92	<15.47↓	<15.47↓	189.32	186.81
4251	HB2	97.1	<1.22↓	<1.22↓		<1.22↓	<15.47↓	98.83		147.46
4247	HB1	141.6	7.3	4.05	<1.22↓	<1.22↓	147.46	137.64	57.85	142.63
4250	HB5	156.6	6.54	4.57	10.04	2.05	105.45	<15.47↓	153.67	86.88
4248	HB3	141.6	1.05	1.85	1.59	<.66	208.2	67.84	59.68	<24.28
4249	HB4	158	<.66	<.66	<.66	<.66	<24.28	<24.28	<24.28	<24.28
4252	HB6	158.5	14.72	12.89	9.63	10.86	134.22	253.33	140.98	184.27

Rat Plasma Panel

Animal	Exposure	Refl. Impulse kPa-ms	MIP-2 pg/ml				TNF-a pg/ml			
			B-line	3 hr	24 hr	48 hr	B-line	3 hr	24 hr	48 hr
4169	LB1	0		88.02	79.58			<1.51↓	<1.51↓	
4170	Control1	58			106.24				<1.51↓	
4171	LB2	57.3		118.26	115.91	138.27		<1.51↓	<1.51↓	<1.51↓
4172	Control2	0	120.58				<1.51↓			
4173	LB3	56.9				61.21				<1.51↓
4174	Control3	0	70.67	102.49	93.42		<1.51↓	<1.51↓	<1.51↓	
4205	LB4	0		67.58	113.54	73.7		<1.51↓	<1.51↓	<1.51↓
4206	Control4	57.1	215.77				<1.51↓			
4207	LB5	0	88.02		76.67	47.5	<1.51↓		<1.51↓	<1.51↓
4208	Control5	56		558.2				<1.51↓		
4210	LB6	59.3		61.21	73.7	47.5		<1.51↓	<1.51↓	<1.51↓
4224	MLB1	100.5	79.58		88.02	67.58	<1.51↓		<1.51↓	<1.51↓
4225	MLB2	104.3	54.53	90.74	90.74	69.14	<1.51↓	<1.51↓	<1.51↓	<1.51↓
4226	MLB3	96.5	64.43	98.66	125.14	121.73	<1.51↓	<1.51↓	<1.51↓	1.77
4228	MLB5	157	78.13	98.66	61.21	90.74	<1.51↓	<1.51↓	<1.51↓	<1.51↓
4229	MLB6	97.9	52.81	51.06	106.24	97.36	<1.51↓	<1.51↓	<1.51↓	<1.51↓
4251	HB2	97.1	108.71	113.54		90.74	<1.51↓	<1.51↓		<1.51↓
4247	HB1	141.6	101.22	119.42	99.94	96.06	<1.51↓	<1.51↓	<1.51↓	<1.51↓
4250	HB5	156.6	76.67	64.43	76.67	43.84	<1.51↓	<1.51↓	<1.51↓	<1.51↓
4248	HB3	141.6	86.77	71.06	85.59	59.64	<1.08	<1.08	<1.08	<1.08
4249	HB4	158	<23.51	<23.51	<23.51	<23.51	<1.08	<1.08	<1.08	<1.08
4252	HB6	158.5	523.74	505.32	607.99	478.38	7.26	8.24	9.05	12.77

Rat Plasma Panel

Animal	Exposure	Reflected Impulse kPa-ms	RANTES pg/ml			
			Baseline	3 hr	24 hr	48 hr
4169	LB1	0		<3.13↓	<3.13↓	
4170	Control1	58			<3.13↓	
4171	LB2	57.3		<3.13↓	<3.13↓	<3.13↓
4172	Control2	0	<3.13↓			
4173	LB3	56.9				<3.13↓
4174	Control3	0	<3.13↓	<3.13↓	<3.13↓	
4205	LB4	0		<3.13↓	<3.13↓	<3.13↓
4206	Control4	57.1	<3.13↓			
4207	LB5	0	<3.13↓		<3.13↓	<3.13↓
4208	Control5	56		<3.13↓		
4210	LB6	59.3		<3.13↓	<3.13↓	<3.13↓
4224	MLB1	100.5	<3.13↓		<3.13↓	<3.13↓
4225	MLB2	104.3	<3.13↓	<3.13↓	<3.13↓	<3.13↓
4226	MLB3	96.5	<3.13↓	<3.13↓	<3.13↓	<3.13↓
4228	MLB5	157	<3.13↓	<3.13↓	<3.13↓	<3.13↓
4229	MLB6	97.9	<3.13↓	<3.13↓	<3.13↓	<3.13↓
4251	HB2	97.1	<3.13↓	<3.13↓		<3.13↓
4247	HB1	141.6	<3.13↓	<3.13↓	<3.13↓	<3.13↓
4250	HB5	156.6	<3.13↓	<3.13↓	<3.13↓	<3.13↓
4248	HB3	141.6	<4.47	<4.47	<4.47	<4.47
4249	HB4	158	<4.47	<4.47	<4.47	<4.47
4252	HB6	158.5	29.96	12.56	9.34	14.31